Uniwersytet Zieologórski
University of Zielona Góra

Dziedzina nauk ścisłych i przyrodniczych
Dyscyplina nauk fizycznych

Field: **natural sciences**
Discipline: **physical sciences**

VINH LE DUC

Korelacje kwantowe w układach $\mathcal{PT}$-symetrycznych
Quantum Correlations in $\mathcal{PT}$-symmetric Systems

Akceptacja promotora:

.....

Promotor:
prof. dr hab. Wiesław Leoński

Promotor pomocniczy:
dr inż. Konrad Marek Gruszka

Zielona Góra
2 czerwca 2022

Acknowledgments

I need to admit that my dissertation would not be done without the help, support, and advice from my family, supervisors and friends. Firstly, I would like to express my sincere gratitude to my supervisor, Professor Wiesław Leoński, for his patience, enthusiasm and insightful guidance throughout my PhD study. He is the person who always gives me a lot of good advice and teaches me how to be more professional in research.

I would like to express my sincere gratitude to my supervisor, Dr. Konrad Marek Gruszka, for his exceptional patience and scientific support. I am deeply indebted to dr. Kalaga from Institute of Physics, University of Zielona Gora for her advice and mentoring in a scientific career.

I would like to thank Professor Van Cao Long for introducing me to the university and giving me some good advice. He is also the person who always encourage and support to me when I feel like things are getting tough.

I also would like to express my gratitude to all staffs of the faculty of physics for their help. I really appreciate what they kindly did for me during the time I was here.

Finally, I would like to be thankful to my family and my friends for support me during the time I have been in Poland for my PhD study.

Streszczenie

Korelacje kwantowe należą do jednej z głównych koncepcji mechaniki kwantowej i są szczególnie istotne z punktu widzenia kwantowej teorii informacji. Korelacje takie pokazują nam, jak stan kwantowy podukładu, który jest częścią układu składającego się z dwóch lub większej liczby podukładów, jest ściśle powiązany ze stanami odpowiadającymi pozostałym podukładom. Innymi słowy, pomiary wykonywane na jednym podukładzie wpływają na stan oraz na wyniki pomiarów wykonywanych na pozostałych podukładach. Te zależności pomiędzy podukładami mogą wykazywać różne właściwości jak i siłę. Korelacjami kwantowymi są na przykład splątanie kwantowe, sterowanie kwantowe czy nielokalność Bella. I tak, spośród tych trzech rodzajów korelacji, najsilniejszą jest nielokalność Bella, a najsłabszą splątanie. Takie korelacje były przedmiotem różnych badań poświęconych nie tylko informacji kwantowej, ale także badaniom podstawowym dotyczącym kwantowej natury świata. W ogromnej większości prac, takie przejawy skorelowania pomiędzy układami jak np. splątanie były zwykle analizowane w modelach opisywanych przez hamiltoniany hermitowskie.

Niemniej jednak w ostatnim czasie dużą uwagę zaczęto zwracać na modele zakładające, że hamiltonian nie jest hermitowski. Okazało się bowiem, że hermitowskość hamiltonianu nie jest jedynym warunkiem posiadania przez niego rzeczywistych wartości własnych. W roku 1998 Bender i Boettcher [1] wykazali, że niehermitowski hamiltonian wykazujący symetrię $\mathcal{PT}$ może posiadać również rzeczywiste wartości własne. W związku z tym prezentowana tutaj rozprawa dotyczy zagadnień, które uwzględniają różnego rodzaju korelacje kwantowe pojawiające się w układach z symetrią typu $\mathcal{PT}$. W szczególności, kwantowe układy tutaj rozważane, to układy składające się z oddziałujących ze sobą dwóch lub trzech podukładów przy jednoczesnym założeniu, że w tych wielomodowych układach mamy równowagę między zyskiem a utratą energii.

Niniejsza rozprawa składa się z czterech części. W rozdziale pierwszym rozprawy, omówione zostaną różne rodzaje korelacji kwantowych. W szczególności, opisane zostanie splątanie kwantowe, sterowanie kwantowe i nielokalność typu Bella oraz relacje między nimi. Dodatkowo w rozdziale tym omówione zostaną korelacje pierwszego i drugiego rzędu pola elektromagnetycznego. Dla wszystkich wymienionych tu korelacji opisane zostaną metody ich kwantyfikacji.

W rozdziale drugim przedstawione zostaną ogólne idee dotyczące opisu układów kwantowych przez niehermitowskie hamiltoniany, które wykazują symetrię typu $\mathcal{PT}$. Gdy taka symetria nie jest naruszona, wartości własne takich hamiltonianów są rzeczywiste i pozwalają opisać właściwości fizyczne rozważanych modeli. Zazwyczaj modele takie oddziałują z zewnętrznym środowiskiem, a dokładniej pozyskują energię ze środowiska oraz ją tracą, a strata i zysk związane z interakcją z otoczeniem równoważą się wzajemnie.

W pozostałych dwóch rozdziałach rozprawy omówione zostaną otrzymane przez nas wyniki dotyczące różnych postaci korelacji kwantowych i relacji między nimi uzyskane dla modeli dwu- i trójdzielnych (odpowiednio, rozdziały 3 i 4). Rozważane w tych rozdziałach modele obejmują dwie lub trzy oddziałujące ze sobą wnęki. Dodatkowo zakładamy, że jedna z nich zyskuje energię z otoczenia, a druga ją traci. Wszystkie rozważane modele są opisane przez $\mathcal{PT}$-symetryczne hamiltoniany dla których znajdujemy warunki, dla których symetria $\mathcal{PT}$ nie jest łamana. W omawanych tutaj przypadkach skoncentrujemy się na takich sytuacjach, w których parametry opisujące układy zapewniają rzeczywiste wartości hamiltonianów. Innymi słowy, otrzymujemy wartości parametrów opisujących korelacje kwantowe i omawiamy relacje między nimi, właśnie gdy symetria $\mathcal{PT}$ nie jest łamana. Pokazujemy także, jak te parametry ewoluują w czasie i jak zależą one od siły interakcji między podukładami oraz od zysków i strat energii całego układu.

W ostatnim (czwartym) rozdziale zaprezentowany zostanie model trójdzielny, który składa się z trzech wnęk. Ponieważ analizowany układ obejmuje trzy podukłady, dlatego omówione zostanie nie tylko splątanie dwudzielne, ale także jego trójdzielny odpowiednik. Ponadto, przedstawiony zostanie wpływ dodatkowego sprzężenia pomiędzy wnękami na generowane korelacje. To dodatkowe sprzężenie zmienia geometrię układu z liniowej w trójkątną, a co za tym idzie zmienia charakterystykę układu, w tym parametry opisujące korelacje i kwantowy charakter modelu.

Abstract

Quantum correlations belong to one of the central concepts of quantum mechanics, and they are especially relevant from the quantum information theory point of view. Such correlations show how the quantum state of a subsystem of a multi-party one is closely related to those corresponding to the remaining subsystems. In other words, measurements performed on one subsystem affects the state and results of measurements performed on the remaining ones. The quantum correlations can exhibit their various characteristics and be of different strengths. For instance, they can be of the quantum entanglement, quantum steering, or Bell nonlocality type. Such correlations were subjects of various studies devoted not only to quantum information but also to fundamental research concerning the nature of the quantum world. Naturally, such correlations were usually considered in the models described by the Hermitian Hamiltonians.

Nevertheless, recently, great attention was paid to the models assuming that the Hamiltonian is not Hermitian but exhibits the $\mathcal{PT}$-symmetry. It has appeared that the Hamiltonian's hermiticity is not only one condition for obtaining its real eigenvalues. In 1998 Bender and Boettcher [1] showed that non-hermitian Hamiltonian exhibiting $\mathcal{PT}$-symmetry can also possess real eigenvalues. Thus, presented here dissertation concerns the topics which incorporate the quantum correlations of various types and descriptions with the application of the $\mathcal{PT}$-symmetry formalism. In particular, we concentrate here on the studies of bipartite and tripartite $\mathcal{PT}$-symmetric systems in which the balance between the gain and loss of the system's energy is assumed.

In the first chapter of the dissertation, we introduce the concepts of quantum correlations of various types. In particular, we mention the quantum entanglement, quantum steering, and Bell-type nonlocalities, pointing out the relations among them. Additionally, in that chapter, we present an introduction devoted to first- and second-order

correlations of the electromagnetic field. For all mentioned in the chapter correlations, we describe the methods of their quantification.

The second chapter is devoted to an introduction to the topics and main ideas related to the description of quantum systems by non-Hermitian Hamiltonians, primarily those exhibiting $\mathcal{PT}$-symmetric properties. When such symmetry is not broken, the eigenvalues of such Hamiltonians are real and allow to describe the physical properties of considered models. Usually, the models with balanced gain and loss related to the interaction with an environment and other external couplings are considered for such cases.

The remaining part of the dissertation is devoted to the discussion of our results concerning various forms of quantum correlations and relations among them for bi- and tripartite models (Chapters 3 and 4, respectively). Considered in those chapters, models involve two (three) interacting cavities. Additionally, we assume that one of them is excited, whereas another loses its energy. All considered models are described by the $\mathcal{PT}$-symmetric Hamiltonians, and we find the conditions for which such symmetry is not broken. We concentrate just on such situations and assume that the parameters describing the systems ensure the real values of the Hamiltonians. For such cases, we get the parameters describing the quantum correlations and discuss the relations among the latter. We show how such parameters evolve in time and depend on the interactions between cavities and the pumping/losses strength.

Finally, in the last (fourth) chapter, we discuss the tripartite model involving three cavities. As we deal with three subsystems, we discuss not only the bipartite entanglement but also its tripartite counterpart. Additionally, we show how the additional coupling between cavities, changing the model's geometry from the linear to a triangle one, changes the characteristics of the system, including the parameters describing the correlations and quantum character of the model.

Table of Contents

List of Figures

Introduction

Since the concept of quantum space-time was first introduced in 1969 [2], the idea of performing quantum computations and quantum information respectively was given by Alexander Holevo and Charles H. Bennett in 1973 [3]. In 1980, the working mechanism of a quantum computer was described for the first time by Paul Benioff [4], and then, his original model of a quantum mechanical Turing machine was developed in 1982 [5]. At this point one should mention the famous lectures given in 1984 by Rychard P. Feynman at 1984, where he provided the complete framework for the idea of quantum computing (see the book [6]. In 1998, the first experimental demonstration of a quantum algorithm by a working 2-qubit NMR quantum computer was presented in [7]. The computer solved Deutsch-Jozsa problem. After many proposals of quantum computers, the largest superconducting 127-qubit quantum computer was created by IBM in 2021.

In parallel, with the development of quantum computers, the idea of quantum teleportation as a technique for transferring quantum information has appeared for the first time in 1993 by Bennett [8]. Such technique was experimentally realized by many research groups [9–11]. In 2014, Wolfgang Pfaff and his co-worker performed an experiment in which the transfer data by quantum teleportation over a distance of 3 meters with a zero percent error rate [12] was performed. That step is especially important for the implementation of the idea of quantum Internet. It became even more promising when Xiao-Song Ma and his group reported the experiment of quantum teleportation over 143 kilometers between the La Palma and Tenerife islands [13]. The future of quantum internet became more clear when the distance of quantum teleportation increased up to $1,400$ km in an experiment of quantum information transition between ground and satellite was reported by the research group of Jian-Wei Pan in 2017 [14].

One of the key problems is finding physical systems that could be able to implement the

protocols of quantum computation and quantum teleportation, in which the existence of quantum correlations is vital. Quantum entanglement is a necessary condition for many quantum protocols [15], while quantum steering plays a special role in quantum information processing, especially in quantum cryptography and quantum teleportation [16]. The systems that can be used in implementation of quantum protocols have to be quantum correlation sources. For that goal, there are many physical systems that have been studied. For instance there are quantum dots [17], two-level atoms [18–20], the systems involving an atom and a molecule [21], micromechanical oscillators [22], or semiconductor quantum wires [23].

For a long time, scientists focused only on the systems that are described by Hermite Hamiltonian because of the existence of their real eigenvalue spectra. The systems that are described by non-Hermite Hamiltonians are believed not to have real spectra of eigenvalues and were not especially discussed. However, after Beder *et.al* showed that real eigenvalues spectra in such systems can exist when they are $\mathcal{PT}$-symmetric, and fulfill the condition in which the symmetry is unbroken [1, 24]. Such systems are called $\mathcal{PT}$-symmetric ones. Since then, such systems have attracted a lot of attention and many publications devoted to those system have appeared. Therefore, in this dissertation, we will focus on quantum correlations appearing in $\mathcal{PT}$-symmetric systems. Thus, that purpose, the dissertation will be organized as follows:

In the first chapter, we will present some basic concepts concerning quantum correlations such as quantum entanglement, quantum steering, Bell nonlocality, and quantum correlation functions. Besides the definition of quantum correlations, we will present the quantities that can be used to quantify them. We will emphasize that such the quantities can be expressed as combinations of the bosonic creation and annihilation operators.

The second chapter is devoted to the introduction of idea of $\mathcal{PT}$-symmetry, definitions

of the parity- and time-reversal operators and their properties. We will also present the conditions determining whether the real eigenvalue spectrum in a $\mathcal{PT}$-symmetric system appear, and finally, the concept of the phase-transition point in $\mathcal{PT}$-symmetric systems.

In the third chapter, we consider the model of a bipartite $\mathcal{PT}$-symmetric system involving two cavities with the balance between the energy gain and loss. For such the model we concentrate on the level of quantum coherence between two subsystems in the model (described by the first- and second-order correlation functions) After finding conditions determining the location of the phase-transition (the position of the point in which the $\mathcal{PT}$-symmetry is broken), we discuss the quantum correlations such as the entanglement and quantum steering. We discuss there the case when the symmetry is unbroken.

Finally, in the last chapter, we focus on the model involving three cavities. For such a system we show how the quantum bipartite and tripartite entanglement and quantum steering can be generated. Similar to the previous chapter, we concentrate on the case when the $\mathcal{PT}$-symmetry is not broken, and the balance of energy gain and loss is preserved. Additionally, we discuss the influence of the interaction between the first and last subsystems, that transforms the system from a linear to a triangular one.

Chapter 1

Quantum correlations – quantum entanglement and steering, Bell-type non-locality, correlation functions of EM field.

1.1 Quantum entanglement

1.1.1 Entangled states and separable states

One of types of quantum correlations is quantum entanglement. It plays a crucial role in quantum information theory. An entangled system is a system that is generated so that the quantum state of each subsystem can not be independently described from the quantum state of others. In that case, subsystems share an entangled state. If we perform a measurement in a subsystem, we also determine the quantum state of others. Contrary to an entangled state, a separable state describes the system in which the quantum state of each subsystem can be independently represented from the state of others. Let us start this section by considering a system of N parties defined in N individual Hilbert spaces $\mathcal{H}_1$, $\mathcal{H}_2$, ..., $\mathcal{H}_N$. The space of the whole system's state will be a Hilbert space that is a result of tensor product $\mathcal{H} = \mathcal{H}_1 \otimes \mathcal{H}_2 \otimes ... \otimes \mathcal{H}_N$. The number of dimensions of such space is $d = \prod_{i=1}^{N} d_i$, where d_i is the dimension of Hilbert space $\mathcal{H}_i$. On the other side, we can not generally write the state of the whole system as a

tensor product of the states describing subsystems. This shows the formal statement of entanglement phenomena. In this section, we will introduce some definitions in which the difference between entangled state and separable state will be indicated.

Before considering the discrimination between quantum entangled state and quantum separable state, we will introduce concepts of pure and mixed states. A state $|\psi\rangle$ will be a pure state if it can not be represented as a convex combination of the other states [25].

If a system is in a pure state, we can obtain the exact information about the quantum system. For such a case, the outcome of the measurement of the observable A can be its expectation value that is calculated as

$$A = \langle\psi| \hat{A} |\psi\rangle , \tag{1.1}$$

where $\hat{A}$ is the operator characterizing observable A. The density matrix of the system $\hat{\rho} = |\psi\rangle \langle\psi|$ gives us two simple tests to determine whether the system is in pure state or not. For pure state, we always have $\hat{\rho}^2 = \hat{\rho}$ or the purity $\gamma_P \equiv \mathrm{Tr}(\hat{\rho}^2) = 1$ [26]. We can illustrate it by considering a 1/2 spin particle system. For this system, there are two individual states as

$$\left|\psi_{(+)}\right\rangle = \frac{1}{\sqrt{2}} \left(|\uparrow\rangle + |\downarrow\rangle\right) , \tag{1.2}$$

and

$$\left|\psi_{(-)}\right\rangle = \frac{1}{\sqrt{2}} \left(|\uparrow\rangle - |\downarrow\rangle\right) , \tag{1.3}$$

where $|\uparrow\rangle$ and $|\downarrow\rangle$ represents the state of spin up and spin down, respectively. In the computational basis $\{|\uparrow\rangle , |\downarrow\rangle\} = \left\{ \begin{bmatrix} 1 \\ 0 \end{bmatrix} , \begin{bmatrix} 0 \\ 1 \end{bmatrix} \right\}$, the density matrices corresponding to

$\left|\psi_{(+)}\right\rangle$ and $\left|\psi_{(+)}\right\rangle$ can be represented by the following 2×2 matrices

$$\hat{\rho}_{(\pm)} = \begin{bmatrix} 1/2 & \pm 1/2 \\ \pm 1/2 & 1/2 \end{bmatrix}. \tag{1.4}$$

It is easy to check that $\mathrm{Tr}(\hat{\rho}_{\pm}^2) = 1$. It means that $\left|\psi_{(+)}\right\rangle$ and $\left|\psi_{(+)}\right\rangle$ are pure states.

In contrary to pure state, a state represented by $\hat{\rho}$ is a mixed state if it can not be expressed in terms of only one pure state density matrix. For such the case $\hat{\rho}$ can be written as

$$\hat{\rho} = \sum_{i=1}^{N} p_i \left|\psi_i\right\rangle \left\langle\psi_i\right|, \tag{1.5}$$

where p_i are the probabilities of pure states $|\psi_i\rangle$, and $\sum\limits_i p_i = 1$. A pure state can be represented by a state vector $|\psi\rangle$. Meanwhile, for the case of a mixed state, it is always represented by a density matrix $\hat{\rho}$. We can say that a mixed state $\hat{\rho}$ is a statistical ensemble of pure states $\{\psi_1, \psi_2 ..., \psi_N\}$. For a mixed state, the purity has to satisfies $\frac{1}{d} \leq \gamma_P \equiv \mathrm{Tr}(\hat{\rho}^2) < 1$, where d is is the dimension of the Hilbert space upon which the state is defined [27]. A mixed state will be a maximally mixed state if it has uniform probability distribution for every pure state involved. For such the case, we have $\gamma_P \equiv \mathrm{Tr}(\hat{\rho}^2) = \frac{1}{d}$.

As previously, we can use the system of two 1/2-spin particles as an example of a mixed state that takes the form

$$\hat{\rho} = \frac{1}{2} \left|\psi_{(+)}\right\rangle \left\langle\psi_{(+)}\right| + \frac{1}{2} \left|\psi_{(-)}\right\rangle \left\langle\psi_{(-)}\right|, \tag{1.6}$$

where $\left|\psi_{(+)}\right\rangle$ and $\left|\psi_{(-)}\right\rangle$ are the same as in (1.2) and (1.3).

Now, we are in a position to introduce the separable and entangled states. The difference between the entangled states and the separable ones can be easily presented in the case of a pure state. A pure state $|\psi\rangle$ in Hilbert space $\mathcal{H}$ will be a separable state if it can be written as a tensor product of states describing subsystems as follows

$$|\psi\rangle = |\psi\rangle_1 \otimes |\psi\rangle_2 \otimes ... \otimes |\psi\rangle_N , \tag{1.7}$$

where $|\psi\rangle_i$ is the individual state of subsystem i defined in the Hilbert space $\mathcal{H}_i$.

We can go back the exemplary system of two 1/2 spin particles to show a possible separable pure state $|\psi\rangle = \frac{1}{2}(|0\rangle|0\rangle - |0\rangle|1\rangle + |1\rangle|0\rangle - |1\rangle|1\rangle)$. It is the separable pure

state because we can express this state as a tensor product of two different pure state describing two subsystems as follows

$$|\psi\rangle = \frac{1}{\sqrt{2}}\left(|0\rangle + |1\rangle\right) \otimes \frac{1}{\sqrt{2}}\left(|0\rangle - |1\rangle\right) = \left|\psi_{(+)}\right\rangle \otimes \left|\psi_{(-)}\right\rangle. \tag{1.8}$$

Based on the definition of the separable pure state presented above, we can easily introduce the definition of the entangled pure state. Accordingly, a pure state $|\psi\rangle$ in Hilbert space $\mathcal{H}$ will be an entangled pure state if it is not a separable pure state.

We can illustrate entangled pure states by the well-known maximally entangled states for the case of two-qubit systems. They are Bell states for two-qubit systems [28]:

$$\begin{aligned}
\left|\phi^{+}\right\rangle &= \frac{1}{\sqrt{2}}\left(|0\rangle\,|0\rangle + |1\rangle\,|1\rangle\right) \\
\left|\phi^{-}\right\rangle &= \frac{1}{\sqrt{2}}\left(|0\rangle\,|0\rangle - |1\rangle\,|1\rangle\right) \\
\left|\psi^{+}\right\rangle &= \frac{1}{\sqrt{2}}\left(|0\rangle\,|1\rangle + |1\rangle\,|0\rangle\right) \\
\left|\psi^{-}\right\rangle &= \frac{1}{\sqrt{2}}\left(|0\rangle\,|1\rangle - |1\rangle\,|0\rangle\right)
\end{aligned} \tag{1.9}$$

The definition of mixed entangled states is more complicated than that for pure states. Nevertheless, it describes realistic laboratory situations, where decoherence and imperfect operations lead to incomplete information about the state vector describing the system [29]. In this case, a mixed state $\hat{\rho}$ belonging to a positive operator $\mathcal{S}(\mathcal{H})$ acting on Hilbert space $\mathcal{H}$ is separable if it can be written in a convex combination of tensor products of pure states as [30, 31]

$$\hat{\rho} = \sum_{i} p_i \left|\psi_{i1}\right\rangle \left\langle\psi_{i1}\right| \otimes \left|\psi_{i2}\right\rangle \left\langle\psi_{i2}\right| \otimes ... \otimes \left|\psi_{iN}\right\rangle \left\langle\psi_{iN}\right|, \tag{1.10}$$

where $|\psi_{ij}\rangle$ are the possible pure states in Hilbert space $\mathcal{H}_j$, and p_i are positive numbers (probabilities) that satisfy $\sum\limits_{i} p_i = 1$.

Consequently, a mixed state $\hat{\rho}$ defined in the space $\mathcal{S}(\mathcal{H})$ is entangled if it is not separable. Let us assume that a system consisting of two subsystems A and B that share a state $\hat{\rho}$. The states that describe the subsystems A and B are $\hat{\rho}^A$ and $\hat{\rho}^B$, respectively. The state of the system will be an entangled state if it can not be written as a convex combination of product states as follows

$$\hat{\rho}^{AB} = \sum_{\lambda} p\left(\lambda\right) \hat{\rho}_{\lambda}^{A} \otimes \hat{\rho}_{\lambda}^{B}. \tag{1.11}$$

Additionally, for the separable states, when performing local measurements $\hat{M}_{a|x}$ and $\hat{M}_{b|y}$ on the subsystems A and B, the probabilities to get the outcomes a and b corresponding to the observable quantities x and y, respectively, are

$$p\left(a,b\left|x,y\right.\right)=\sum_{\lambda}p\left(\lambda\right)Tr\left(\hat{M}_{a|x}\hat{\rho}_{\lambda}^{A}\right)Tr\left(\hat{M}_{b|y}\hat{\rho}_{\lambda}^{B}\right). \tag{1.12}$$

For the case of the entangled states, (1.12) is not satisfied. Thus, any measurement performed on the first subsystem will cause an effect on the measurement that is performed on the second one and vice versa.

1.1.2 Quantification of quantum entanglement

There are many ways to quantify quantum entanglement. One of them is quantifying quantum entanglement by using von Neumann entropy. This quantifier is special simply for pointing out the strength of quantum entanglement, and can be applied when we are dealing with pure states.

Let us assume that we deal with a bipartite system involving two parties A and B in which its state is described by a density matrix $\hat{\rho}=\sum_{i}p_{i}\left|\psi_{i}\right\rangle\left\langle\psi_{i}\right|$, where p_i are the probabilities corresponding to pure states $|\psi_i\rangle$. The von Neumann entropy of each subsystem is defined as

$$E\left(\left|\psi_{i}\right\rangle\right)=S\left(\hat{\rho}_{A}\right)=S\left(\hat{\rho}_{B}\right)=-\sum_{j}\lambda_{j}^{A}\log_{2}\lambda_{j}^{A}=-\sum_{k}\lambda_{k}^{B}\log_{2}\lambda_{k}^{B}, \tag{1.13}$$

where λ_k^A and λ_k^B are the eigenvalues of reduced density matrices $\hat{\rho}_A$ and $\hat{\rho}_B$, respectively. Such matrices can be obtained by tracing out one of the two subsystems, *i.e.* $\hat{\rho}_A = \mathrm{Tr}_B(\hat{\rho})$ and $\hat{\rho}_B = \mathrm{Tr}_A(\hat{\rho})$. The strength of quantum entanglement of systems's state can be quantified as follows

$$E\left(\hat{\rho}\right)=\min\sum_{i}p_{i}E\left(\left|\psi_{i}\right\rangle\right). \tag{1.14}$$

In [32], F. Pan *et.al* have proposed a simple way to evaluate the entanglement of multipartite pure states. This method was simplified by C. Wangcang [33]. In [33], the entanglement of multipartite pure states is quantified by introducing a quantity called *average entropy* defined as

$$E(\hat{\rho})=\frac{1}{N}\sum_{i=1}^{N}E_{i}\left(\hat{\rho}_{i}\right), \tag{1.15}$$

where $E_i(\hat{\rho}_i) = -Tr\left(\hat{\rho}_i \log_2 \hat{\rho}_i\right)$ is the reduced von Neumann entropy for i-th subsystem when the other subsystems are traced out ($\hat{\rho}_i$ is reduced density matrix with respect to i-th subsystem). The value of $E(\hat{\rho})$ is only different from zero when $E_i(\hat{\rho}_i) \neq 0$ for all i. If for any i the condition $E_i(\hat{\rho}_i) = 0$ is fulfilled, $E(\hat{\rho})$ will be equal to zero.

We can easily see that it is quite explicitly and easily to quantify the entanglement of two-qubit states by using von Neumann entropy calculation. However, for many-party systems, this calculation becomes more complicated and difficult.

In 1998, William K. Wootters proposed another method to quantify the entanglement of two-qubit system states proposing the parameter called the *concurrence* [34]. To find the concurrence we only need to perform multiplications of matrices and find the eigenvalues.

The concurrence corresponding to the state $\hat{\rho}$ is defined as

$$C\left(\hat{\rho}\right)=\max\left\{0,\sqrt{\lambda_1}-\sqrt{\lambda_2}-\sqrt{\lambda_3}-\sqrt{\lambda_4}\right\}, \tag{1.16}$$

where λ_j (j=1,...,4) are the positive eigenvalues (in decreasing order) of Hermitian matrix

$$\hat{R}=\hat{\rho}\left(\sigma_y\otimes\sigma_y\right)\hat{\rho}^*\left(\sigma_y\otimes\sigma_y\right). \tag{1.17}$$

The operator $\sigma_y=\begin{bmatrix}0 & -i\\ i & 0\end{bmatrix}$ is the Pauli spin matrix and $\hat{\rho}^*$ is the complex conjugation of $\hat{\rho}$. The concurrence is equal to 0 when $\hat{\rho}$ represents separable state and is equal to the unity for maximally entangled state.

In 2004, F. Mintert *et.al* introduced a method to calculate concurrence of multi-party state $|\psi\rangle$ of N-qubit states [35] that is simplified as in the following expression [36]

$$C\left(|\psi\rangle\right)=2^{1-\frac{N}{2}}\sqrt{2^N-2-\sum_{k=1}^{2^N-2}Tr\hat{\rho}_k^2}, \tag{1.18}$$

where $\hat{\rho}_k$ is the reduced density matrix corresponding to the k-th subset with a total number of 2^N-2 possible subsets of the N subsystems.

For the case of mixed states, the concurrence of mixed state $\hat{\rho}$ can be calculated as follows

$$C(\hat{\rho})=\min_{\{p_1|\psi_i\rangle\}}\sum_j p_j C\left(|\psi_j\rangle\right). \tag{1.19}$$

This has to be done over all possible state decomposition $\hat{\rho}=\sum_j p_j\left|\psi_j\right\rangle\left\langle\psi_j\right|$, $p_j\geq 0$, and $\sum_j p_j=1$.

C. S. Yu and H. S. Song introduced another way to measure multipartite entanglement by considering a definition of semi-separable state [37]. In their method, the system consisting of N subsystems is separated on two groups. The first one consists of n subsystems, whereas the other one contains $N-n$ subsystems. A state of N-party system $\hat{\rho}$ is called semi-separable state if it can be written in the following way

$$\hat{\rho}=\sum_i p_i\hat{\rho}_i^n\otimes\hat{\rho}_i^{N-n}, \tag{1.20}$$

where the sum is taken over all possible bipartite grouping corresponding to the probability p_i satisfying condition $\sum_i p_i = 1$. Moreover, $\hat{\rho}_i^n$ and $\hat{\rho}_i^{N-n}$ are the quantum state of the group of n and $N-n$ subsystems, respectively. Additionally, $n \in [1, M]$, where $M = \frac{N}{2}$ if N is even, and $M = \frac{N-1}{2}$ if N is odd. The system's separation can be done in $S = \sum_{m=1}^{M} C_N^m$ ways with $C_N^m = \frac{N!}{(N-m)!m!}$. Thus, the entanglement measure of the whole system can be expressed as follows [37]

$$E(\hat{\rho}) = \sum_j^S \frac{E_j}{S}, \tag{1.21}$$

where E_j is the bipartite entanglement measure of the j-th possible bipartite grouping.

In 2002, Vidal and Werner have proposed a quantum entanglement measure for bipartite quantum states by using bipartite negativity [38]. Let $\mathcal{H}_A$ and $\mathcal{H}_B$ be complex Hilbert spaces of subsystems A and B, with dimensions d_A and d_B, respectively. The negativity that quantifies the entanglement of a bipartite quantum state of A and B is defined as follows

$$N(\hat{\rho}) = \frac{\left\|\hat{\rho}^{T_A}\right\| - 1}{2}, \tag{1.22}$$

where $\hat{\rho}^{T_A}$ is the partial transpose of $\hat{\rho}$ with respect to subsystem A, and $\left\|\hat{\rho}^{T_A}\right\|$ shows the trace norm of $\hat{\rho}^{T_A}$. The matrix elements of $\left\|\hat{\rho}^{T_A}\right\|$ can be written as follows

$$\langle m_A| \otimes \langle n_B| \hat{\rho}^{T_A} |p_A\rangle \otimes |q_B\rangle \equiv \langle p_A| \otimes \langle n_B| \hat{\rho} |m_A\rangle \otimes |q_B\rangle, \tag{1.23}$$

where $|m_A\rangle \otimes |n_B\rangle$ is a product basis state defined in a Hilbert space $\mathcal{H}_A \otimes \mathcal{H}_B$. The value of negativity will be equal to 0 when $\hat{\rho}$ represents separable state, and it will be unity for maximally entangled state.

Although using negativity to evaluate quantum entanglement is quite simple and effective for bipartite quantum states, there is still no precise method for calculating negativity for multipartite quantum states. In 2008, C. Sabin and G. García-Alcaine proposed a simple method of finding negativity for tripartite quantum systems based on finding bipartite negativities for possible bipartite groupings. [39]. In this method, we assume that a system consists of three subsystems labeled by 1, 2, and 3, Thus, let us assume that the quantum state describing the whole system is $\hat{\rho}$. We separate the system into two parts. The first part is one of three subsystems, whereas the other part comprises two remaining subsystems. In this way, we have three possibilities of separation: 1-23, 2-13, and 3-12. The tripartite negativity of state $\hat{\rho}$ now can be calculated as follows

$$N(\hat{\rho}) = \sqrt[3]{N_{1-23} N_{2-13} N_{3-12}}, \tag{1.24}$$

where bipartite negativities N_{i-jk} are defined as in (1.22), *i.e.* $N_{i-jk} = \frac{\left\|\hat{\rho}^{T_i}\right\|-1}{2}$, and $\hat{\rho}^{T_i}$ is partial transpose of $\hat{\rho}$ with respect to subsystem i, $\{i = 1, 2, 3\}$, and $\{jk = 23, 13, 12\}$, respectively. As previously, the value of negativity N will be equal to 1 for the case of maximally entangled states, and be equal to zero for separable ones.

1.2 Quantum steering

Quantum steering is a special type of nonlocal quantum correlations. This concept arose from the famous debate of Einstein, Podolsky, and Rosen in 1935 concerning the completeness of quantum mechanics [40]. They proposed a system consisting of two particles sharing an entangled state. If we are interested in measurements of the position and momentum of both particles, the results of measurement performed on the first particle will allow us to predict the result of measurement on the second one. This is caused by the quantum correlation between the particles. Approximately at the same time, Schrödinger published another article to show his opinion concerning that phenomenon [41,42]. He suggested that if we choose the type of measurement of the position or momentum of the first particle, we can steer the state of the second particle when the wave-function collapses into the eigenstates of the position or momentum operators. However, at that time, such idea did not attract much attention, as Schrödinger has also admitted that it is still a some kind of "magical" process, and it can not be used in the transmition of quantum information. Such situation was not changed until 2007 when Wiseman *et.al.* presented an idea of quantum information process. They have shown that quantum steering indicates that the conditional states can not be described as a product of their parts by the local hidden variables (LHV) model [43]. They also showed that quantum steering represents quantum correlations that are located in some sense between the entanglement and Bell non-locality. It means that every quantum state violating Bell inequalities should be steerable, and all steerable states are also entangled. However, the statement in the opposite direction is not necessarily true. Since then, the concept of quantum steering has also received more attention of physicists, and that is one of the reasons why quantum steering became one of the hot research topics in the current research.

In the following subsections, we will mention some of the concepts related to quantum steering based on the above point of view. We shall also apply the ideas and parameters given by Cavalcanti *et.al.* [44].

1.2.1 Definition of quantum steering

It will be easier for us to understand the main idea of quantum steering by taking a look at what Einstein, Podolsky, and Rosen said in their publication in 1935 [40]. Let us assume that we have a system of two subsystems A and B. Let $\{a_n\}$ $(n = 1, 2, 3, ...)$ are the eigenvalues of a physical quantity M_1 characterized by operator $\hat{M}_1$ that is related to subsystem A. The related eigenfunctions can be correspondingly written as $\{u_n(x_1)\}$, where x_1 characterizes the variables describing subsystem A. In such a way, the wave function of the whole system can be expressed as

$$\psi(x_1, x_2) = \sum_{n=1}^{\infty} \psi_n(x_2) u_n(x_1), \tag{1.25}$$

where $\psi_n(x_2)$ can be seemed as the coefficients of the expansion of $\psi(x_1, x_2)$ into orthogonal functions $\{u_n(x_1)\}$, and x_2 characterize the variables describing subsystem B. If we do a measurement of the quantity M_1 on subsystem A and get the value a_i corresponding to eigenfunction $u_i(x_1)$, the wave function describing subsystem B will immediately collapse into $\psi_i(x_2)$.

It is obviously that the set of $\{u_n(x_1)\}$ depends on the measured quantity. Therefore, if we consider quantity M_2 instead of M_1, the related eigenvalues will be $\{b_m\}$ $(m = 1, 2, 3, ...)$ corresponding to eigenfunctions $\{v_m(x_1)\}$. As a result, the wave function of the whole system in (1.25) will take the following form

$$\psi(x_1, x_2) = \sum_{m=1}^{\infty} \varphi_m(x_2) v_m(x_1), \tag{1.26}$$

where $\varphi_m(x_2)$ are the coefficients of the expansion of $\psi(x_1, x_2)$ into orthogonal functions $\{v_n(x_1)\}$. Now, if we measure quantity M_2 on subsystem A and get the value b_j corresponding to eigenfunction $v_j(x_1)$, the wave function describing subsystem B will collapse into $\varphi_i(x_2)$. Therefore, we can see that the consequence of choosing two different bases of measurement performed on subsystem A leads to the fact that subsystem B will be in the states described by two set of the states. In other words, by choosing the kind of measurement performed on subsystem A, we can steer the quantum state describing subsystem B. That is the main idea of the quantum steering phenomenon.

Now, we can go further by showing the definition of quantum steering applying probabilistic and information theory concepts. Let us start by considering a two-particle system held by Alice and Bob sharing an unknown quantum state described by the density matrix $\hat{\rho}^{AB}$. Alice can perform a measurement of observable x and obtain the corresponding output of a. Immediately after Alice performs the above measurement, the state of the particle held by Bob will change to state $\hat{\rho}_{a|x}$ with the corresponding probability $p(a\,|x)$. This state is called post-measurement state. Let us assume that Bob is in complete control of his measurements while the characteristics of the measurements performed by Alice is unknown. In that case, all the things that we have are the post-measurement state $\hat{\rho}_{a|x}$ and the conditional probability $p(a\,|x)$ corresponding to the result of the measurement that Alice made. They do not depend on any information about how she made her measurements. Those post-measurement states and corresponding conditional probabilities form a group of normalized quantum states called assemblage $\left\{\hat{\sigma}_{a|x}\right\} \equiv \left\{p\left(a\,|x\right)\hat{\rho}_{a|x}\right\}$. The elements of the assemblage can be determined by tracing of the components of the matrix that we get after acting measure-specific operator $\hat{M}_{a|x}$ related to the Alice′s measurement on the state of the system [44]

$$\hat{\sigma}_{a|x} = Tr_A\left[\left(\hat{M}_{a|x} \otimes \hat{\mathbb{I}}\right)\hat{\rho}^{AB}\right], \tag{1.27}$$

where the operator $\hat{M}_{a|x}$ is positive, and satisfies the condition $\sum_a \hat{M}_{a|x} = \hat{\mathbb{I}}$ for every measurement of observable x and the corresponding output a. The post-measurement

state of the subsystem on the Bob's side will be a combination of all components of the assemblage $\left\{\hat{\sigma}_{a|x}\right\}$. It means $\hat{\rho}^B = \sum_a \hat{\sigma}_{x|a}$. Besides that, the assemblage $\left\{\hat{\sigma}_{a|x}\right\}$ is normalized, *i.e.* $Tr\left(\sum_a \hat{\sigma}_{x|a}\right) = \hat{\mathbb{I}}$. In addition, the tracing of each element of the assemblage gives us the probability of the corresponding measurement $Tr\left(\hat{\sigma}_{x|a}\right) = p\left(a\,|x\right)$.

Similar to the way in which we defined quantum entangled states after considering the definition of separable states, we can introduce the definition of steerable states by defining unsteerable ones. Such definition is based on the introduction of the local hidden state (LHS) model. In such the model, we assume that the initial state of the particle in Bob's side was one of hidden states $\hat{\zeta}_\lambda$ corresponding to the probabilities $p\left(\lambda\right)$ for a hidden variable λ. They create a local hidden state assemblage $\left\{p\left(\lambda\right), \hat{\zeta}_\lambda\right\}$. The hidden variable λ directs the measurement of Alice to get outcome a with corresponded probability $p\left(a|\,x,\lambda\right)$ when she does a measurement on the particle she holds. The whole possibility of getting outcome a for measuring observable x can be calculated as

$$p\left(a|\,x\right) = \sum_\lambda p\left(\lambda\right) p\left(a|\,x,\lambda\right). \tag{1.28}$$

By this assumption, what Bob can get is not only the outcomes of Alice's measurement but also their corresponded probabilities. Therefore, the component $\hat{\sigma}_{a|x}$ of the state assemblage $\{\hat{\sigma}_{a|x}\}$ on Bob's side, corresponding to Alice's measurement assemblage $\left\{\hat{M}_{a|x}\right\}$, can be written as follows

$$\hat{\sigma}_{a|x} = \sum_\lambda p\left(\lambda\right) p\left(a|\,x,\lambda\right)\hat{\zeta}_\lambda. \tag{1.29}$$

Tracing of each element of that assemblage gives us the whole possibility of getting outcome a for measuring observable x, $p\left(a|\,x\right) = Tr(\hat{\sigma}_{a|x})$. A state $\hat{\rho}^{AB}$ will be unsteerable if a local hidden state assemblage $\left\{p\left(\lambda\right), \hat{\zeta}_\lambda\right\}$ exists and (1.29) is satisfied for arbitrary measurement x and corresponded state $\hat{\sigma}_{a|x}$ in the state assemblage $\left\{\hat{\sigma}_{a|x}\right\}$. By this way a state will be steerable if it is not unsteerable. From (1.29), one can see that if the state of a two-party system is steerable, then the choice of measurement assemblage for local measurements performed on the first subsystem will affect the post-measure state of the second one. If Bob performs a local measurement of the quantity y by applying the operator $\hat{M}_{b|y}$ on the state of the particle he holds, the joint probability corresponding to getting the outcomes a (in the Alice′s measurement) and b (in the Bob′s measurement) is

$$p\left(a,b\,|x,y\right) = Tr(\hat{M}_{b|y}\,\hat{\sigma}_{a|x}). \tag{1.30}$$

Substituting (1.29)into (1.30) gives us

$$p\left(a,b\,|x,y\right) = \sum_\lambda \Big[p\left(\lambda\right) p\left(a\,|x\,,\lambda\right) Tr(\hat{M}_{b|y}\,\hat{\zeta}_{a|x})\Big]. \tag{1.31}$$

1.2.2 Quantification of quantum steering

To introduce the parameters that could be useful in quantification of quantum steering, we will start our discussion from quantifiers that can quantify quantum steering corresponding to a chosen assemblage. The task is to find out how much quantum steering an assemblage indicates. For that goal, the first quantum steering quantifier was supposed to be steering weight [45]. The idea of such a kind of steering quantifier comes from the idea of considering the best separable approximation [46] allowing to distinguish entangled states from separable states. Such approach is based on the fact that we always decompose an assemblage $\hat{\sigma}_{a|x}$ as a convex combination of an assemblage in local hidden state model $\hat{\sigma}^{LHS}_{a|x}$ and a compatible assemblage $\hat{\varrho}_{a|x}$ that fulfills the relation

$$\hat{\sigma}_{a|x} = q\hat{\varrho}_{a|x} + (1-q)\,\hat{\sigma}^{LHS}_{a|x}, \tag{1.32}$$

where $0 \leq q \leq 1$, $\hat{\varrho}_{a|x}$ has to satisfy

$$\sum_a \hat{\varrho}_{a|x} = \sum_a \hat{\varrho}_{a|x'} \quad \forall x, x', \tag{1.33}$$

and

$$Tr \sum_a \hat{\varrho}_{a|x} = 1 \quad \forall x, \quad \hat{\varrho}_{a|x} \geq 0 \quad \forall a, x. \tag{1.34}$$

Equation (1.32) shows that the greater value of q, the better demonstration of steering assemblage $\hat{\sigma}_{a|x}$ does. That allows to introduce a steering quantifier referred to as steering weight $SW\left(\hat{\sigma}_{a|x}\right)$. The value of such a quantity can be calculated as the minimal value of q as

$$SW\left(\hat{\sigma}_{a|x}\right) = \min_{\hat{\sigma}_{a|x}} (q)\,, \tag{1.35}$$

where the minimum of q is understood to be overall possible decomposition of $\hat{\sigma}_{a|x}$ in the form of (1.32).

There is another quantification method that comes from the idea analogous to that related to the robustness of entanglement [47]. In such approach, we start by considering a given assemblage $\hat{\sigma}_{a|x}$, and then finding out another assemblage $\hat{\theta}_{a|x}$ that we need to add to $\hat{\sigma}_{a|x}$ for it to become an assemblage of local hidden state model $\hat{\sigma}^{LHS}_{a|x}$ fulfilling the following relation [44]

$$\hat{\sigma}^{LHS}_{a|x} = \frac{\hat{\sigma}_{a|x} + \mu\hat{\theta}_{a|x}}{1+\mu} \quad (\mu \geq 0), \tag{1.36}$$

where $\hat{\theta}_{a|x}$ also has to fulfill conditions

$$\sum_a \hat{\theta}_{a|x} = \sum_a \hat{\theta}_{a|x'} \quad \forall x, x', \tag{1.37}$$

and

$$Tr \sum_a \hat{\theta}_{a|x} = 1 \quad \forall x, \quad \hat{\theta}_{a|x} \geq 0 \quad \forall a, x. \tag{1.38}$$

When $\mu = 0$, assemblage $\hat{\sigma}_{a|x}$ becomes that corresponding to local hidden state $\hat{\sigma}_{a|x}^{LHS}$. The greater value μ takes, the more distinct demonstration of steering assemblage $\hat{\sigma}_{a|x}$ shows. Similarly to the case of steering weight, this also allows us to consider a steering quantifier called *robustness of steering*. Such a kind of quantity can be determined by finding the minimal value of μ over all possible decompositions of $\hat{\sigma}_{a|x}$ satisfying (1.36) as follows

$$SR\left(\hat{\sigma}_{a|x}\right) = \min_{\hat{\sigma}_{a|x}} \left(\mu\right). \tag{1.39}$$

The accuracy of the quantum steering quantification by using the steering weight and the robustness was proved in [48] where the steering monotones were defined. In that article, the authors also considered the relative entropy as a steering quantifier. The approach presented there is based on the quantum von Neumann relative entropy between two density matrices $\hat{\varrho}$ and $\hat{\varrho}'$ as

$$S_Q\left(\hat{\varrho}\,|\hat{\varrho}'\right) = Tr\left(\hat{\varrho}\log\left(\frac{\hat{\varrho}}{\hat{\varrho}'}\right)\right), \tag{1.40}$$

and classical relative entropy for any two probability distributions p and p' corresponding to measurements of observable x in the form

$$S_C\left(p\,|p'\right) = \sum_x \left(p(x)\log\left(\frac{p(x)}{p'(x)}\right)\right). \tag{1.41}$$

Next, we assume that Alice and Bob share a bipartite system. Alice applies a set of classical measurements $\{x\}$ to get a set of outcomes $\{a\}$. The probability corresponding to each measurement is $p(a,x)$. Meanwhile, Bob can apply a quantum measurements to his party. After Alice's measurement, the state of the subsystem on the Bob's side can be a combination of elements of an assemblage $\{\hat{\sigma}_{a|x}(x)\}$ as $\hat{\rho}^B = \sum_a \hat{\sigma}_{x|a}$. The element $\hat{\sigma}_{a|x}(x)$ can be written as follows:

$$\hat{\sigma}_{a|x} = \sum_a p(a,x)\hat{\varsigma}_a, \tag{1.42}$$

where $\{\hat{\varsigma}_a\}$ is an orthonormal basis of an auxiliary Hilbert space on the Alice's side, corresponding to her measurement outcome a. Assuming that $\{\hat{\sigma}_{a|x}^{LHS}\}$ is the assemblage in the local hidden state model that fulfills (1.29), and its elements can be represented as

$$\hat{\sigma}_{a|x}^{LHS} = \sum_\lambda p\left(\lambda\right) p^{LHS}(a,x)\hat{\varsigma}_\lambda, \tag{1.43}$$

where $p\left(\lambda\right)$ is probability corresponding to a hidden state $\hat{\varsigma}_\lambda$ for a hidden variable λ, $p^{LHS}(a,x)$ is the probability corresponding to the measurement of observable x to get outcome a (if Alice makes that measurement in the scenario of local hidden state model). The distinguishability between $\hat{\sigma}_{a|x}$ and $\hat{\sigma}_{a|x}^{LHS}$ comes from two parts. The first one is the distinguishability between two classical objects $p(a,x)$ and $p^{LHS}(a,x)$. The second

one is the distinguishability between quantum objects $\hat{\varsigma}_a$ and $\hat{\varsigma}_\lambda$ weighted by $p(\lambda)$ and averaged over all values of a. Thus, we can write the von Neumann relative entropy between $\hat{\sigma}_{a|x}$ and $\hat{\sigma}_{a|x}^{LHS}$ as

$$S_Q\left(\sigma_{a|x}(x)\left|\sigma_{a|x}^{LHS}(x)\right.\right) = S_C\left(p(x)\left|p^{LHS}(x)\right.\right) + \sum_a p(\lambda) S_Q\left(\varsigma_a\left|\varsigma_\lambda\right.\right), \tag{1.44}$$

where $p(x)$ and $p^{LHS}(x)$, respectively, are the distribution over all a that are taken from $p(a,x)$ and $p^{LHS}(a,x)$ when x is fixed. As a result, the assemblage relative entropy of $\hat{\sigma}_{a|x}(x)$ respect to $\hat{\sigma}_{a|x}^{LHS}(x)$ can be written as follows [48]

$$S_A\left(\hat{\sigma}_{a|x}(x)\left|\hat{\sigma}_{a|x}^{LHS}(x)\right.\right) = \max_{P(x,b),\left\{\hat{M}_b\right\}}(X), \tag{1.45}$$

where

$$X = \left[S_C\left(P_B(b)\left|P_B{}'(b)\right.\right) + \sum_{x,b} P(x,b) P_B(b) S_Q\left(\frac{\hat{\mathbb{I}}\otimes\hat{M}_b\hat{\sigma}_{a|x}}{P_B(b)}\left|\frac{\hat{\mathbb{I}}\otimes\hat{M}_b\hat{\sigma}^{LHS}{}_{a|x}}{P_B{}'(b)}\right.\right)\right], \tag{1.46}$$

$\hat{M}_b$ is the measurement operator acting on the subsystem on Bob's side to get outcomes b that fulfill $\sum\limits_b \hat{M}_b = \hat{\mathbb{I}}$. $P(x,b)$ is distribution of conditional probability corresponding to x when the value of b is given, $P_B(b)$ and $P_B{}'(b)$ and takes the following forms

$$P_B(b) = Tr\left(\hat{\mathbb{I}}\otimes\hat{M}_b\hat{\sigma}_{a|x}(x)\right), P_B{}'(b) = Tr\left(\hat{\mathbb{I}}\otimes\hat{M}_b\hat{\sigma}_{a|x}^{LHS}(x)\right). \tag{1.47}$$

The greater is the value of $S_A\left(\sigma_{a|x}(x)\left|\sigma_{a|x}^{LHS}(x)\right.\right)$, the difference between the values of $\hat{\sigma}_{a|x}$ $\hat{\sigma}_{a|x}^{LHS}$ becomes more and more pronounced. By the definition (1.45), we can finally define the relative entropy of steering SE of an assemblage $\{\hat{\sigma}_{a|x}\}$ respect to assemblage $\{\hat{\sigma}_{a|x}^{LHS}\}$ as

$$SE(\hat{\sigma}_{a|x}) = \min_{\hat{\sigma}_{a|x}^{LHS}} S_A\left(\hat{\sigma}_{a|x}\left|\hat{\sigma}_{a|x}^{LHS}\right.\right), \tag{1.48}$$

where the minimum is taken over all possible assemblages $\hat{\sigma}_{a|x}^{LHS}$ corresponding to local hidden state model. The greater value of $SE(\hat{\sigma}_{a|x})$, the better demonstration of steering assemblage $\{\hat{\sigma}_{a|x}\}$ shows.

1.3 Bell non-locality

In the interpretation of the local theory, each influence on an object will only have an immediate effect on the objects surrounding it. This is related to a concept called "spooky action at a distance" (that term was used for the first time in the inthea letter to Max Born written by Albert Einstein on 3 March 1947) according to which an action

at one point can affect another point in space, and an interaction propagation period is required. In addition, the influence must be propagated through a space between two points at a speed not exceeding the speed of light in a vacuum. However, in 1935, A. Einstein, B. Podolsky, and N. Rosen formulated the EPR paradox which states that quantum mechanics can be non-local [40]. They showed that it is possible to an entangled state in a system of two separate particles. Then, making a measurement on the first particle will simultaneously cause a collapse of the wave function on the second. However, this violation also can not be used in the propagation of quantum information beyond the limit of the speed of light in a vacuum because the collapse of wave function is still a statistical nature. Experimental results of A. Aspect *et.al* in 1982 reported the first evidence of Bell non-locality [49]. Thereafter, practical evidence continued to be reported. In 2015, three different experiments were performed by three research groups by B. Hensen [50], L. K. Shalm [51] and M. Giustina [52] and showed the clearest evidence of Bell non-locality.

1.3.1 Definition of Bell non-locality

Similar to the way to get the definition of quantum entanglement and quantum steering, we will define Bell non-locality by introducing the concept of Bell locality. Bell locality states that, in a system, the process acting in each subsystem, generates the outcome that does not bring into account the input of the other subsystems. So, to formalize Bell locality, let us start by the simplest case of a two-particle system held by Alice and Bob sharing the state $\hat{\rho}^{AB}$. They perform measurements characterized by the measurement sets x and y respectively for the particles held by them. To do that, they can apply measurement operators $\hat{M}_{a|x}$ and $\hat{M}_{b|y}$ acting on the state $\hat{\rho}^{AB}$ to obtain the expected outputs of a and b with the probabilities $p\left(a|\, x, \lambda\right)$ and $p\left(b|\, y, \lambda\right)$, respectively. Such description comes from the interpretation of the local hidden variable model (LHV) in which each hidden variable occurs with probability $p(\lambda)$. The joint probability for obtained outcomes a and b can be calculated as

$$p\left(a, b|\, x, y\right) = \sum_{\lambda} p\left(\lambda\right) p\left(a\,|x, \lambda\right) p\left(b\,|y, \lambda\right), \tag{1.49}$$

where $p\left(\lambda\right)$ is the probability distribution that shows us how often a concrete process in which λ is used. The state of a system will be Bell locality if there exist a local hidden variable assemblage $\{p\left(\lambda\right), \lambda\}$, in which the statistics (1.49) can be written for arbitrary x and y measurements. In the opposite case, the state of the system exhibits Bell non-locality.

In the steering scenario, the measurement on the Bob's side corresponds to the observable quantity that we expect, and Bob's response function can be derived from the rules of quantum mechanics concerning measurements. In consequence, after Alice's measurement, the state of the particle that Bob holds is $\hat{\sigma}_{a|x} = \sum_{\lambda} p\left(\lambda\right) p\left(a|\, x, \lambda\right) \hat{\varsigma}_{\lambda}$ for each

outcome a of Alice's measurement. Therefore, after Alice got outcome a for her measurement, if Bob does a measurement on his particle, the joint probability corresponding to getting outcome b is

$$p\left(a,b\left|x,y\right.\right)=Tr\left(\hat{M}_{b|y}\hat{\sigma}_{a|x}\right)=\sum_{\lambda}p\left(\lambda\right)p\left(a\left|x\right.,\lambda\right)Tr\left(\hat{M}_{b|y}\hat{\varsigma}_{\lambda}\right). \tag{1.50}$$

The state of a system will be unsteerable if there exist a local hidden state assemblage $\{p\left(\lambda\right),\hat{\varsigma}_{\lambda}\}$ by that the statistics (1.50) can be written for an arbitrary measurement x. In the other cases, the state of the system is steerable.

Now, we assume that the measurements in both Bob's and Alice's sides completely correspond to the observable quantity we expected, and they can be derived from the measurement's rule of quantum mechanics, $p\left(a\left|x\right.\right)=Tr\left(\hat{M}_{a|x}\hat{\sigma}^{A}\right)$ and $p\left(b\left|y\right.\right)=Tr\left(\hat{M}_{b|y}\hat{\sigma}^{B}\right)$, where $\hat{\sigma}^{A}$ and $\hat{\sigma}^{B}$ are the states of the particles that Alice and Bob hold, respectively. Consequently, the joint probability of distributed measurements is as follows

$$p\left(a,b\left|x,y\right.\right)=\sum_{i}p_{i}Tr\left(\hat{M}_{a|x}\hat{\sigma}_{i}^{A}\right)Tr\left(\hat{M}_{b|y}\hat{\sigma}_{i}^{B}\right), \tag{1.51}$$

where p_i are distributed probabilities corresponding to the measurements. In this scenario, the state of a system will be separable if the probability (1.51) can be defined for arbitrary measurements x and y. In the other cases, the state of the system will be entangled. We can see from (1.78), (1.79) and (1.51) that quantum steering is a level of quantum correlation that is between quantum entanglement and Bell non-locality. In consequence, any state that is Bell non-local will be steerable, any steerable state will be entangled. However, in the opposite direction of that conclusion, there will be entangled states that can not be used for steering, and there will be steerable states that are not non-local in the Bell sense.

Let us go to a general case in which we consider a system of N parties. For such the situation, we apply the measurement operators $\left\{\hat{M}_{a_i|x_i}\right\}$ corresponding to measurements $\{x_i\}$ to get the results $\{a_i\}$ $(i=1,2,...,N)$ respectively. The probability for joint measurements of all parties can be written as

$$p\left(a_1,a_2,...,a_N\left|x_1,x_2,...,a_N\right.\right)=\sum_{\lambda}\left(p_{\lambda}\prod_{i=1}^{N}p\left(a_i\left|x_i,\lambda\right.\right)\right), \tag{1.52}$$

where $p\left(a_i\left|x_i,\lambda\right.\right)$ is the response function corresponding to the measurement on the i-th particle, $p(\lambda)$ is distributed probability corresponding to the local hidden variable λ.

Now, we assume that only the measurement results of T first parties do not correspond to the observable quantity we expected. It means that such T first parties are trusted. The measurements on those parties follow the measurement rules of quantum mechanics by tracing out after applying measurement operators on the state of those particles. The

results of measurement on the other parties do not correspond to the observable quantity we expected. It means that they are not trusted. In this case, the probability for joint measurements can be rewritten as follows

$$p\left(a_1, a_2, ..., a_N \left| x_1, x_2, ..., a_N \right.\right) = \sum_{\lambda} \left(p_\lambda \prod_{i=1}^{T} Tr\left(\hat{M}_{a_i|x_i} \hat{\varsigma}_i\right) \prod_{j=T+1}^{N} p\left(a_j \left| x_j, \lambda \right.\right) \right), \quad (1.53)$$

where $p\left(a_j \left| x_j, \lambda \right.\right)$ is the contribution of untrusted party j, $\hat{\varsigma}_i$ is the state of trusted party i. Such attempt is called local causal (LC) model. Let LC(T, N) denotes (1.53) when only T from N parties are trusted. The violation LC(T, N) with the different values of T indicate different quantum correlations. The violation LC$(0, N)$ indicates Bell non-locality while the violation LC(N, N) implies a standard entanglement test. The violation LC$(1, N)$ indicates the case of steering while the violation LC(T, N) with $1 < T < N$ associates to the entanglement in the presence of $N - T$ untrusted parties, but uncertainly shows quantum steering or Bell nonlocality. Fig.1.1 shows the relations

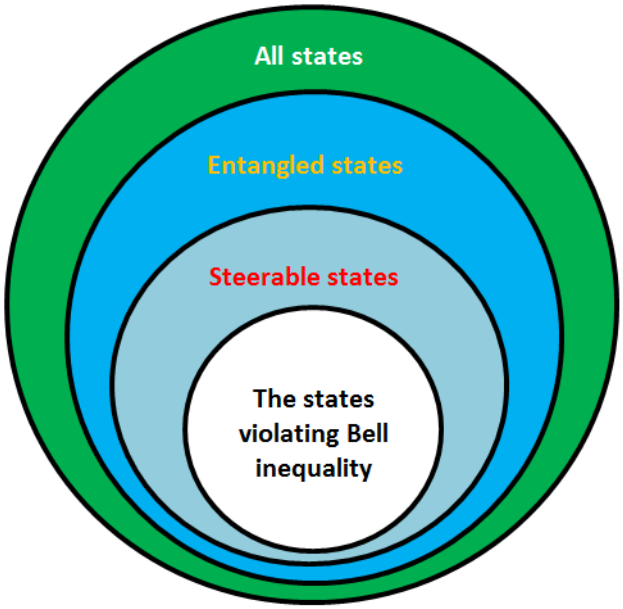

Fig. 1.1: The relations among Bell inequality violation, quantum steering, and entanglement

among groups of quantum states with respect to the level of non-local quantum correlation. In that relation, the set of all quantum states is convex. Entangled states are a special group of steerable states, and steerable state forms a special group of the states that violate Bell inequality.

1.3.2 Quantification of Bell non-locality

To quantify Bell non-locality, we will start from finding the form of multipartite non-locality inequalities. To do that, we consider the following complex function [53, 54]

$$F_j^{\pm} = X_j \pm iY_j, \tag{1.54}$$

where X_j and Y_j are measurement outcomes of each party j corresponding to measurement operators $\hat{X}_j$ and $\hat{Y}_j$. For each value of local hidden variable λ, we get

$$\left\langle F_j^{\pm} \right\rangle_\lambda = \langle X_j \rangle_\lambda \pm i \langle Y_j \rangle_\lambda, \tag{1.55}$$

and

$$\left\langle F_j^{s_j} \right\rangle_\lambda^2 = \langle X_j \rangle_\lambda^2 + \langle Y_j \rangle_\lambda^2, \tag{1.56}$$

where $\langle X_j \rangle_\lambda = \sum_{X_j} p\left(X_j \left|\lambda\right.\right) X_j$ and $\langle Y_j \rangle_\lambda = \sum_{Y_j} p\left(Y_j \left|\lambda\right.\right) Y_j$. It is necessary to point out that for the measurement results of untrusted parties, $p\left(X_j \left|\lambda\right.\right)$ and $p\left(Y_j \left|\lambda\right.\right)$ will be replaced by response functions $p_R\left(X_j \left|\lambda\right.\right)$ and $p_R\left(Y_j \left|\lambda\right.\right)$, respectively. By using such a complex function, for each equation (1.52), we have

$$\left\langle \prod_{j=1}^{N} F_j^{s_j} \right\rangle = \sum_{\lambda} \left(\prod_{j=1}^{N} \left\langle F_j^{s_j} \right\rangle p\left(\lambda\right) \right), \tag{1.57}$$

where $s_j \in \{+, -\}$ shows the sign of the function $F_j^{s_j}$, $p(\lambda)$ is distributed probability corresponding to local hidden variable λ. Because the standard variance for every function $F_j^{s_j}$ is always positive, we can write

$$\left(\Delta F_j^{s_j}\right)^2 = \left\langle \left(F_j^{s_j}\right)^2 \right\rangle - \left\langle F_j^{s_j} \right\rangle^2 > 0. \tag{1.58}$$

Therefore, we have $\left\langle F_j^{s_j} \right\rangle^2 < \left\langle \left(F_j^{s_j}\right)^2 \right\rangle$ and consequent inequality

$$\left| \left\langle \prod_{j=1}^{N} F_j^{s_j} \right\rangle \right|^2 \leq \left\langle \prod_{j=1}^{N} \left(F_j^{s_j}\right)^2 \right\rangle = \left\langle \prod_{j=1}^{T} \left(F_j^{s_j}\right)^2 \prod_{j=T+1}^{N} \left(F_j^{s_j}\right)^2 \right\rangle. \tag{1.59}$$

For the measurement results of trusted parties T, we have to restrict ourselves by using the following uncertainty relation

$$\left(\Delta X_j\right)^2 + \left(\Delta Y_j\right)^2 \geq Z_j \tag{1.60}$$

where Z_j depends on the choice of measurement operators giving measurement outcomes X_j and Y_j. We can also rewrite (1.60) in more detailed form as

$$\left\langle X_j^2 \right\rangle - \left\langle X_j \right\rangle^2 + \left\langle Y_j^2 \right\rangle - \left\langle Y_j \right\rangle^2 \geq Z_j. \tag{1.61}$$

After some simple transformations, we achieve

$$\langle X_j\rangle^2 + \langle Y_j\rangle^2 \leq \langle X_j^2\rangle + \langle Y_j^2\rangle - Z_j. \tag{1.62}$$

From (1.56) and (1.62), we can rewrite the contribution of trusted parties in (1.59) as:

$$\left\langle \prod_{j=1}^{T} \left(F_j^{s_j}\right)^2 \right\rangle = \prod_{j=1}^{T} \left(\langle X_j\rangle^2 + \langle Y_j\rangle^2\right) \leq \prod_{j=1}^{T} \left(\langle X_j^2\rangle + \langle Y_j^2\rangle - Z_j\right). \tag{1.63}$$

Consequently, non-locality inequalities (1.59) become

$$\left| \left\langle \prod_{j=1}^{N} \left(F_j^{s_j}\right) \right\rangle \right|^2 \leq \left\langle \prod_{j=1}^{T} \left(X_j^2 + Y_j^2 - Z_j\right) \prod_{j=T+1}^{N} \left(X_j^2 + Y_j^2\right) \right\rangle. \tag{1.64}$$

No,w we can determine the non-locality inequalities by considering canonical operators

$$X_j = \hat{q}_j = \frac{\hat{a}_j^\dagger + \hat{a}_j}{\sqrt{2}}, \tag{1.65}$$

and

$$Y_j = \hat{p}_j = i\frac{\hat{a}_j^\dagger - \hat{a}_j}{\sqrt{2}}, \tag{1.66}$$

where $\hat{a}_j^\dagger$ and $\hat{a}_j$ are bosonic creation and annihilation operators of the party j, respectively. As a result, we have

$$F_j^+ = \sqrt{2}\hat{a}_j^\dagger, \tag{1.67}$$

$$F_j^- = \sqrt{2}\hat{a}_j, \tag{1.68}$$

and

$$X_j^2 + Y_j^2 = \frac{1}{2}\left[\left(\hat{a}_j^\dagger + \hat{a}_j\right)^2 + \left(\hat{a}_j^\dagger - \hat{a}_j\right)^2\right] = \hat{a}_j^\dagger\hat{a}_j + \hat{a}_j\hat{a}_j^\dagger. \tag{1.69}$$

As the bosonic creation and annihilation operators have to obey the commutation rule $\left[\hat{a}_j, \hat{a}_k^\dagger\right] = \delta_{jk}$, we have $\hat{a}_j\hat{a}_j^\dagger = \hat{a}_j^\dagger\hat{a}_j + 1$ and the above relation becomes

$$X_j^2 + Y_j^2 = 2\hat{a}_j^\dagger\hat{a}_j + 1 = \hat{n}_j + 1, \tag{1.70}$$

where $\hat{n}_j$ is number operator of party j.

For the trusted parties, we apply the procedure proposed in [54] and the commutator $[X_j, Y_j] = i$ what leads to the relation $(\Delta X_j)^2 + (\Delta Y_j)^2 \geq 1$. It means that $Z_j = 1$ and we can write non-locality inequalities (1.64) as

$$\left| \left\langle \prod_{j=1}^{N} \left(F_j^{s_j}\right) \right\rangle \right|^2 \leq \left\langle \prod_{j=1}^{T} \left(X_j^2 + Y_j^2 - 1\right) \prod_{j=T+1}^{N} \left(X_j^2 + Y_j^2\right) \right\rangle. \tag{1.71}$$

After substituting (1.67), (1.68) and (1.69) into (1.71), we achieve the new form of non-locality inequalities:

$$\left|\left\langle \prod_{j=1}^{N} a_j^{s_j} \right\rangle\right|^2 \leq \left\langle \prod_{j=1}^{T} \left(\hat{a}_j^\dagger \hat{a}_j\right) \prod_{j=T+1}^{N} \left(\hat{a}_j^\dagger \hat{a}_j + \frac{1}{2}\right) \right\rangle, \tag{1.72}$$

where $\hat{a}_j^+ = \hat{a}_j^\dagger$ and $\hat{a}_j^- = \hat{a}_j$.

When $T = 0$, all the measurement results are not trusted, and thus, non-locality inequalities for Bell non-locality takes the form

$$\left|\left\langle \prod_{j=1}^{N} a_j^{s_j} \right\rangle\right|^2 \leq \left\langle \prod_{j=1}^{N} \left(\hat{a}_j^\dagger \hat{a}_j + \frac{1}{2}\right) \right\rangle. \tag{1.73}$$

The violation of this non-locality inequalities will implies the Bell's non-locality correlation.

When $T = 1$, only the measurement of the first party is trusted. For such the case non-locality inequalities becomes

$$\left|\left\langle \prod_{j=1}^{N} a_j^{s_j} \right\rangle\right|^2 \leq \left\langle \hat{a}_1^\dagger \hat{a}_1 \prod_{j=2}^{N} \left(\hat{a}_j^\dagger \hat{a}_j + \frac{1}{2}\right) \right\rangle. \tag{1.74}$$

If such inequality is violated, we have quantum steering scenario.

Lastly, for the case when $T = N$, non-locality inequalities (1.72) takes the form

$$\left|\left\langle \prod_{j=1}^{N} a_j^{s_j} \right\rangle\right|^2 \leq \left\langle \prod_{j=1}^{N} \left(\hat{a}_j^\dagger \hat{a}_j\right) \right\rangle. \tag{1.75}$$

If such non-locality inequalities is not satisfied, a multi-mode entanglement scenario that has been shown by Hillery and Zubairy [55] is present.

If we limit the system to a bipartite system, condition determining the existence of bipartite quantum steering becomes

$$\left\langle \hat{a}_j \hat{a}_k^\dagger \right\rangle \left\langle \hat{a}_j^\dagger \hat{a}_k \right\rangle > \left\langle \hat{a}_j^\dagger \hat{a}_j \left(\hat{a}_k^\dagger \hat{a}_k + \frac{1}{2}\right) \right\rangle. \tag{1.76}$$

In such the case, we can define a quantity called steering parameter that can be expressed in the following form:

$$S_{jk} = \left|\left\langle \hat{a}_j \hat{a}_k^\dagger \right\rangle\right|^2 - \left\langle \hat{a}_j \hat{a}_j^\dagger \left(\hat{a}_k \hat{a}_k^\dagger + \frac{1}{2}\right) \right\rangle = \left\langle \hat{a}_j \hat{a}_k^\dagger \right\rangle \left\langle \hat{a}_j^\dagger \hat{a}_k \right\rangle - \left\langle \hat{a}_j \hat{a}_j^\dagger \left(\hat{a}_k \hat{a}_k^\dagger + \frac{1}{2}\right) \right\rangle. \tag{1.77}$$

The value of such the quantity directly shows the possibility of the existence of a steerable state that shares two modes. In such sense, we can say that mode k can steer mode j when the value of S_{jk} is positive. For other cases, mode k can not steer mode j. The symmetric steering appears when both S_{jk} and S_{kj} take the same positive values. If S_{jk} and S_{kj} take different positive values, the steering between modes j and k is asymmetric. For the case in which only one of them is greater than zero, we achieve a one-way steering between j and k modes. Similarly to the steering parameter S, we also can consider a quantity that quantifies Bell's non-locality B called the non-locality parameter. From (1.73), we can define B as:

$$B = \left| \left\langle \prod_{j=1}^{N} a_j^{s_j} \right\rangle \right|^2 - \left\langle \prod_{j=1}^{N} \left(\hat{a}_j^\dagger \hat{a}_j + \frac{1}{2} \right) \right\rangle . \tag{1.78}$$

For the case of bipartite system, that parameter B becomes

$$B_{jk} = \left\langle \hat{a}_j \hat{a}_k^\dagger \right\rangle \left\langle \hat{a}_j^\dagger \hat{a}_k \right\rangle - \left\langle \left(\hat{a}_j \hat{a}_j^\dagger + \frac{1}{2} \right) \left(\hat{a}_k \hat{a}_k^\dagger + \frac{1}{2} \right) \right\rangle . \tag{1.79}$$

If the value of B_{jk} is negative, non-locality inequalities is not violated. This is related to the local scenario. In the opposite case, when the value of B_{jk} is positive, non-locality inequalities will be violated and be corresponding to the non-local scenario.

1.4 Correlation functions for electromagnetic field

In nature, there are a lot of optical phenomena that are related to coherence, especially interference, and radiation of fluctuating sources [56,57]. To investigate these effects, we can use one of the most powerful theoretical tools called correlation functions that are mentioned in well-known monographs [58–61]. In the last years of the previous century, correlation functions were considered for quantitative description of spatial statistics not only in one-mode system [62], but also in multi-mode ones [63]. The correlation functions provide interesting information concerning optical systems. The first-order correlation function describes the correlations of amplitudes while the second-order correlation function correspond to correlations between intensities of electromagnetic field. The values of correlation functions can give us the information concerning the appearance of anti-bunching effect [64]. Such phenomenon is a typical example of the effects that occurs in non-classical systems. Besides that, the correlation functions help us detect the appearance of another phenomenon called *photon blockade*. This phenomenon attracted deeply attention of many physicists [65–69].

In 1954, the experiment concerning correlation function of the intensities was firstly done by Hanbury Brown and Twiss who analyzed the measurement of the correlation functions of the light coming from the telescope to determine the radius of stars [70]. After that, there are other experimental problems that have been studied, such as characterization of photons [71, 72], quantum imaging for intensity correlated photons [73],

ghost imaging with the use of the variance of the different photons [74,75] and measurements of coherent and chaotic states by a time-multiplexed detection [76]. Besides the first- and the second-order correlation functions, the higher order correlation functions have also been discussed by Chopra and Mandel who used the third order correlation function to characterize laser beams [77] and by Ivanova [78] who considered normalized intensity correlation functions of fourth order. In this section, we will concentrate on the first- and the second-order correlation functions as those most commonly considered in the literature

1.4.1 The first-order correlation function

In quantum optics, the first-order correlation function is considered for quantifying the coherence between electrical fields. The idea of this function came from the calculation of the intensity at a point M due to the linear interference phenomenon. The most common example is the interference appearing in double slit experiment. For such the case, we assume that the observation point M is separated from slits by distances s_1 and s_2, and the electrical fields at the positions of slits are $\vec{E}_1(\vec{x}_1, t)$ and $\vec{E}_2(\vec{x}_2, t)$. As a result of interference phenomenon, the electrical field at the given point M can be calculated as a superposition of two electrical fields coming from the two slits

$$\vec{E}(\vec{x}, t) = \vec{E}_1(\vec{x}_1, t) + \vec{E}_2(\vec{x}_2, t + \tau), \tag{1.80}$$

where time delay $\tau = (s_1 - s_2)/c$, and c is the speed of electrical field propagation. Thus, the intensity of the electric field at the given point M is

$$\begin{aligned} I(\vec{x}, t) = \left\langle \vec{E}^*(\vec{x}, t)\vec{E}(\vec{x}, t) \right\rangle &= \left\langle \vec{E}_1^*(\vec{x}_1, t)\vec{E}_1(\vec{x}_1, t) \right\rangle + \left\langle \vec{E}_2^*(\vec{x}_2, t + \tau)\vec{E}_2(\vec{x}_2, t + \tau) \right\rangle \\ &+ \left[\left\langle \vec{E}_1^*(\vec{x}_1, t)\vec{E}_2(\vec{x}_2, t + \tau) \right\rangle + \left\langle \vec{E}_1(\vec{x}_1, t)\vec{E}_2^*(\vec{x}_2, t + \tau) \right\rangle \right]. \end{aligned} \tag{1.81}$$

Because $\left\langle \vec{E}_1^*(\vec{x}_1, t)\vec{E}_2(\vec{x}_2, t + \tau) \right\rangle$ and $\left\langle \vec{E}_1(\vec{x}_1, t)\vec{E}_2^*(\vec{x}_2, t + \tau) \right\rangle$ are complex conjugate of each other, we can rewrite (1.81) as follows

$$I(\vec{x}, t) = I_1(\vec{x}_1, t) + I_2(\vec{x}_2, t + \tau) + 2\,\mathrm{Re}\left[\left\langle \vec{E}_1^*(\vec{x}_1, t)\vec{E}_2(\vec{x}_2, t + \tau) \right\rangle \right]. \tag{1.82}$$

In (1.82), the first two terms represent the intensities produced by two slits. They do not make any effect on the visibility of interference fringes. In contrast, the contribution of the third term will correspond to the interference effects. It involves the first-order coherence function of electrical fields at the times t and $t + \tau$ that is defined as [58]

$$\gamma_{12}^{(1)}(\vec{x}_1, \vec{x}_2, \tau) = \left\langle \vec{E}_1^*(\vec{x}_1, t)\vec{E}_2(\vec{x}_2, t + \tau) \right\rangle = \frac{1}{T} \int_T \vec{E}_1^*(\vec{x}_1, t)\vec{E}_2(\vec{x}_2, t + \tau)dt, \tag{1.83}$$

where T is the period of electrical field oscillations. From the statistical point of view, the degree of temporal coherence can be determined as the normalized form of the first-order coherence function

$$g_{12}^{(1)}(\vec{x}_1, \vec{x}_2, \tau) = \frac{\left\langle \vec{E}_1^*(\vec{x}_1, t)\vec{E}_2(\vec{x}_2, t+\tau) \right\rangle}{\sqrt{\left\langle \vec{E}_1^*(\vec{x}_1, t)\vec{E}_1(\vec{x}_1, t) \right\rangle \left\langle \vec{E}_2^*(\vec{x}_2, t+\tau)\vec{E}_2(\vec{x}_2, t+\tau) \right\rangle}}. \tag{1.84}$$

By considering such a function, equation (1.82) can be rewritten as follows

$$I(\vec{x}, t) = I_1(\vec{x}_1, t) + I_2(\vec{x}_2, t+\tau) + 2\sqrt{I_1 I_2}\,\mathrm{Re}\left[g_{12}^{(1)}(\vec{x}_1, \vec{x}_2, \tau)\right]. \tag{1.85}$$

Because $g_{12}^{(1)}(\vec{x}_1, \vec{x}_2, \tau)$ is a complex function, we can express it in the form

$$g_{12}^{(1)}(\vec{x}_1, \vec{x}_2, \tau) = \left|g_{12}^{(1)}(\vec{x}_1, \vec{x}_2, \tau)\right| exp(i\Phi_{12}) = G_{12}^{(1)}(\vec{x}_1, \vec{x}_2, \tau) exp(i\Phi_{12}), \tag{1.86}$$

where Φ_{12} is the phase factor, and the function

$$G^{(1)}(\vec{x}_1, \vec{x}_2, \tau) = \frac{\left|\left\langle \vec{E}^*(\vec{x}_1, t)\vec{E}(\vec{x}_2, t+\tau) \right\rangle\right|}{\sqrt{\left\langle \left|\vec{E}(\vec{x}_1, t)\right|^2 \right\rangle \left\langle \left|\vec{E}(\vec{x}_2, t+\tau)\right|^2 \right\rangle}} \tag{1.87}$$

can be seemed as the first-order correlation function. Thus, the equation 1.85 takes the form

$$I(\vec{x}, t) = I_1(\vec{x}_1, t) + I_2(\vec{x}_2, t+\tau) + 2\sqrt{I_1 I_2} G_{12}^{(1)}(\vec{x}_1, \vec{x}_2, \tau) cos(\Phi_{12}). \tag{1.88}$$

The correlation function defined in (1.87) shows us the correlation between two fields at two different times t and $t+\tau$. It is the cross-correlation function. The value of $G^{(1)}(\vec{x}_1, \vec{x}_2, \tau)$ indicates the types of coherence, that are

$$\begin{aligned} &G^{(1)}(\vec{x}_1, \vec{x}_2, \tau) = 1 && \text{full coherence,} \\ &0 < G^{(1)}(\vec{x}_1, \vec{x}_2, \tau) < 1 && \text{partial coherence,} \\ &G^{(1)}(\vec{x}_1, \vec{x}_2, \tau) = 0 && \text{the lack of coherence.} \end{aligned} \tag{1.89}$$

For a stationary light beam, to express the correlation between two fields at the same point, but at different times, we can use the first-order auto-correlation function that is defined as

$$G^{(1)}(\tau) = \frac{\left|\left\langle \vec{E}^*(t)\vec{E}(t+\tau) \right\rangle\right|}{\left\langle \vec{E}^*(t)\vec{E}(t) \right\rangle}. \tag{1.90}$$

We can easily see that $\left\langle \vec{E}_1^*(t)\vec{E}_2(t-\tau)\right\rangle = \left\langle \vec{E}_1^*(t+\tau)\vec{E}_2(t)\right\rangle = \left\langle \vec{E}_2^*(t)\vec{E}_1(t+\tau)\right\rangle^*$. Therefore, from the definition (1.90), the first-order correlation function fulfills the following relation

$$G_{12}^{(1)}(-\tau) = G_{12}^{(1)}(\tau)^*. \tag{1.91}$$

The value of the first-order correlation function (1.90) shows us the coherence level of the light beam. If $G^{(1)}(\tau) = 1$, the light is fully coherent. If $G^{(1)}(\tau) = 0$, the light is completely not coherent. The light is partially coherent when $0 < G^{(1)}(\tau) < 1$. Besides that, we can say the value of the first-order correlation function depends on the value of time-delay τ. When that delay is equal to zero ($\tau = 0$), (1.90) shows that $G^{(1)}(0) = 1$. If the time-delay is much smaller than coherence time τ_c, it means $\tau << \tau_c$, the value of $G^{(1)}(\tau) \simeq 1$, and the light approximately remains fully coherent. If the time-delay is much greater than the coherence time τ_c, *i.e.* $\tau >> \tau_c$, the value of $G^{(1)}(\tau)$ tends to be zero. It means the light at two well separated points in space-time is incoherent.

The first-order correlation function is also related to a quantity called fringe visibility that is defined by Rayleigh as follows [79]

$$\nu = \frac{I_{max} - I_{min}}{I_{max} + I_{min}}. \tag{1.92}$$

This quantity corresponds to the contrast of the pattern in the interference experiment. From (1.88), when $cos\Phi_{12} = 1$, we get

$$\begin{aligned} I_{max} &= I_1 + I_2 + 2\sqrt{I_1 I_2}G^{(1)}(\vec{x}_1, \vec{x}_2, \tau), \\ I_{min} &= I_1 + I_2 - 2\sqrt{I_1 I_2}G^{(1)}(\vec{x}_1, \vec{x}_2, \tau). \end{aligned} \tag{1.93}$$

Substituting (1.93) into (1.92) gives us

$$\nu = \frac{2\sqrt{I_1 I_2}}{I_1 + I_2}G^{(1)}(\vec{x}_1, \vec{x}_2, \tau). \tag{1.94}$$

It is easy to see that, for the full coherence, the visibility for fringes in the interference experiment reaches its maximal value

$$\nu_{max} = \frac{2\sqrt{I_1 I_2}}{I_1 + I_2}. \tag{1.95}$$

For the case when we are dealing with a completely incoherent light, the visibility takes its minimal value that is equal to zero because of $G^{(1)}(\vec{x}_1, \vec{x}_2, \tau) = 0$.

We can convert the form of the first-order correlation function into its quantized form by representing electrical field vectors in terms of creation and annihilation operators. In such the way, the first-order cross-correlation function between two modes for the time delay τ can be written as

$$G_{12}^{(1)}(\tau) = \frac{\left|\left\langle \hat{a}_1^\dagger(t)\hat{a}_2(t+\tau)\right\rangle\right|}{\sqrt{\left\langle \hat{a}_1^\dagger(t)\hat{a}_1(t)\right\rangle \left\langle \hat{a}_2^\dagger(t+\tau)\hat{a}_2(t+\tau)\right\rangle}}, \tag{1.96}$$

where $\hat{a}_i^\dagger$ and $\hat{a}_i$ are creation and annihilation operators corresponding to mode i ($i = 1, 2$),respectively. They satisfy commutation relation

$$\left[\hat{a}_i, \hat{a}_j^\dagger\right] = \delta_{ij}. \tag{1.97}$$

When we discuss the auto-correlation function, the first-order correlation function will take the form

$$G^{(1)}(\tau) = \frac{\left|\left\langle \hat{a}^\dagger(t)\hat{a}(t+\tau\right\rangle\right|}{\sqrt{\langle \hat{a}^\dagger(t)\hat{a}(t)\rangle \langle \hat{a}^\dagger(t+\tau)\hat{a}(t+\tau)\rangle}}. \tag{1.98}$$

Such function shows the coherence between the electrical fields at the same position, but for two different times t and $t+\tau$.

1.4.2 The second-order correlation function

In the previous subsection, we considered the first-order correlation function as the degree of the temporal coherence between the electrical fields at two different points in space-time. In a similar fashion, we will continue to consider the second-order correlation function as a quantity that can quantify intensity fluctuation. The idea of this function came from the Brown-Twiss experiment in which the correlations of light intensities at two different points in space-time were measured. Let consider two different points $(\vec{x}_1, t)$ and $(\vec{x}_2, t+\tau)$ in space-time. For such the case, the classical second-order intensity correlation function can be written in the form [80]

$$G_{12}^{(2)}(\tau) = \frac{\langle I_1(t) I_1(t+\tau\rangle}{\langle I_1(t)\rangle \langle I_1(t+\tau\rangle} = \frac{\left\langle \vec{E}_1(\vec{x}_1, t)\vec{E}_2(\vec{x}_2, t+\tau)\vec{E}_2^*(\vec{x}_2, t+\tau)\vec{E}_1^*(\vec{x}_1, t)\right\rangle}{\left\langle \vec{E}_1^*(\vec{x}_1, t)\vec{E}_1(\vec{x}_1, t)\right\rangle \left\langle \vec{E}_2^*(\vec{x}_2, t+\tau)\vec{E}_2(\vec{x}_2, t+\tau)\right\rangle}. \tag{1.99}$$

Applying the second quantization formalism, we can transform classical quantities to their equivalent counterparts and rewrite electrical field vector $\hat{E}(t)$ in terms of the bosonic creation and annihilation operators as [81]

$$\begin{aligned} \hat{E}_k^*(t) &\sim \hat{a}_k \exp\left[-i\left(\omega_k t - \vec{k}\vec{x}_k\right)\right], \\ \hat{E}_k(t) &\sim \hat{a}_k^\dagger \exp\left[-i\left(\omega_k t - \vec{k}\vec{x}_k\right)\right]. \end{aligned} \tag{1.100}$$

Applying (1.100), the second-order-correlation function (1.99) can be rewritten as

$$G_{12}^{(2)}(\tau) = \frac{\left\langle \hat{a}_1^\dagger(t)\hat{a}_2^\dagger(t+\tau)\hat{a}_2(t+\tau)\hat{a}_1(t)\right\rangle}{\left\langle \hat{a}_1^\dagger(t)\hat{a}_1(t)\right\rangle \left\langle \hat{a}_2^\dagger(t+\tau)\hat{a}_2(t+\tau)\right\rangle}. \tag{1.101}$$

The value of $G_{12}^{(2)}(\tau)$ shows the probability of detecting a photon at a point $(\vec{x}_2, t+\tau)$ after detecting another photon at $(\vec{x}_1, t)$. For a quantized light the second-order auto-correlation function takes the form

$$G^{(2)}(\tau) = \frac{\langle I(t)I(t+\tau)\rangle}{\langle I(t)\rangle \langle I(t+\tau)\rangle} = \frac{\left\langle \hat{a}^\dagger(t)\hat{a}^\dagger(t+\tau)\hat{a}(t+\tau)\hat{a}(t)\right\rangle}{\langle \hat{a}^\dagger(t)\hat{a}(t)\rangle \langle \hat{a}^\dagger(t+\tau)\hat{a}(t+\tau)\rangle}. \tag{1.102}$$

The value of $G^{(2)}(\tau)$ in (1.102) gives the information concerning the probability of detection a photon at the time $t+\tau$ after detecting another photon at the time t at the same point. Speaking more generally, it describes the correlations between the number of simultaneously detected photons at the times t and $t+\tau$. When the time-delay $\tau \to 0$, $G^{(2)}(\tau)$ tends to be zero, the second-order auto-correlation function takes the following form

$$G_{12}^{(2)}(0) = \frac{\left\langle \hat{a}^\dagger(t)\hat{a}^\dagger(t)\hat{a}(t)\hat{a}(t)\right\rangle}{\langle \hat{a}^\dagger(t)\hat{a}(t)\rangle^2}. \tag{1.103}$$

By using the number photon operator $\hat{n} = \hat{a}^\dagger(t)\hat{a}(t)$ and the commutator $\left[\hat{a}, \hat{a}^\dagger\right] = 1$, we can rewrite (1.103) as

$$G^{(2)}(0) = \frac{\langle \hat{n}(\hat{n}-1)\rangle}{\langle \hat{n}\rangle^2} = \frac{\langle \hat{n}^2\rangle - \langle \hat{n}\rangle}{\langle \hat{n}\rangle^2} = \frac{\left\langle (\Delta\hat{n})^2\right\rangle + \langle \hat{n}\rangle^2 - \langle \hat{n}\rangle}{\langle \hat{n}\rangle^2}, \tag{1.104}$$

where the variance $\left\langle (\Delta\hat{n})^2\right\rangle = \langle \hat{n}^2\rangle - \langle \hat{n}\rangle^2$. The value of zero-time delay auto-correlation function shows the probability of detecting the second photon at the time of detecting the first photon. To be more precise, it tell us how often we can detect two photons at two times that are very close to each other. Such defined second-order auto-correlation function is an important measure of temporal coincidences of photons that can help to distinguish different states of light. For the coherent light (an ideal laser light, for instance) the number of photons is proportional to the intensity of the light that is constant over time, whereas, the variance of number of photons $\left\langle (\Delta\hat{n})^2\right\rangle = \langle \hat{n}\rangle$. As a result, $G^{(2)}(0) = G^{(2)}(\tau) = 1$. That means that the number of detected photons at the moments of time t and $t+\tau$ are uncorrelated for any τ. For a classical light (thermal or chaotic light) we can observe some intensity fluctuations. Therefore, events of detection tend to be closer to each other. For such cases, the value of the zero-time delay second-order auto-correlation function $G^{(2)}(0) > G^{(2)}(\tau) \geq 1$. That means that if the photon is detected at the time t, the probability of photon detection at times very close to t increases. For example, in the case of thermal light, the variance of photon number $\left\langle (\Delta\hat{n})^2\right\rangle = \langle \hat{n}\rangle^2 + \langle \hat{n}\rangle$. Substituting this result into (1.104) gives us $G^{(2)}(0) = 2$. Such a kind of light is called bunched light [60]. For the opposite situation, we can get $G^{(2)}(0) < 1$. For such the case, the mentioned probability of the second detection decreases. In other words, the detection of photon at time t reduces the probability of detecting another photon at times very close to time t. Such effect is called photon anti-bunching. Such a kind of light is called anti-bunched one, and is highly non-classical. For example, in the case of Fock-state, the variance of photon number $\left\langle (\Delta\hat{n})^2\right\rangle = 0$. As a result, $G^{(2)}(0) = 1 - 1/n < 1$ $(n \geq 1)$ [60]. Thus, for the light exhibiting anti-bunching,

we have $G^{(2)}(0) < G^{(2)}(\tau)$. So, it is seemed that the second-order correlation function is very important in characterization of the quantumness of the light states.

1.5 Summary

In this chapter, we have presented some basic concepts related to quantum correlations. First, we reviewed the difference between entangled quantum states and quantum separable states. Besides that, some ways of quantification of quantum entanglement were also presented. Among them, negativity is especially emphasized as an useful way to quantify quantum entanglement, which will be used in Chapters 3 and 4. Secondly, we gave an introduction to the quantum steering and Bell-nonlocality concepts. Similarly, as for the entanglement, we also discussed some quantifiers that can be used to quantify those two kinds of quantum correlations. Moreover, we have shown the relations among those three levels of quantum correlations. Finally, we have concentrated on the first- and second-order correlation functions that depict the coherence between electric fields and intensity fluctuations, respectively. Those concepts will be applied in the discussion presented in Chapter 3. The parameters quantifying quantum correlations were expressed as functions of the photon creation and annihilation operators, and will be used in numerical calculations, which results will be presented in Chapters 3 and 4.

In the next chapter, we shall present the basic ideas related to $\mathcal{PT}$-symmetric systems. The concepts of the parity and time-reversal operators, and the conditions for the existence of the unbroken $\mathcal{PT}$-symmetric phase will also be presented.

Chapter 2

$\mathcal{PT}$-symmetry – general ideas

2.1 History of $\mathcal{PT}$-symmetry research and exemplary applications

In the 20th century, the theory of quantum mechanics was proposed and improved to describe and explain the physical phenomena in reality that can not be done by classical physics. Such theory is based on a set of fundamental postulates. One of them concerns operators that characterize the actions over a physical state by giving another physical one. Some of those operators also characterize measurable quantities. As the measurable quantities are described by real parameters, the eigenvalues of the related operators also have to be real. Consequently, the Hamiltonian operator characterizing the energy of a system also has to be Hermitian. Such a point of view remained dominant until Bender *et al.* showed that some operators still have a spectrum of real eigenvalues, even when they are non-Hermitian ones [1, 24]. Consequently, we can find out some systems that, although described by non-Hermitian Hamiltonians, have real eigenvalues spectra. However, such a situation only happens when the Hamiltonian describing the system is invariant under the actions of space reflection $\mathcal{P}$ and time-reversal $\mathcal{T}$ operators. Mathematically speaking, such Hamiltonians have to commute with $\hat{P}\hat{T}$ operator:

$$\hat{H}\hat{P}\hat{T} = \hat{P}\hat{T}\hat{H}. \tag{2.1}$$

A system that is described by such a Hamiltonian is called $\mathcal{PT}$-symmetric one. That kind of system behaves as a system described by a Hermitian Hamiltonian and has real energy levels, even when it exchanges energy with the external environment. However, such behaviors are only shown when the system is in the unbroken $\mathcal{PT}$-symmetry phase. Such phase is separated from the broken one by an exceptional point, called phase-transition point.

More than two decades from the time when Bender's research results were published, there have been many confirmations for the existence of $\mathcal{PT}$-symmetry systems by reported experiments. For instance, in the field of electric systems, they can be those involving a finite superconducting wire subjected to an electric current [82], designed for a wireless power transfer [83], electronic circuits in an electronic dimer [84], or trimer [85]. At the microscopic scale one can mention semiconductor exciton-polariton condensate [86], superconducting resonators [87], microscopic power grids connecting

harmonic oscillators [88] and Cooper pairs in the superconducting weak link model [89]. In the optical area, one of the most studied $\mathcal{PT}$-symmetric systems are those of dual coupled waveguides. Studies are carried out comprehensively from theory building [90, 91], determination of the phase transitions [92, 93], the properties [94–96] and formation of solitons [97]. The above mentioned research were confirmed experimentally by observing the occurrence of phase transitions [98], spontaneous $\mathcal{PT}$-breaking and power oscillations violating [99], and evolution of the system from the unbroken $\mathcal{PT}$-symmetry phase to its broken counterpart [100–103]. Besides that, the nonlinear and nonlocal properties of light were also studied in systems of multi-core coupled waveguides [104–106]. In recent years, $\mathcal{PT}$-symmetry in optical lattices has attracted still increasing attention. For example, there are research concerning beam's dynamics theoretically studied [107–109] and verified by experimental observations in [110]. Optical lattices were also considered as objects for the studies of the existence, stability, and propagation dynamics of solitons [111–117], light rectification, the formation of discrete solitons [118–121], and other special effects appearing as a result of Bragg scattering [122, 123]. The experimental results were also reported for a $\mathcal{PT}$-symmetric systems of ultra-cold atoms confined in optical lattices [124]. In the field of lasers, the breaking of $\mathcal{PT}$-symmetry is also intensively investigated [125–129].

In quantum optics, $\mathcal{PT}$-symmetric systems are mainly considered in the context of models involving coupled quantum oscillators. For such kinds of system, the researches concentrated on investigating the breaking of $\mathcal{PT}$-symmetry in micro-resonators coupled to fibers [130, 131] or optical dimer [132–137] and trimer [138–141]. Besides that, the nonlinear properties [142–144], light transmission [145, 146] and the effects of quantum noise [147, 148] in such $\mathcal{PT}$-symmetric systems were also studied. The other $\mathcal{PT}$-symmetric systems considered in that group discussed models of microwave billiards [149–151] in the area of microwave cavities, nonlinear split-ring resonators [152, 153] or coupled waveguides [154, 155] in the field of meta materials.

In the following sections, we will present and discuss the basic concepts concerning the mathematical description of $\mathcal{PT}$-symmetry and the conditions of getting a real spectrum of eigenvalues for Hamiltonians describing $\mathcal{PT}$-symmetric systems.

2.2 Parity- and time-reversal operators

The action of parity-reversal operator $\hat{P}$ on the state of a system changes the sign of all coordinates appearing in the wave-function characterizing that state

$$\hat{P}\,|\psi(\vec{x},\vec{p},t)\rangle = |\psi(-\vec{x},-\vec{p},t)\rangle\,, \tag{2.2}$$

where $\vec{x}$ and $\vec{p}$ are the position and momentum of the system, respectively. Such action corresponds to the change of the system's location to the that located at the opposite side with respect to the origin point of the coordinate axes. The change of the coordinate sign leads to the change of the sign of mean values $\langle x\rangle$ and $\langle p\rangle$. Therefore, the transformation

of coordinate and momentum operators under the action of the parity conversion have the following form

$$\hat{P}^{\dagger}\hat{x}\hat{P} = -\hat{x}, \tag{2.3}$$

and

$$\hat{P}^{\dagger}\hat{p}\hat{P} = -\hat{p}, \tag{2.4}$$

where $\hat{x}$ and $\hat{p}$ are coordinate and momentum operators, respectively.

The parity operator is an unitary operator. Indeed, if $\hat{P}$ acts on $|\psi(\vec{x},\vec{p},t)\rangle$ twice in succession, the result only differs from $|\psi(\vec{x},\vec{p},t)\rangle$ by a phase term $\exp(i\alpha)$. Therefore, we can write

$$\hat{P}^2 |\psi(\vec{x},\vec{p},t)\rangle = \exp(i\alpha) |\psi(\vec{x},\vec{p},t)\rangle . \tag{2.5}$$

Because parity is an observable, the parity operator $\hat{P}$ has to be self-adjoin operator. It means $\hat{P}^{\dagger} = \hat{P}$. As a result, the phase term in this case has to be unity ($\exp(i\alpha) = 1$). That directly leads to the relation $\hat{P}^{\dagger}\hat{P} = \hat{P}^2 = \hat{1}$, and we can say that $\hat{P}$ is unitary.

We also see that $\hat{P}$ is linear operator. According to [156], an operator $\hat{L}$ is a linear operator if for an arbitrary complex constant a and an arbitrary state $|\psi(\vec{x},t)\rangle$ we have

$$\hat{L}\left(a|\psi(\vec{x},t\rangle\right) = a\hat{L}|\psi(\vec{x},t\rangle , \tag{2.6}$$

and an operator $\hat{N}$ will be nonlinear operator if

$$\hat{N}\left(a|\psi(\vec{x},t\rangle\right) = a^{*}\hat{N}|\psi(\vec{x},t\rangle . \tag{2.7}$$

To check whether the operator $\hat{P}$ is a linear operator, we start our considerations with setting $a = i$ and $|\psi(\vec{x},t)\rangle = \hbar\hat{1}$, and then, substitute them into (2.3) and (2.4). One should remember the commutation relation between $\hat{x}$ and $\hat{p}$ is $[\hat{x},\hat{p}] = i\hbar\hat{1}$. Applying the actions of $\hat{P}$ onto the commutator, we get

$$\begin{aligned}\hat{P}^{\dagger}\left[\hbar(i\hat{1})\right]\hat{P} = \hat{P}^{\dagger}[\hat{x},\hat{p}]\hat{P} &= \hat{P}^{\dagger}\hat{x}\hat{p}\hat{P} - \hat{P}^{\dagger}\hat{p}\hat{x}\hat{P} = \hat{P}^{\dagger}\hat{x}\hat{P}\hat{P}^{\dagger}\hat{p}\hat{P} - \hat{P}^{\dagger}\hat{p}\hat{P}\hat{P}^{\dagger}\hat{x}\hat{P} \\ &= (\hat{x})(\hat{p}) - (\hat{p})(\hat{x}) = [\hat{x},\hat{p}] = i(\hbar\hat{1}).\end{aligned} \tag{2.8}$$

The result shows that the action of operator $\hat{P}$ does not change the value of constant a. It means that $\hat{P}$ is a linear operator. For arbitrary operators $\hat{A}_i$ and arbitrary constants c_i (i=1,2, ...), we can easily write

$$\hat{P}^{\dagger}(c_1\hat{A}_1 + c_2\hat{A}_2 + ... + c_c\hat{A}_n)\hat{P} = c_1\hat{P}^{\dagger}\hat{A}_1\hat{P} + c_2\hat{P}^{\dagger}\hat{A}_2\hat{P} + ... + c_n\hat{P}^{\dagger}\hat{A}_n\hat{P} \tag{2.9}$$

and

$$\hat{P}^{\dagger}\left(\hat{A}_i\hat{A}_j\right)\hat{P} = \left(\hat{P}^{\dagger}\hat{A}_i\hat{P}\right)\left(\hat{P}^{\dagger}\hat{A}_j\hat{P}\right). \tag{2.10}$$

Therefore, if the Hamiltonian of a system can be written as a combination of coordinate and momentum operators, we can write

$$\hat{P}^{\dagger}\hat{H}(\hat{x},\hat{p},t)\hat{P} = \hat{H}(\hat{P}^{\dagger}\hat{x}\hat{P},\hat{P}^{\dagger}\hat{p}\hat{P},t) = \hat{H}(-\hat{x},-\hat{p},t). \tag{2.11}$$

A system will be invariant respect to the parity inversion if such inversion does not change the form of the Hamiltonian. For example, if a system is described by the Hamiltonian $\hat{H}(\hat{x},\hat{p},t) = \frac{\partial^2}{\partial t^2}\hat{x} + \hat{p}^2$ will be parity-invariant because

$$\hat{P}^\dagger \hat{H}(\hat{x},\hat{p},t)\hat{P} = \hat{H}(-\hat{x},-\hat{p},t) = \hat{H}(\hat{x},\hat{p},t). \tag{2.12}$$

In such the case, we also easily see that parity operator $\hat{P}$ commutes with the Hamiltonian $\hat{H}$. Indeed, because $\hat{P}$ is unitary and $\hat{H}$ is invariant under parity transformation, we have $\hat{H}\hat{P} = \hat{P}\hat{H}\hat{P}^\dagger\hat{P} = \hat{P}\hat{H}$ and $\left[\hat{H},\hat{P}\right] = 0$.

When the time-reversal operator $\hat{T}$ acts on a time dependent polynomial of parameters and variables, the time variable changes its sign ($t \to -t$). Concerning the operators, we can easily see that the action of $\hat{T}$ does not change the sign of coordinate operators but does change the sign of operators that are time dependent. For example, the momentum $\hat{p} = -i\hbar\nabla$ and angular momentum $\hat{j} = \hat{x} \times \hat{p}$ operators change their signs under the action of $\hat{T}$. Therefore, we can write

$$\hat{T}^\dagger \hat{x} \hat{T} = \hat{x}, \tag{2.13}$$

$$\hat{T}^\dagger \hat{p} \hat{T} = -\hat{p}, \tag{2.14}$$

$$\hat{T}^\dagger \hat{j} \hat{T} = -\hat{j}. \tag{2.15}$$

To find out whether the time-reversal operator $\hat{T}$ is an unitary, we follow the way that we used for the operator $\hat{P}$. When $\hat{T}$ acts on a quantum state $|\psi(\vec{x},\vec{p},t)\rangle$ twice, we will get a state that is only different from $|\psi(\vec{x},\vec{p},t)\rangle$ by a phase term $\exp(i\beta)$. Therefore, we have:

$$\hat{T}^2 |\psi(\vec{x},\vec{p},t)\rangle = \exp(i\beta) |\psi(\vec{x},\vec{p},t)\rangle . \tag{2.16}$$

If $\hat{T}$ acts on $|\psi(\vec{x},\vec{p},t)\rangle$ one more time, we get

$$\hat{T}(\hat{T}^2 |\psi(\vec{x},\vec{p},t)\rangle) = \hat{T}(\exp(i\beta) |\psi(\vec{x},\vec{p},t)\rangle). \tag{2.17}$$

After performing a transformation of this equation, we achieve

$$\hat{T}^2(\hat{T} |\psi(\vec{x},\vec{p},t)\rangle) = \exp(-i\beta)(\hat{T} |\psi(\vec{x},\vec{p},t)\rangle). \tag{2.18}$$

Comparing (2.16) and (2.17) we see that $\exp(i\beta) = \exp(-i\beta)$ because the action of $\hat{T}^2$ on the different states gives the same phase factor. This leads to the result $\beta = 0$ and we have

$$\hat{T}^2 |\psi(\vec{x},\vec{p},t)\rangle = \pm |\psi(\vec{x},\vec{p},t)\rangle . \tag{2.19}$$

The equation (2.19) says that $\hat{T}$ is not unitary. It is an anti-unitary operator.

To check whether $\hat{T}$ is a linear- or nonlinear operator, we apply (2.19) with setting $\hat{N} = \hat{T}, a = i$ and $|\psi(\vec{x},t)\rangle = \hbar\hat{1}$. The transformation with use of $\hat{T}$ can be written as

$$\begin{aligned}
\hat{T}^\dagger \left[\hbar(i\hat{1})\right] \hat{T} &= \hat{T}^\dagger [\hat{x},\hat{p}] \hat{T} = \hat{T}^\dagger\hat{x}\hat{p}\hat{T} - \hat{T}^\dagger\hat{p}\hat{x}\hat{T} = \hat{T}^\dagger\hat{x}\hat{T}\hat{T}^\dagger\hat{p}\hat{T} - \hat{T}^\dagger\hat{p}\hat{T}\hat{T}^\dagger\hat{x}\hat{T} \\
&= \left(\hat{T}^\dagger\hat{x}\hat{T}\right)\left(\hat{T}^\dagger\hat{p}\hat{T}\right) - \left(\hat{T}^\dagger\hat{p}\hat{T}\right)\left(\hat{T}^\dagger\hat{x}\hat{T}\right) = (\hat{x})(\hat{p}) - (\hat{p})(\hat{x}) \\
&= -\hat{x}\hat{p} + \hat{p}\hat{x} = -[\hat{x},\hat{p}] = -i\hbar\hat{1} = -i(\hbar\hat{1}) = (i)^*(\hbar\hat{1}).
\end{aligned} \tag{2.20}$$

The result shows that $\hat{T}$ is nonlinear- and anti-unitary operator. For a wave function, the action of $\hat{T}$ on that function can be expressed as follows:

$$\hat{T}\left|\psi(\vec{x},\vec{p},t)\right\rangle = \left|\psi(\vec{x},-\vec{p},-t)\right\rangle. \tag{2.21}$$

Because $\hat{T}$ is a nonlinear operator, the relation (2.9) is not satisfied. However, its successive actions such as those presented in (2.10) are possible. It means for every operator $\hat{A}_i$ and $\hat{A}_j$, we also have

$$\hat{T}^\dagger\left(\hat{A}_i\hat{A}_j\right)\hat{T} = \left(\hat{T}^\dagger\hat{A}_i\hat{T}\right)\left(\hat{T}^\dagger\hat{A}_j\hat{T}\right). \tag{2.22}$$

As the result, the action of time-reversal operator on the Hamiltonian describing a considered system can be shown in the following way

$$\hat{T}^\dagger\hat{H}(\hat{x},\hat{p},t)\hat{T} = \hat{H}(\hat{x},-\hat{p},-t). \tag{2.23}$$

A system will be invariant with respect to a time-reversal if the action of the time-reversal operator does not change the form of Hamiltonian

$$\hat{H}(\hat{x},\hat{p},t) = \hat{H}(\hat{x},-\hat{p},-t). \tag{2.24}$$

Even when Hamiltonian operators are time-reversal invariant, we can not assert exactly whether operator $\hat{T}$ commutes with Hamiltonian $\hat{H}$ or not. After making the transformation $\hat{H}\hat{T} = \hat{T}\hat{H}\hat{T}^\dagger\hat{T}$ and looking at (2.19) we see that $\left[\hat{H},\hat{T}\right] = 0$ if $\hat{T}^2\left|\psi(\vec{x},\vec{p},t)\right\rangle = \left|\psi(\vec{x},\vec{p},t)\right\rangle$ and anti-commutator $\left\{\hat{H},\hat{T}\right\} = 0$ for the other cases.

We can contract the combination of two operators $\hat{P}$ and $\hat{T}$ by considering the operator $\hat{D} = \hat{P}\hat{T}$. The action of $\hat{D}$ on a quantum state is a combination of subsequent actions of $\hat{P}$ and $\hat{T}$. Because $\hat{P}$ is an linear and unitary, while $\hat{T}$ is nonlinear and anti-unitary, $\hat{D}$ is nonlinear- and anti-unitary. Combine (2.3) and (2.4) with respect of (2.13) and (2.14), we get

$$\hat{D}^\dagger\hat{x}\hat{D} = \hat{P}^\dagger\hat{P}^\dagger\hat{x}\hat{P}\hat{T} = -\hat{x}, \tag{2.25}$$

$$\hat{D}^\dagger\hat{p}\hat{D} = \hat{P}^\dagger\hat{P}^\dagger\hat{p}\hat{P}\hat{T} = \hat{p}, \tag{2.26}$$

and

$$\hat{D}^\dagger\hat{j}\hat{D} = \hat{P}^\dagger\hat{P}^\dagger\hat{j}\hat{P}\hat{T} = \hat{j}. \tag{2.27}$$

If the Hamiltonian describing a system is a polynomial of coordinate and momentum operators, we can describe the action of operator $\hat{D}$ as follows

$$\hat{D}^\dagger\hat{H}(\hat{x},\hat{p},t)\hat{D} = \hat{P}^\dagger\hat{T}^\dagger\hat{H}(\hat{x},\hat{p},t)\hat{P}\hat{T} = \hat{H}(\hat{P}^\dagger\hat{T}^\dagger\hat{x}\hat{P}\hat{T},\hat{P}^\dagger\hat{T}^\dagger\hat{p}\hat{P}\hat{T},t) = \hat{H}^*(-\hat{x},\hat{p},-t). \tag{2.28}$$

A system is $\mathcal{PT}$-symmetric if the Hamiltonian describing that system does not change its form under simultaneous actions of $\hat{P}$ and $\hat{T}$:

$$\hat{H}^*(-\hat{x},\hat{p},-t) = \hat{H}(\hat{x},\hat{p},t). \tag{2.29}$$

In general, the potential energy of a system usually has a complex form $\hat{V}(\vec{x}) = \hat{V}_R(\vec{x}) + i\hat{V}_I(\vec{x})$, where $\hat{V}_R(\vec{r})$ and $\hat{V}_I(\vec{x})$ are real and imaginary terms, respectively. The condition (2.29) is only fulfilled when $\hat{V}_R(\vec{x})$ is an even function of coordinates, while $\hat{V}_I(\vec{x})$ is an odd function. We see that for $\mathcal{PT}$-symmetric systems, we can obtain a set of eigenstates with a real spectrum of eigenvalues of the Hamiltonian, even when the Hamiltonian is non-Hermitian. To do that, we have to consider a new concept of inner product and some conditions that will be discussed in the next section.

2.3 Conditions for a real spectrum of eigenvalues of $\mathcal{PT}$-symmetric Hamiltonian

In quantum mechanics, if an operator commutes with a Hamiltonian, it will share a set of eigenstates with such Hamiltonian. In complex quantum mechanics, the story is very different. Even when the operator $\hat{P}\hat{T}$ commutes with a Hamiltonian, they can or can not share the same eigenstates together. The result depends on the particular, considered situation. For such the case the important role plays a boundary called a phase-transition point. At the one side of the phase-transition point, the Hamiltonian has an absolutely real spectrum of eigenvalues. for such the case, the system is characterized in an unbroken $\mathcal{PT}$-symmetry phase. On the other side of the phase-transition phase, we are dealing with the broken $\mathcal{PT}$-symmetry phase, where the Hamiltonian has a complex spectrum of its eigenvalues. In complex quantum mechanics, if a system is in an unbroken phase, it is characterized by positive probabilities, and such probability of the system being in a given state is only conserved if we consider a new concept of the inner product.

It is well known that for a Hermitian Hamiltonian, we will find out a set of eigenstates with real spectrum eigenvalues. However, for a non-Hermitian Hamiltonian, it is necessary to commute with combination of $\hat{P}$ and $\hat{T}$ operators

$$\left[\hat{H}, \hat{P}\hat{T}\right] = 0. \tag{2.30}$$

Moreover, it is also shown in [157,158] that the non-degenerated eigenvalues E_n (n=1,2...) of a $\mathcal{PT}$-symmetric system will be real if and only if its eigenfunctions $|\psi_n\rangle$ are $\mathcal{PT}$-symmetric. To demonstrate this condition, fist of all, we will show that if the eigenfunction of $\mathcal{PT}$-symmetric system is invariant with $\mathcal{PT}$-transformation, its eigenvalues will be real.

Let us assume that the eigenfunction of $\mathcal{PT}$-symmetric system is invariant with $\mathcal{PT}$-transformation

$$\hat{P}\hat{T}\,|\psi_n\rangle = |\psi_n\rangle\,. \tag{2.31}$$

Because $|\psi_n\rangle$ are eigenfunction corresponding to eigenvalues E_n, we can write

$$\hat{H}\,|\psi_n\rangle = E_n\,|\psi_n\rangle\,. \tag{2.32}$$

If we apply $\mathcal{PT}$-transformation to both sides of (2.32) and remember that Hamiltonian $\hat{H}$ is invariant with $\mathcal{PT}$-transformation, we can rewrite (2.32) as

$$\hat{H}\left|\psi_n\right\rangle = \hat{P}\hat{T}(E_n\left|\psi_n\right\rangle). \tag{2.33}$$

Because $\hat{P}$ and $\hat{T}$ are linear and nonlinear operators respectively, we apply (2.6) and (2.7) and continue to modify (2.33)

$$\hat{H}\left|\psi_n\right\rangle = \hat{P}\hat{T}(E_n\left|\psi_n\right\rangle) = \hat{P}(E_n^*\left|\psi_n\right\rangle) = E_n^*\left|\psi_n\right\rangle. \tag{2.34}$$

The equation (2.32) and (2.34) are only satisfied simultaneously if ${E_n}^* = E_n$. That means the eigenvalues of the $\mathcal{PT}$-symmetric system are real.

Now, we will continuously indicate that, in the converse direction of condition,*i.e.* if the eigenvalues of a $\mathcal{PT}$-symmetric system are real, the eigenfunctions have to be invariant under $\mathcal{PT}$-transformation. Let us assume that the eigenfunction of the system $\left|\psi_n\right\rangle$ is changed to the state $\left|\varphi_n\right\rangle$ under $\mathcal{PT}$-transformation. Thus, we have

$$\hat{P}\hat{T}\left|\psi_n\right\rangle = \left|\varphi_n\right\rangle. \tag{2.35}$$

If we apply $\mathcal{PT}$-transformation to both sides of (2.32), we get

$$\hat{P}\hat{T}\hat{H}\left|\psi_n\right\rangle = \hat{P}\hat{T}(E_n\left|\psi_n\right\rangle). \tag{2.36}$$

Now, remembering that E_n are real and operator $\hat{P}\hat{T}$ commutes with the Hamiltonian $\hat{H}$ ($\hat{P}\hat{T}\hat{H} = \hat{H}\hat{P}\hat{T}$), we can write the result of transformation as

$$\hat{H}\hat{P}\hat{T}\left|\psi_n\right\rangle = E_n\hat{P}\hat{T}\left|\psi_n\right\rangle \tag{2.37}$$

or

$$\hat{H}(\left|\varphi_n\right\rangle) = E_n\left|\varphi_n\right\rangle. \tag{2.38}$$

The equations (2.32) and (2.38) show that $\left|\psi_n\right\rangle$ and $\left|\varphi_n\right\rangle$ have the same eigenvalues. Because the spectrum of Hamiltonian is non-degenerate, then there is no more than one eigenfunction that share an eigenvalue. It means $\left|\psi_n\right\rangle = \left|\varphi_n\right\rangle$ and after substituting it into (2.35) we have

$$\hat{P}\hat{T}\left|\psi_n\right\rangle = \left|\varphi_n\right\rangle = \left|\psi_n\right\rangle.$$

The result directly shows that the eigenfunctions of the $\mathcal{PT}$-symmetric system are invariant under $\mathcal{PT}$-transformation. Obviously, when a system is described by a Hermitian Hamiltonian, its eigenfunctions $\left|\psi_i\right\rangle$ not only have a real spectrum of their eigenvalues, but also provide a set of orthonormal basic obeying $\left\langle\psi_i\right|\left.\psi_j\right\rangle = \delta_{ij}$. Beside that, time-dependent Schrödinger equation

$$i\frac{\partial}{\partial t}\left|\psi(\vec{x},t)\right\rangle = \hat{H}\left|\psi(\vec{x},t)\right\rangle \tag{2.39}$$

gives us the time-dependent eigensolution $|\psi_n(\vec{x},t)\rangle = \exp(iE_nt)\,|\psi_n(\vec{x},0)\rangle$. The complex conjugate of the Schrödinger equation has the form

$$-i\frac{\partial}{\partial t}\langle\psi_n(\vec{x},t)| = \langle\psi_n(\vec{x},t)|\,\hat{H}^\dagger. \tag{2.40}$$

Subtracting (2.39) from (2.40) and multiplying both sides of (2.39) by $\langle\psi_n(\vec{x},t)|$ on the left and both sides of (2.40) by $|\psi(\vec{x},t)\rangle$ on the right, we achieve

$$\frac{\partial}{\partial t}\langle\psi(\vec{x},t)|\,\psi(\vec{x},t)\rangle = i\,\langle\psi(\vec{x},t)|\left(\hat{H}^\dagger - \hat{H}\right)|\psi(\vec{x},t)\rangle\,. \tag{2.41}$$

If the Hamiltonian is Hermitian ($\hat{H} = \hat{H}^\dagger$) we directly have $\frac{\partial}{\partial t}\langle\psi(\vec{x},t)|\,\psi(\vec{x},t)\rangle = 0$. It means that the probability is preserved.

To check whether eigenfunctions of non-Hermitian Hamiltonian are orthogonal, we expand the state of the system in the basis of eigenfunctions

$$|\psi(\vec{x},t)\rangle = \sum_n c_n\,|\psi_n(\vec{x},t)\rangle\,, \tag{2.42}$$

and rewrite the left side of (2.41) as follow

$$\begin{aligned}\frac{\partial}{\partial t}\langle\psi(\vec{x},t)|\psi(\vec{x},t)\rangle &= \frac{\partial}{\partial t}\left(\sum_m c_m^*\,\langle\psi_m(\vec{x},t)|\sum_n c_n\,|\varphi_n(\vec{x},t)\rangle\right)\\ &= \frac{\partial}{\partial t}\left(\sum_m\sum_n c_m^*c_n\,\langle\psi_m\left(\vec{x},t\right)|\varphi_n\left(\vec{x},t\right)\rangle\right).\end{aligned} \tag{2.43}$$

Because the Hamiltonian is non-Hermitian, the right side of (2.41) is different from zero. Therefore, the left side of that equation also differs from zero,

$$\frac{\partial}{\partial t}\langle\psi(\vec{x},t)|\psi(\vec{x},t)\rangle = \frac{\partial}{\partial t}\left(\sum_{m\neq n} c_m^*c_n\,\langle\psi_m\left(\vec{x},t\right)|\varphi_n\left(\vec{x},t\right)\rangle\right) \neq 0. \tag{2.44}$$

Consequently, we have $\langle\psi_m(\vec{x},t)|\,\psi_n(\vec{x},t)\rangle \neq 0$ for $m \neq n$. That means that the eigenfunctions of the Hamiltonian are not orthogonal.

However, when the system is $\mathcal{P}$-symmetric, the situation changes considerably. Let us multiply both sides of (2.39) by $\langle\psi_n(\vec{x},t)|\,\hat{P}$ on the left and both sides of (2.40) by $\hat{P}\,|\psi(\vec{x},t)\rangle$ on the right then subtract such obtained results, we achieve

$$i\frac{\partial}{\partial t}\langle\psi(\vec{x},t)|\,\hat{P}\,|\psi(\vec{x},t)\rangle = \langle\psi(\vec{x},t)|\,\hat{H}^\dagger\hat{P} - \hat{P}\hat{H}\,|\psi(\vec{x},t)\rangle\,. \tag{2.45}$$

At this point we should remember that $\hat{T}\hat{H}\hat{T} = \hat{H}^\dagger$. Therefore, if $\hat{P}^\dagger\hat{H}\hat{P} = \hat{P}\hat{H}\hat{P} = \hat{H}^\dagger$, we will have $\hat{T}\hat{H}\hat{T} = \hat{P}\hat{H}\hat{P}$. Consequently, we can get the following transformation

$$\hat{H}^\dagger\hat{P} = \hat{T}\hat{H}\hat{T}\hat{P} = \hat{P}\hat{H}\hat{P}\hat{P} = \hat{P}\hat{H}. \tag{2.46}$$

By substituting (2.46) into (2.45) we achieve $i\frac{\partial}{\partial t}\langle\psi(\vec{x},t)|\,\hat{P}\,|\psi(\vec{x},t)\rangle = 0$. That means that the probability is preserved if we consider a new concept of bra vector as $\langle\psi(\vec{x},t)|\,\hat{P}$. With this, we also have the new definition of expectation value of observable quantity Q that is characterized by operator $\hat{Q}$. It can be expressed as

$$\left\langle \hat{Q} \right\rangle = \langle\psi(\vec{x},t)|\,\hat{P}\hat{Q}\,|\psi(\vec{x},t)\rangle\,. \tag{2.47}$$

2.4 Summary

In this chapter, we provided an introduction to the original ideas of the $\mathcal{PT}$-symmetric systems considered by Bender *et.al* [1, 24] and the insight into current research devoted to various physical models described by the formalism of $\mathcal{PT}$-symmetry. Besides that, we also presented the space-reflection and time-reversal operator concepts and their properties. We showed that the first of them is a unitary and linear operator, whereas the time-reversal operator is a nonlinear and anti-unitary one. Moreover, we discussed the conditions determining whether the Hamiltonian describing a $\mathcal{PT}$-the symmetric system can give us a real spectrum of eigenvalues as a condition for the existence of unbroken $\mathcal{PT}$-symmetric phase. The next chapter will be devoted to the discussion of quantum correlations in a bipartite $\mathcal{PT}$-symmetric model. We will concentrate on quantum entanglement and quantum steering appearing in such the model. Additionally, the coherence functions describing the correlations of the electric fields and light intensities that are generated in the system will also be shown.

Chapter 3

Quantum correlations in a bipartite $\mathcal{PT}$-symmetric model of two cavities

3.1 The $\mathcal{PT}$-symmetric model of two cavities

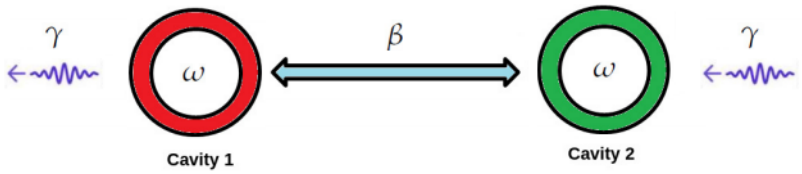

Fig. 3.1: Schematic illustration of a bipartite $\mathcal{PT}$-symmetric system of two cavities considered here. The cavities are labeled as 1 (active) and 2 (passive).

We consider here the model of a bipartite $\mathcal{PT}$-symmetric system consisting of two cavities interacting linearly with each other (Fig.3.1). Additionally, the cavity labeled as 1 (called passive) is excited by the interaction with an external environment, whereas the cavity 2 (active) emits its energy. Usually, when the $\mathcal{PT}$-symmetric systems are considered, those two processes are balanced with each other, so they are described by the same parameter γ. The non-Hermitian Hamiltonian that characterizes the system can be written as:

$$\hat{H} = (\omega - i\gamma)\hat{a}_1^\dagger \hat{a}_1 + (\omega + i\gamma)\hat{a}_2^\dagger \hat{a}_2 + \beta(\hat{a}_1^\dagger \hat{a}_2 + \hat{a}_2^\dagger \hat{a}_1), \tag{3.1}$$

where $\hat{a}_1^\dagger$ and $\hat{a}_2^\dagger$ are the creation operators, while $\hat{a}_1$ and $\hat{a}_2$ are annihilation operators corresponding to the cavities that are labeled as 1 and 2, respectively. The parameter ω is the resonance frequency that is assumed to be the same for both cavities, while γ is the loss (gain) rate of energy of the cavity 1 (2). The strength of linear interaction between two cavities is characterized by the parameter β. We can rewrite the Hamiltonian in a matrix form as

$$\hat{H} = \begin{pmatrix} \hat{a}_1^\dagger & \hat{a}_2^\dagger \end{pmatrix} \begin{pmatrix} \omega - i\gamma & \beta \\ \beta & \omega + i\gamma \end{pmatrix} \begin{pmatrix} \hat{a}_1 \\ \hat{a}_2 \end{pmatrix} = \begin{pmatrix} \hat{a}_1^\dagger & \hat{a}_2^\dagger \end{pmatrix} \hat{H}_{eff} \begin{pmatrix} \hat{a}_1 \\ \hat{a}_2 \end{pmatrix}, \tag{3.2}$$

where $\hat{H}_{eff}$ is the effective Hamiltonian that takes the form

$$\hat{H}_{eff} = \begin{pmatrix} \omega - i\gamma & \beta \\ \beta & \omega + i\gamma \end{pmatrix}. \tag{3.3}$$

We can easily see that the Hamiltonian 3.3 is not Hermitian. However, it is $\mathcal{PT}$-symmetric as it is invariant after action of $\hat{P}$ and $\hat{T}$ operators. In fact the operator $\hat{T}$ is a complex conjugate and operator, whereas $\hat{P}$ can be written in the matrix form

$$\hat{P} = \begin{pmatrix} 0 & 1 \\ 1 & 0 \end{pmatrix}. \tag{3.4}$$

After some straightforward algebra, one can get the eigenvalues of the Hamiltonian (3.3). They are:

$$E_1 = \omega + \sqrt{\beta^2 - \gamma^2},$$

and

$$E_2 = \omega - \sqrt{\beta^2 - \gamma^2}. \tag{3.5}$$

We can see that those eigenvalues can be real or complex depending on the relation between β and γ. When $\gamma > \beta$, the system is in the broken $\mathcal{PT}$-symmetry phase. For such a case, the eigenvalue spectrum is complex and has two values that are complex conjugate of each other

$$E_1 = \omega + i\sqrt{\gamma^2 - \beta^2},$$

$$E_2 = \omega - i\sqrt{\gamma^2 - \beta^2}. \tag{3.6}$$

Contrary, when $\gamma < \beta$, all the eigenvalues (3.5) are real. This phase is called the unbroken phase of the $\mathcal{PT}$-symmetry. Finally, the case $\gamma = \beta$ corresponds to the phase-transition point and the only eigenvalue of Hamiltonian is $E = \omega$. The real and imaginary parts of energy eigenvalues are plotted as functions of γ/β in Fig.3.2.

As we are interested in the cases when the $\mathcal{PT}$-symmetry is not broken, we follow the path proposed in [159–163]. They have shown that for the case of the unbroken symmetry phase, we can describe the system's evolution with an application of the master equation in the Lindblad form for the density matrix describing the systems' state. Such equation involves the Hamiltonian $\hat{H}_0$ in which the terms with the parameter γ is removed. For the model considered here, the master equation and $\hat{H}_0$ are:

$$\frac{d}{dt}\hat{\rho} = \frac{1}{i}\left[\hat{H}_0, \hat{\rho}\right] + \hat{\mathcal{L}}\hat{\rho}, \tag{3.7}$$

and

$$\hat{H}_0 = \omega\left(\hat{a}_1^\dagger \hat{a}_1 + \hat{a}_2^\dagger \hat{a}_2\right) + \beta\left(\hat{a}_1^\dagger \hat{a}_2 + \hat{a}_2^\dagger \hat{a}_1\right), \tag{3.8}$$

The Liouvillian superoperator appearing here $\hat{\mathcal{L}}$ acts on $\hat{\rho}$ in the following way:

$$\hat{\mathcal{L}}\hat{\rho} = \gamma\left(2\hat{a}_1\hat{\rho}\hat{a}_1^\dagger - \hat{a}_1^\dagger\hat{a}_1\hat{\rho} - \hat{\rho}\hat{a}_1^\dagger\hat{a}_1\right) + \gamma\left(2\hat{a}_2^\dagger\hat{\rho}\hat{a}_2 - \hat{a}_2\hat{a}_2^\dagger\hat{\rho} - \hat{\rho}\hat{a}_2\hat{a}_2^\dagger\right). \tag{3.9}$$

In equation 3.9, the first term describes the loss of energy to environment, while the second term characterizes the gain of energy.

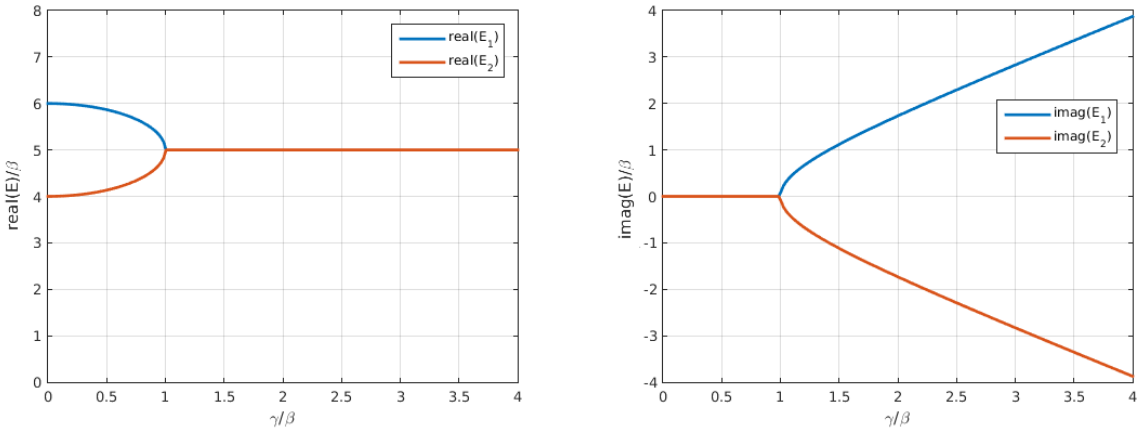

Fig. 3.2: The dependence of real and imaginary parts of eigenvalues of the Hamiltonian as the function of the rate between γ and β when $\omega = 5\beta$.

3.2 Quantum correlation functions in a bipartite $\mathcal{PT}$-symmetric model

We start this section from the discussion of non-classical properties of a bipartite $\mathcal{PT}$-symmetric system. To do that, we calculate the first- and second-order correlation functions with zero time delay that respectively take the forms

$$G_{12}^{(1)}(0) = \frac{\left|\left\langle \hat{a}_1^\dagger(t)\hat{a}_2(t)\right\rangle\right|}{\sqrt{\left\langle \hat{a}_1^\dagger(t)\hat{a}_1(t)\right\rangle \left\langle \hat{a}_2^\dagger(t)\hat{a}_2(t)\right\rangle}}, \tag{3.10}$$

and

$$G_{12}^{(2)}(0) = \frac{\left\langle \hat{a}_1^\dagger(t)\hat{a}_2^\dagger(t)\hat{a}_2(t)\hat{a}_1(t)\right\rangle}{\left\langle \hat{a}_1^\dagger(t)\hat{a}_1(t)\right\rangle \left\langle \hat{a}_2^\dagger(t)\hat{a}_2(t)\right\rangle}, \tag{3.11}$$

where $\hat{a}_i^\dagger$ and $\hat{a}_i$ are creation and annihilation operators, respectively, corresponding to the modes i $(i = 1, 2)$.

We concentrate here on two scenarios in which the system's initial state correspond to the situations when only one of subsystems is excited. It means that the system's initial states will be $\hat{\rho}(t = 0) = |10\rangle\langle 10|$ or $\hat{\rho}(t = 0) = |01\rangle\langle 01|$.

In the first scenario, only the passive cavity is excited, while the active is in the vacuum state. It means that the initial state of our system will be $\hat{\rho}(t = 0) = |10\rangle\langle 10|$. The results of $G_{12}^{(1)}(0)$ and $G_{12}^{(2)}(0)$ evolution are shown in Fig.3.3. We can see that in this scenario, the values of $G_{12}^{(1)}(0)$ and $G_{12}^{(2)}(0)$ clearly depend on the value of γ/β. When the value of γ/β is very small, $\gamma = 0001\beta$, the values of both $G_{12}^{(1)}(0)$ and $G_{12}^{(2)}(0)$ periodically

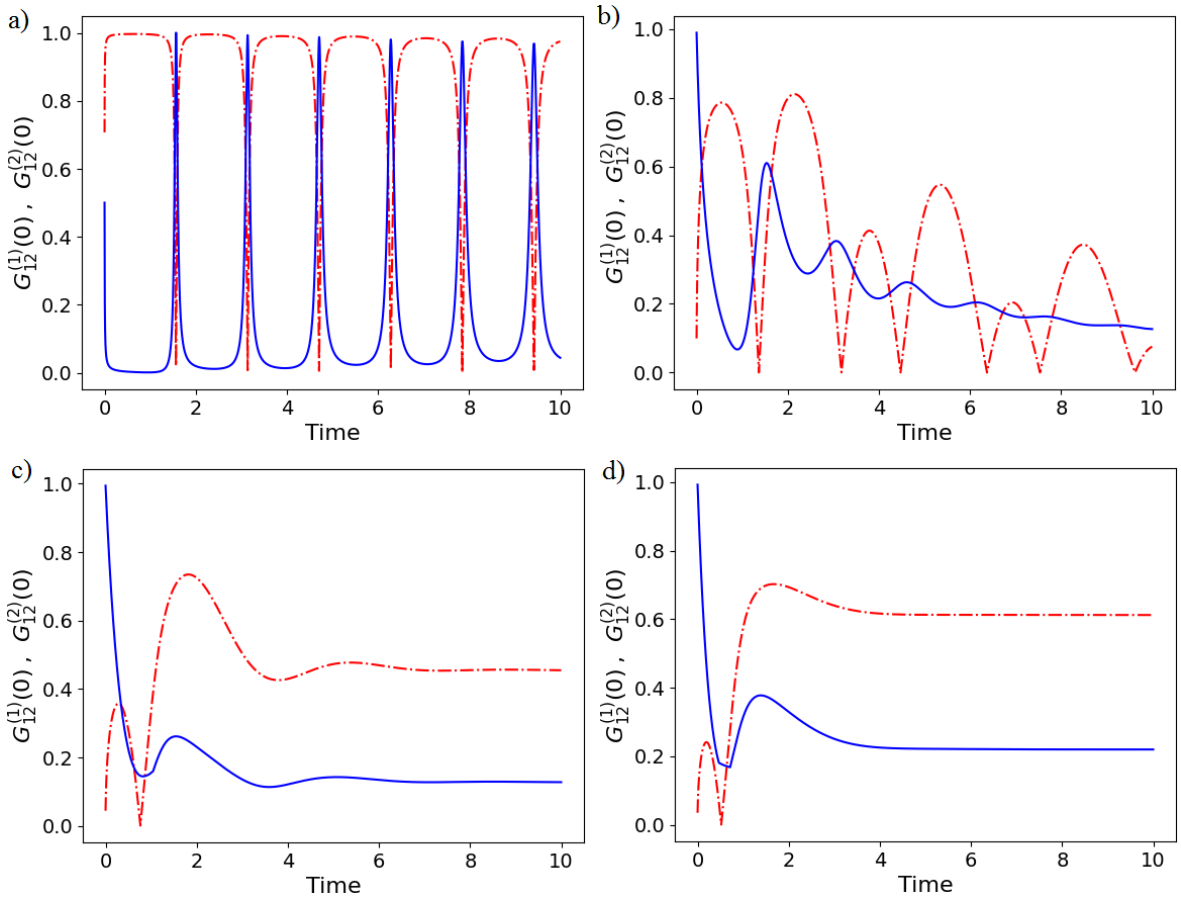

Fig. 3.3: The time-evolution of $G_{12}^{(1)}(0)$ (dash-doted line) and $G_{12}^{(2)}(0)$ (solid line) for the initial state $\hat{\rho}(t=0) = |10\rangle\langle 10|$ and $\gamma = 0001\beta$ (a); $\gamma = 01\beta$ (b); $\gamma = 05\beta$ (c); $\gamma = 08\beta$ (d). The time is scaled in $1/\beta$ units.

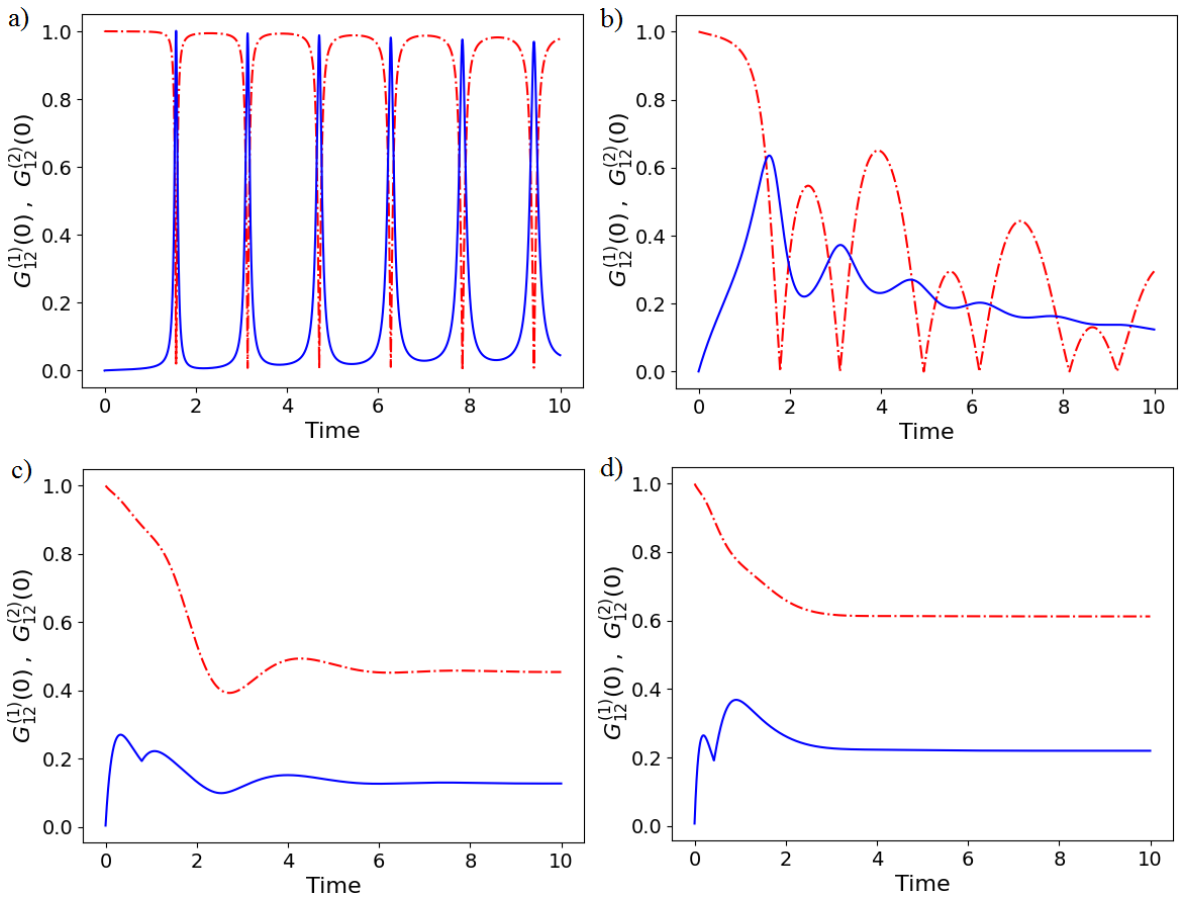

Fig. 3.4: The time evolution of $G_{12}^{(1)}(0)$ (dash-dot line) and $G_{12}^{(2)}(0)$ (solid line) for the initial state $\hat{\rho}(t=0) = |01\rangle\langle 01|$ and $\gamma = 0001\beta$ (a); $\gamma = 01\beta$ (b); $\gamma = 05\beta$ (c); $\gamma = 08\beta$ (d). Time is scaled in $1/\beta$ units.

change in time, and their changes are symmetric with each other We can easily see from Fig.3.3a that when the value of $G_{12}^{(1)}(0)$ reaches its maximum, the value of $G_{12}^{(2)}(0)$ will be minimal, and vice versa. For every period of time, the value of $G_{12}^{(1)}(0)$ reaches its maximal value for a while before decreasing to its minimum. The time interval of that regular change becomes shorter and shorter in time. In such intervals of time, the value of $G_{12}^{(2)}(0)$ also reaches its minimal value before increasing to its maximum. In the period of interest, the maximal values of both $G_{12}^{(1)}(0)$ and $G_{12}^{(2)}(0)$ tend to decrease while their minimal values gradually increase. When $\gamma = 01\beta$, $G_{12}^{(1)}(0)$ and $G_{12}^{(2)}(0)$ still oscillate periodically in time. However, their maximal values rapidly decrease. The minimal value of $G_{12}^{(2)}(0)$ in periods firstly increase from a non zero value to a certain value and next, gradually decreases to zero while the minimal value of $G_{12}^{(1)}(0)$ always remains equal to zero (see Fig.3.3b). When we increase the value of γ/β to 0.5, (Fig.3.3c) the value of $G_{12}^{(2)}(0)$ starts from its value ~ 1, and then rapidly decreases to its minimal value. After several oscillations, it tends to be stable with a certain value. Meanwhile, the value of $G_{12}^{(1)}(0)$ starts from zero, then increases to its maximum. It also stabilizes at some value after several oscillations. For γ/β which is close to the phase-transition point, the values of both $G_{12}^{(1)}(0)$ and $G_{12}^{(2)}(0)$ reach their stable values faster than for the case when $\gamma = 05\beta$. Now, the stable values are greater than in the previous case (see Fig.3.3d).

In the second scenario, the system starts its evolution when only the active cavity is excited. It means that the initial state of the system is $\hat{\rho}(t = 0) = |01\rangle\langle 01|$. The results of our calculation are shown in Fig.3.4. We can also see that the evolution of $G_{12}^{(1)}(0)$ and $G_{12}^{(2)}(0)$ considerably depend on the value of γ/β. When $\gamma = 0001\beta$, we can see in Fig.3.4a that the character of changes in time of $G_{12}^{(1)}(0)$ and $G_{12}^{(2)}(0)$ are approximately the same as those considered in the previous scenario. The only different thing is, in this case, that $G_{12}^{(1)}(0)$ starts its evolution from ~ 1 while $G_{12}^{(2)}(0)$ starts from 0 instead of taking non-zero value as we observed in the scenario when $\hat{\rho}(t = 0) = |10\rangle\langle 10|$. For $\gamma = 01\beta$, at the beginning, the value of $G_{12}^{(1)}(0)$ decreases from ~ 1, then it periodically changes with the decreasing its maxima, while its minimal values are always equal to zero. Meanwhile, the value of $G_{12}^{(2)}(0)$ starts from zero, then it oscillates with the decreasing both maxima and minima. For such the case, the value of $G_{12}^{(1)}(0)$ approximately reaches its maximal values when the value of $G_{12}^{(2)}(0)$ is minimal (see Fig.3.4b). When $\gamma = 05\beta$, the oscillations of $G_{12}^{(1)}(0)$ and $G_{12}^{(2)}(0)$ rapidly disappear after a few periods, and they tend to be finally stable. When the value of γ/β is close to the phase-transition point ($\gamma = 08\beta$) we can see that the value of $G_{12}^{(1)}(0)$ continuously decreases from the value close to the unity to its final stable value. Meanwhile, the value of $G_{12}^{(2)}(0)$ still starts from its zero value, then it exhibits some oscillations to finally become stable. We can see that although $G_{12}^{(1)}(0)$ and $G_{12}^{(2)}(0)$ start their evolution in different ways, their final stable values are still the same for different initial states of the system (compare Fig.3.3d and Fig.3.4d). It put an idea of finding steady-state solutions of both first- and second-order quantum correlation functions.

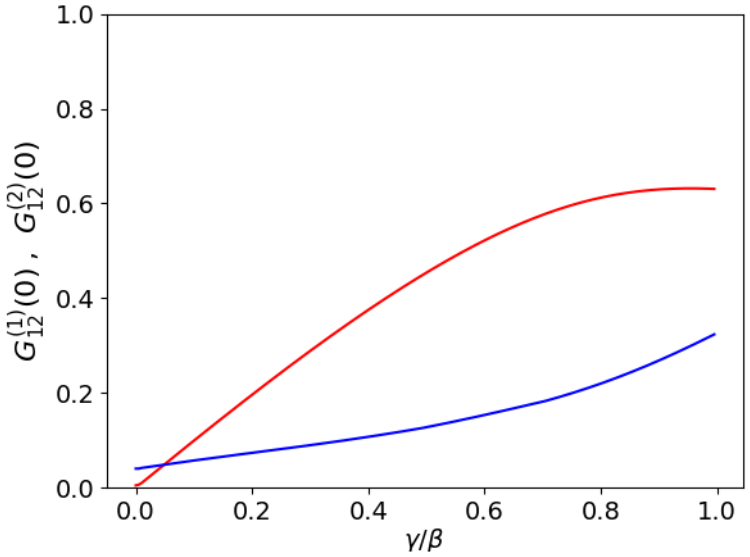

Fig. 3.5: The steady-state solutions for $G_{12}^{(1)}(0)$ (red line) and $G_{12}^{(2)}(0)$(blue line) versus γ/β for $\omega = 5\beta$.

Thus, Fig.3.5 depicts the dependence of $G_{12}^{(1)}(0)$ and $G_{12}^{(2)}(0)$ on γ/β when the time tends to infinity. We can see that the value of $G_{12}^{(1)}(0)$ takes a value that is close to zero for very small value of γ/β, and then it gradually increases with γ/β. When γ/β is close to the phase-transition point of $\mathcal{PT}$-symmetry, the correlation function $G_{12}^{(1)}(0) \simeq 0.63$. Meanwhile, the value of $G_{12}^{(2)}(0)$ is non-zero for very small values of γ/β. When we increase the value of γ/β, $G_{12}^{(2)}(0)$ slightly increases reaching the value around 0.32 When the value of γ/β is close to the phase-transition point. Interestingly, we can achieve stable correlation functions for almost all considered here values of γ/β.

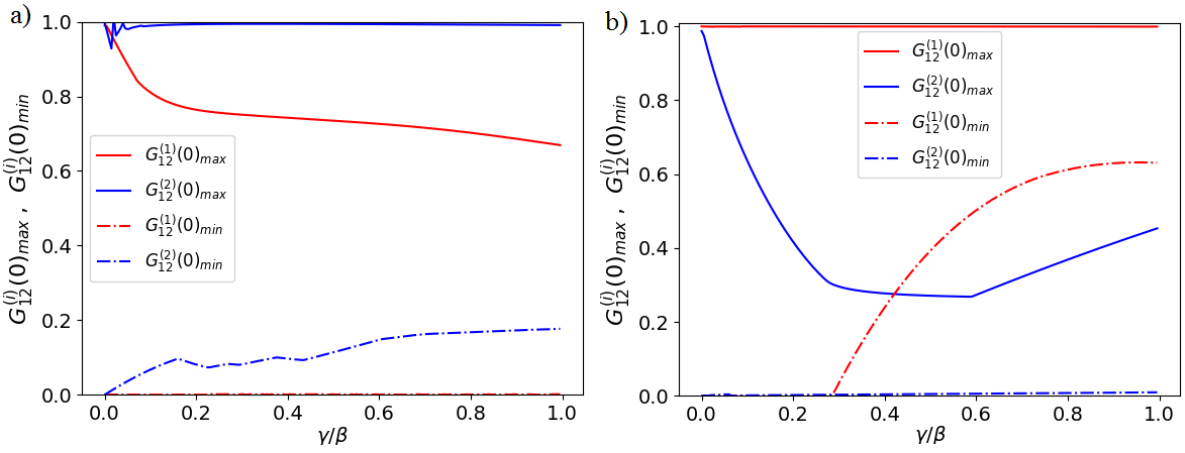

Fig. 3.6: The maximal and minimal values of $G_{12}^{(1)}(0)$ and $G_{12}^{(2)}(0)$ versus γ/β when $\omega = 5\beta$, and for two initial states: (**a**) $\hat{\rho}(t=0) = |10\rangle\langle 10|$; (**b**) $\hat{\rho}(t=0) = |01\rangle\langle 01|$.

In Fig 3.6, we show the maximal and minimal values of both $G_{12}^{(1)}(0)$ and $G_{12}^{(2)}(0)$ depend on γ/β for two cases of different initial states of the system. In the first case, the system's initial state is $\hat{\rho}(t=0) = |10\rangle\langle 10|$. Thus, it is seen that for very small values of γ/β, the maximal value of $G_{12}^{(1)}(0)$ rapidly decreases from ~ 1 to ~ 0.8 when γ/β increases from 0 to 0.1. Then it lightly decreases when we continuously increase the value of γ/β to the phase-transition point. Meanwhile, the minimal value of $G_{12}^{(1)}(0)$ is approximately equal to zero for all values of γ/β. On the side of $G_{12}^{(2)}(0)$, we also see that, for $0 < \gamma/\beta < 0.1$, the maximal value of $G_{12}^{(2)}(0)$ fluctuates between 0.928 and 0.990. For the remaining values of γ/β of the unbroken $\mathcal{PT}$-symmetry phase, the maximal value of $G_{12}^{(2)}(0)$ virtually remains at 0.994. Meanwhile, its minimal value starts from the zero, then slightly oscillates with increasing the value of γ/β from 0 to 0.5. When we continuously increase the value of γ/β to the breaking $\mathcal{PT}$-symmetry phase-transition point, the minimal value of $G_{12}^{(2)}(0)$ slightly increases from 0.114 to 0.177. For the second case ($\hat{\rho}(t=0) = |01\rangle\langle 01|$), the variations of the maxima and minima of $G_{12}^{(1)}(0)$ and $G_{12}^{(2)}(0)$ differ from those corresponding the first case of system's initial state. For such the situation, the maximal value of $G_{12}^{(1)}(0)$ tends to ~ 0.999. Meanwhile, its minimal value is approximately equal to zero when $0 < \gamma/\beta < 0.285$. If we continuously increase γ/β, the minimal value of $G_{12}^{(1)}(0)$ will gradually increase to the value of 0.630. On the side of $G_{12}^{(2)}(0)$, its maximal value rapidly decreases from 0.987 to 0.295 when γ/β increases within the range $0 < \gamma/\beta < 0.3$. If we consecutive increase the value of γ/β, the maximum of $G_{12}^{(2)}(0)$ slightly decreases to 0.268 and next, gradually increasing to 0.453.

3.3 Quantum entanglement in a bipartite $\mathcal{PT}$-symmetric model

In this section, we will discuss the bipartite quantum entanglement between two subsystems of the system. To do that, we use the definition of negativity [38]:

$$N_{12}\left(\hat{\rho}\right) = \frac{\left\|\hat{\rho}^{T_1}\right\| - 1}{2}, \tag{3.12}$$

where $\hat{\rho}^{T_1}$ is the partial transpose of $\hat{\rho}$ with respect to subsystem 1, $\hat{\rho}$ is the density matrix of the whole system, whereas $\left\|\hat{\rho}^{T_1}\right\| = \mathrm{Tr}\sqrt{\rho^{T_1}\rho^{T_1\dagger}}$ is the trace norm of $\hat{\rho}^{T_1}$.

We calculate N_{12} for four different values of γ and two different initial states of the system starting its evolution with a single excitation in one of two subsystems. It means that the initial state can only be $|10\rangle$ or $|01\rangle$. The numerical results of our calculations are represented in Figs.3.7 and 3.8. In the first scenario, the system starts its evolution when the passive cavity is excited while the active one is in the vacuum state. It means $\hat{\rho}(t=0) = |10\rangle\langle 10|$. We plot the results corresponding to this case in Fig.3.7. When

$\gamma = 0001\beta$, one can see, (Fig.3.7a) that the value of N_{12} periodically changes with time and the period of such the oscillations is approximately equal to 1.6 (in units of $1/\beta$). During the evolution, the amplitude of the negativity's oscillations slightly decreases from its maximal value that equal ~ 1 corresponding to the maximally entangled states scenario. At some moments of time, the value of N_{12} becomes equal to zero. It shows that the entanglement in our system instantly disappears at some moments during its evolution. When $\gamma = 01\beta$ (Fig.3.7b), the value of N_{12} also periodically changes in time with the period that is the same as it was in the previous case. Besides that, the maximal values of N_{12} at the first oscillation in those cases are also the same. However, there are still some differences between the two cases. Firstly, in spite of having the same period of oscillation with the previous case, the amplitude of N_{12} oscillation in this case rapidly decreases in time. Secondly, at the beginning of system's evolution, there are some moments in which the entanglement in our system disappears. However, the entanglement disappears for some short interval of time. It seems to be related to the sudden death [164, 165] and rebirth [166, 167] of entanglement. When we increase the value of γ 0.5β, we can easily see (Fig.3.7c) that the maximal value of N_{12} is much smaller than that corresponding to the previous case. After three periods of oscillations, the entanglement in the system disappears and does not appear any more – the negativity N_{12} remains very close to zero during its further evolution. For the last case, when the value of γ becomes close to the phase-transition point ($\gamma = 0.8\beta$) some special features appear. First, instead of decreasing, the maximal value of N_{12} is a little greater than what it was in the case when $\gamma = 0.5\beta$. Next, although the oscillations of N_{12} disappear after only one period of time, its value finally reaches a certain non-zero value instead of its reduction to the zero, as it did in the previous case. That means that the entanglement in our system becomes stronger when the value of γ becomes close to the phase-transition point, but it still remains in the unbroken phase of the $\mathcal{PT}$-symmetry. Moreover, the value of N_{12} becomes unchanged during its further evolution. It means that the quantum entanglement in our system is stable for the greater rate of gain/loss of energy γ. That result suggests the presence of non-zero steady-state solution for the negativity N_{12} when the value of γ/β is great enough.

In the second scenario, the system starts its evolution from the initial state $\hat{\rho}(t = 0) = |01\rangle\langle 01|$ (the active cavity is excited). For such the case we assume that $\gamma = 0.001\beta$, $\gamma = 0.1\beta$, $\gamma = 0.5\beta$, and $\gamma = 0.8\beta$. One see from Fig.3.8, that the time-evolution of the negativity strongly depends on the value of γ/β. Thus, when $\gamma = 0001\beta$, the value of N_{12} periodically changes with the same period of oscillations as for the previous scenario (Fig. 3.8a). The maximal value of N_{12} slightly decreases with time and reduces to ~ 0 for a long-time limit. However, the maximal value of N_{12} is a little smaller than it was observed in the scenario of $\hat{\rho}(t = 0) = |10\rangle\langle 10|$. Besides that, for $t = 0$, the value of N_{12} differs from zero. That means that the bipartite entanglement in the system appears at the beginning of its evolution. Next, when we assume $\gamma = 0.1\beta$, we can see that the value of N_{12} also periodically changes with the same period of oscillations as for the previous case (Fig.3.8b). However, now, the amplitude of N_{12} oscillations decreases faster than previously, when $\gamma = 0.001\beta$. For the third case, when $\gamma = 0.5\beta$, the maximal value of

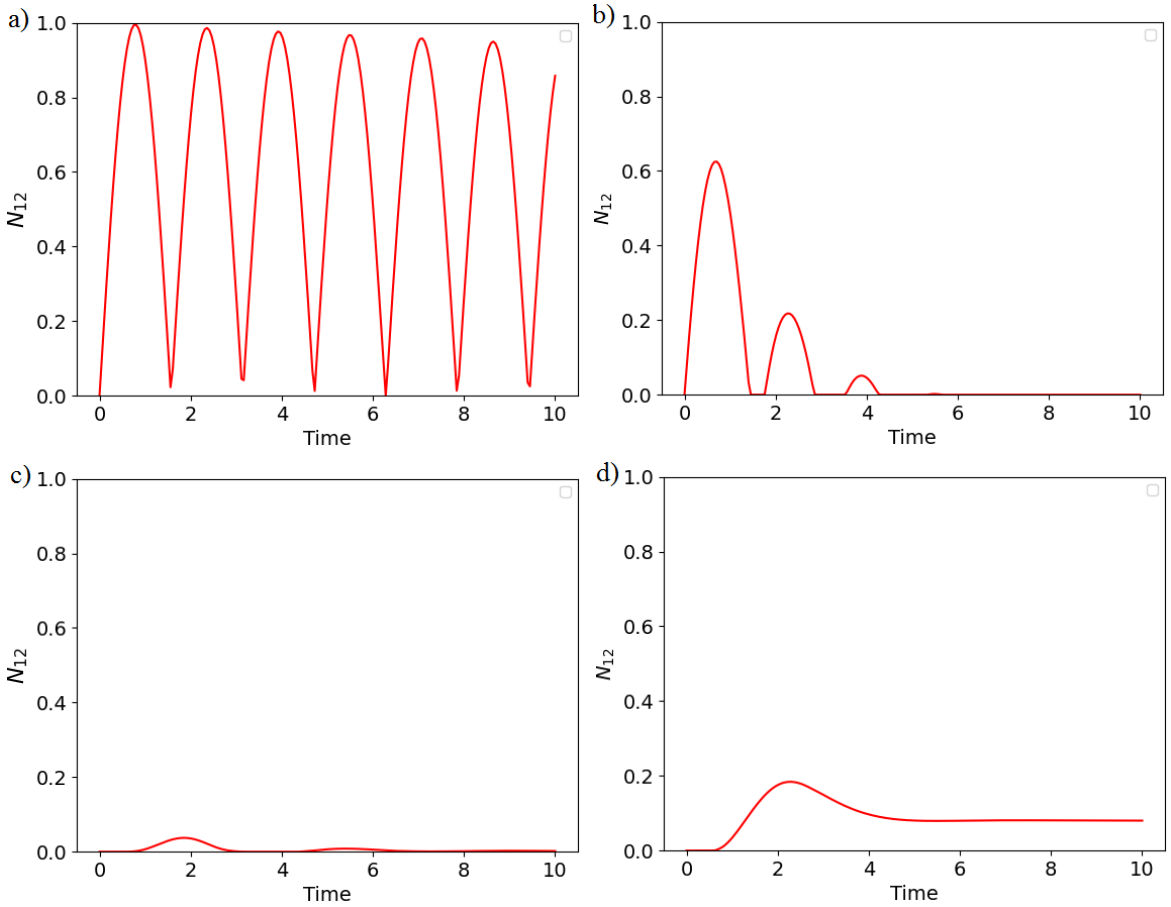

Fig. 3.7: The time evolution of the negativity N_{12} for the initial state $\hat{\rho}(t=0) = |10\rangle\langle 10|$ and $\gamma = 0.001\beta$ (a); $\gamma = 0.1\beta$ (b); $\gamma = 0.5\beta$ (c); $\gamma = 0.8\beta$ (d). Time is scaled in $1/\beta$ units.

N_{12} is much smaller than previously. One can see that after reaching its first maximum, the entanglement practically disappears – only one negligible maximum appears during the further evolution (Fig.3.8c). For the last case, when $\gamma = 0.8\beta$ (see Fig.3.8d), the value of N_{12} firstly increases from the zero and next, after some variations tends to some non-zero final value. Such behavior differs from those observed for the other values of γ.

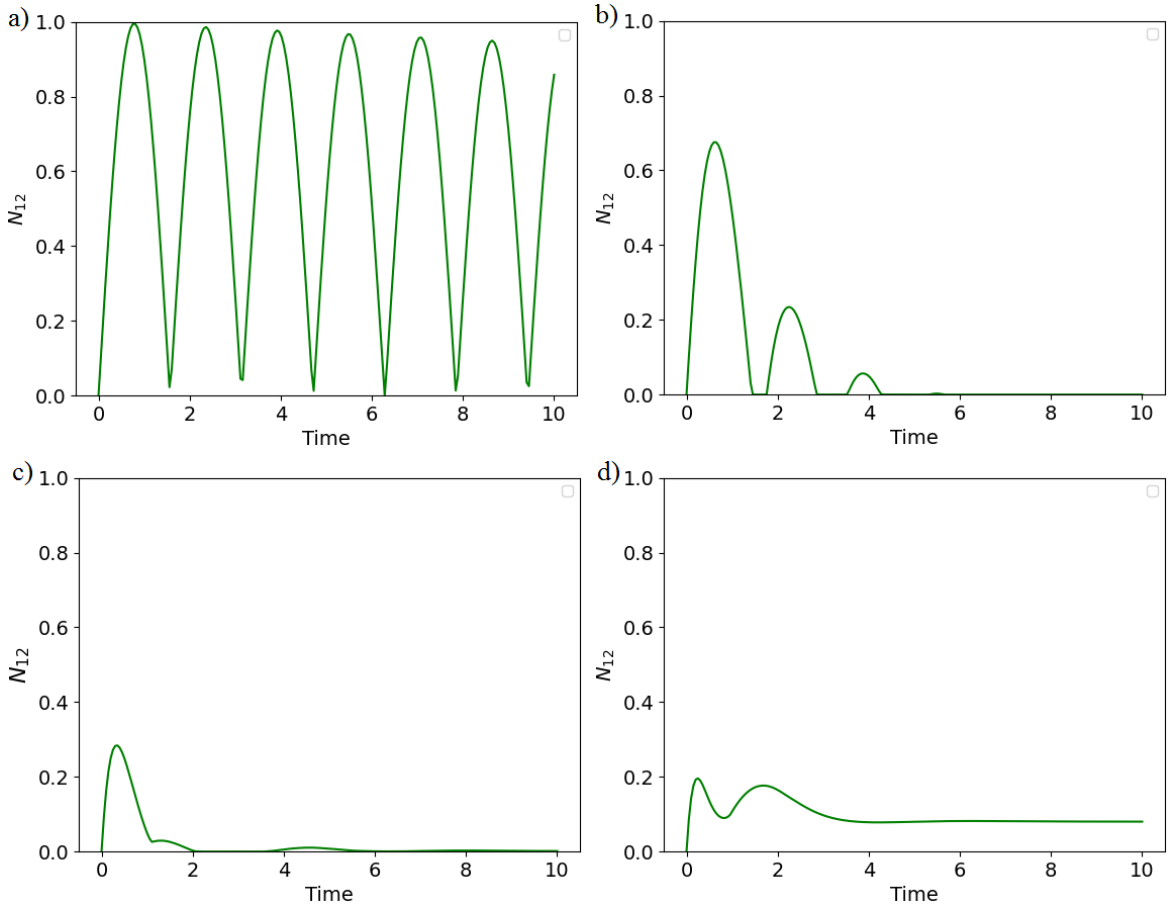

Fig. 3.8: The time evolution of the negativity N_{12} for initial state $\hat{\rho}(t=0) = |01\rangle\langle 01|$ and $\gamma = 0.001\beta$ (a); $\gamma = 0.1\beta$ (b); $\gamma = 0.5\beta$ (c); $\gamma = 0.8\beta$ (d). Time is scaled in $1/\beta$ units.

In Fig.3.9, we show how the maximal value of N_{12} depends on γ/β for the two cases of the system's initial state. Indeed, one can see that the maximal value of N_{12} is strongly γ/β dependent. When we assume that initially the active cavity is excited, the bipartite entanglement in the system is much stronger than for the case when the excitation was in the passive cavity. For very small values of γ/β, the maximal values of N_{12} in both two cases of system's initial state are approximately equal to 1. For the case in which the initial state of the system is $\hat{\rho}(t=0) = |10\rangle\langle 10|$, when we increase the value of γ/β, the maximal value of N_{12} firstly decreases, and then reaches its smallest value when

$\gamma/\beta \simeq 0.463$. If we continue increasing the value of γ/β from that point, the maximal value of N_{12} starts to increase again. Such increasing is approximately linear with γ/β.

For the case when the initial state of our system is $\hat{\rho}(t = 0) = |01\rangle\langle 01|$, when we increase the value of γ/β, the maximal value of N_{12} also decreases. However, in this case, such decreasing is slower than it was in the previously discussed case. Nevertheless, after reaching its smallest value at $\gamma/\beta \simeq 0.817$, it increases linearly up to the point corresponding to the phase-transition point.

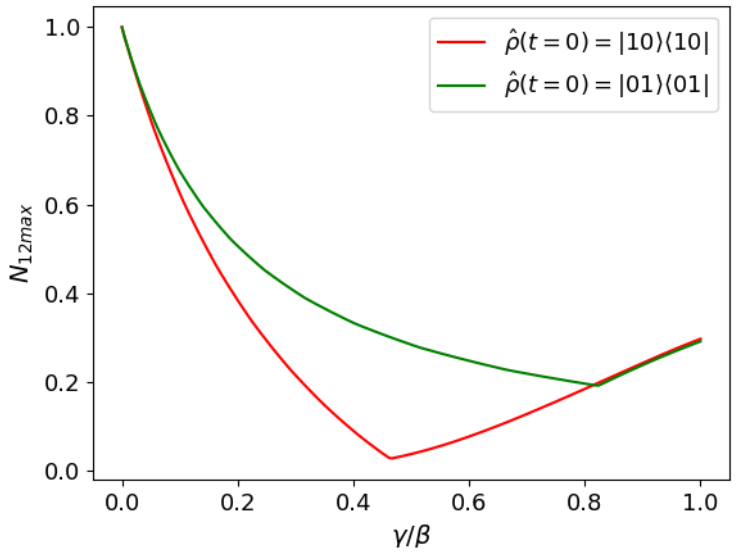

Fig. 3.9: Maximal values of N_{12} versus γ/β for $\omega = 5\beta$, and for two different initial states.

As we see from Fig.3.7d and Fig.3.8d, the value of bipartite negativity N_{12} tends to a steady-state final value, when the value of γ/β becomes close to the phase-transition point. Thus, in Fig.3.10, we show the dependence of the steady-solution of N_{12} on γ/β. We can easily see that, for small values of γ/β, obtained steady-solution of bipartite entanglement in our system is approximately equal to zero for $0 < \gamma/\beta < 0.4$. However, for greater values of γ/β ($0.4 < \gamma/\beta < 1$), the negativity N_{12} starts increasing. Interestingly, the closer to the phase-transition point we are, the greater value of $N_{12}$is achieved. Nevertheless, its final value is not very large ($N_{12} \simeq 0.3$)

3.4 Quantum steering in a bipartite $\mathcal{PT}$-symmetric model

In this section, we concentrate on the quantum steering generation in the system. To determine whether the steering appears and to determine its relative strength, we apply the steering parameter proposed by Cavalcanti *et.al.* [45,168]. It can be calculated with

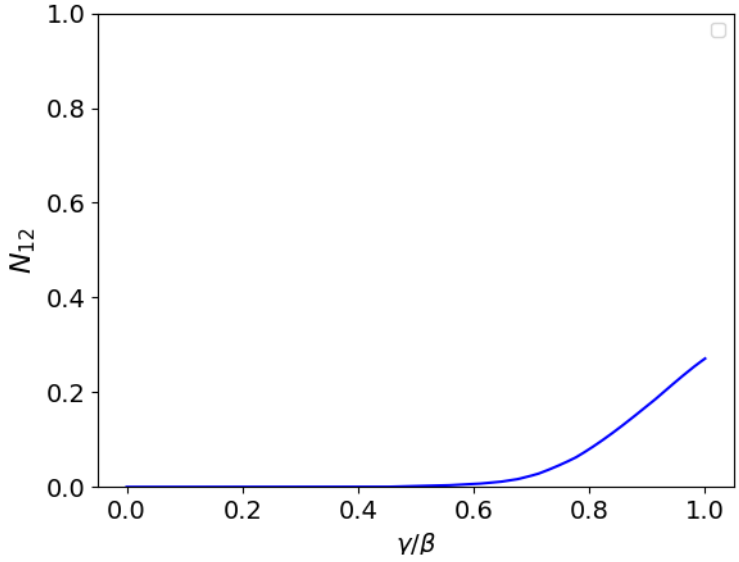

Fig. 3.10: Steady-state values of the negativity N_{12} versus the value of γ/β when $\omega = 5\beta$.

the use of following expression:

$$S_{jk} = \left|\left\langle \hat{a}_j \hat{a}_k^\dagger \right\rangle\right|^2 - \left\langle \hat{a}_j \hat{a}_j^\dagger \left(\hat{a}_k \hat{a}_k^\dagger + \frac{1}{2} \right) \right\rangle = \left\langle \hat{a}_j \hat{a}_k^\dagger \right\rangle \left\langle \hat{a}_j^\dagger \hat{a}_k \right\rangle - \left\langle \hat{a}_j \hat{a}_j^\dagger \left(\hat{a}_k \hat{a}_k^\dagger + \frac{1}{2} \right) \right\rangle, \tag{3.13}$$

where $\hat{a}_j^\dagger$ and $\hat{a}_k^\dagger$ ($\hat{a}_j$ and $\hat{a}_k$) are creation (annihilation) operators corresponding to modes j and k ($j, k = 1, 2$). For the cases considered here we will discuss the steering effects between two qubits, When the parameter S_{jk} is positive, the qubit k steers qubit j. When we perform the mutual replacement of the indices i and j, the parameter S_{ji} describes the steering in the opposite direction.

The same as previously, we will concentrate on the two cases. For the first one, only the passive cavity is excited, and thus, the evolution of the considered system starts from the state $\hat{\rho}(t = 0) = |10\rangle\langle 10|$. From Fig.3.11 one can see that the time-evolution of steering parameters strongly depends on the value of γ. When $\gamma = 0.001\beta$ (Fig.3.11a), at the beginning of the system's evolution, only the steering parameter S_{21} increases reaching positive values while S_{12} is negative. It means that, at the beginning of system's evolution, the steerable states can be generated, and only passive cavity can steers the active one. The value of parameter S_{21} initially increases to its maximal value, and next, decreases to become finally negative. When it starts to be negative, the parameter S_{12} take its turn to be positive. It means that the steering ability in the opposite direction occurs when the steering in the direction $1 \to 2$ disappears. Here, we remind that notation $i \longrightarrow j$ means that subsystem i steers subsystem j. The parameter S_{12} also increases to its maximal value and then disappears in the same way as S_{21} did. The maximal values of S_{12} and S_{21} are approximately the same. After one period of steering for each subsystem, the quantum state becomes unsteerable for a short interval of time. We call this time redirect time because after this interval of time, the order of steering

ability of the cavities will be inverse. The redirect time increases after each steering period. When we increase the value of γ to $\gamma = 0.01\beta$ (see Fig.3.11b) and perform the same analysis, we see that the sequence of steering direction seems to be the same as in the previous case. The maximal values of S_{12} and S_{21} are still approximately the same for the each of periods of steering. However, those maximal values also decrease in time. Finally, after sufficiently long period of time all stirring effects completely disappear.

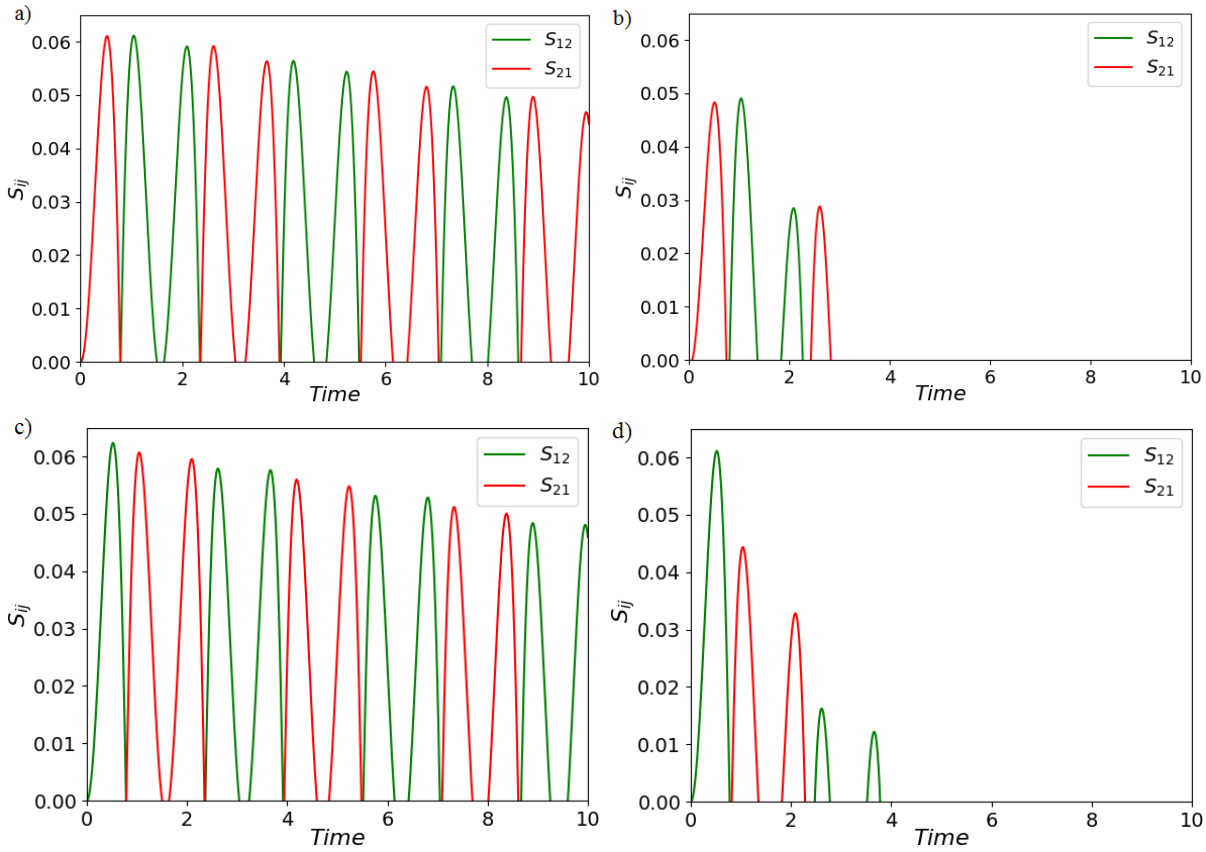

Fig. 3.11: The time evolution of the steering parameters S_{ij}: (**a**) $\hat{\rho}(t=0) = |10\rangle\langle 10|$, $\gamma = 0.001\beta$; (**b**) $\hat{\rho}(t=0) = |10\rangle\langle 10|$, $\gamma = 001\beta$; (**c**) $\hat{\rho}(t=0) = |01\rangle\langle 01|$, $\gamma = 0.001\beta$; (**d**) $\hat{\rho}(t=0) = |01\rangle\langle 01|$, $\gamma = 0.01\beta$. Time is scaled in $1/\beta$ units. We plot only positive values of the parameters.

In the second scenario, our system starts from the state $\hat{\rho}(t=0) = |01\rangle\langle 01|$ (only the active cavity is excited). As in the previous scenario, the evolution of S_{12} and S_{21} strongly depends on the value of γ/β (see Figs.3.11c and 3.11d). When $\gamma = 0.001\beta$ (Fig.3.11c), the steering $2 \longrightarrow 1$ appears as the first one. The value of S_{12} increases to its maximum and then, decreases and becomes negative. After a very short redirect time, the steering in the opposite direction reappears. Then, two subsequent maxima of decreasing heights are visible. In such the case, the maximal value of S_{21} is smaller than that for S_{12}. The maximal values of S_{21} and S_{12} also decrease with time. However, the way in which the decrease differs from that observed it in the previous scenario.

When we increase the value of γ to $\gamma = 0.01\beta$, the steering in the direction $2 \longrightarrow 1$ still appears first. The maximal value of S_{12} is just a little smaller than for the previous case, however, the maximal value of S_{21} is much smaller now. Besides that, after several appearances of the steering, it becomes very weak and then, disappear completely.

Finally, in Fig.3.12, we show how the maximal values of steering parameters S_{ij} depend on the ratio γ/β. Here, we also consider two scenarios of various initial states. For the first case, the passive cavity is initially excited, while the active one is in a vacuum state (Fig.3.12a). We can see that the both paramerts evolwe along the same paths and maximal values of S_{12} and S_{21} are positive only for very small values of γ/β and evolve along the same lines. They decrease linearly up to the point where γ/β is approximately equal to 0.052, and the maximal values of S_{12} and S_{21} become negative. That means that the steering disappears for both directions $2 \longrightarrow 1$ and $1 \longrightarrow 2$ when $\gamma/\beta > 0.052$. So, again, we see that the steering in two directions evolve approximately in the same way.

For the second case, when only the active cavity is excited one (Fig.3.12b), we see that the behavior of the steering differs from that described above. First, we see that the two steerings in two directions differ each other. Moreover, passive cavity can steer the active one only for the very small values of γ/β ($0 < \gamma/\beta < 0.035$). The steering in the opposite direction, from the active cavity to the passive one, appears for all the values of γ/β corresponding to the unbroken phase of $\mathcal{PT}$-symmetry. Next, for all the values of γ/β, for which the steering is achievable for two opposite directions, the steering from the active cavity to the passive one is always much stronger than that acting in the opposite direction. It is should also be emphasized that for $0 < \gamma/\beta < 0.035$, the steering between subsystems is asymmetric. For the remaining values of γ/β in the unbroken phase of $\mathcal{PT}$-symmetry, the steering between subsystems is a one-way steering.

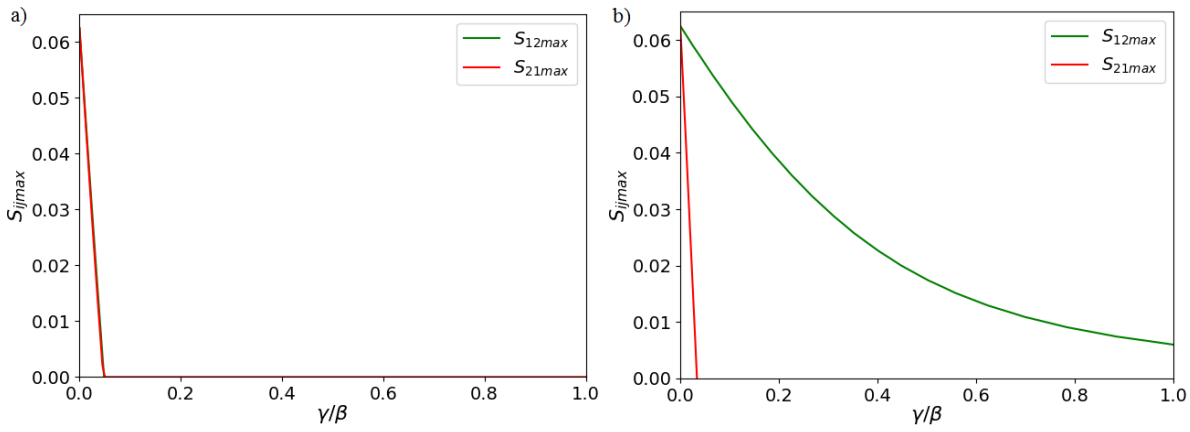

Fig. 3.12: Maximal values of the steering parameters S_{ij} versus γ/β when $\omega = 5\beta$ and for two initial states: (**a**) $\hat{\rho}(t=0) = |10\rangle\langle 10|$; (**b**) $\hat{\rho}(t=0) = |01\rangle\langle 01|$.

3.5 Summary

In this chapter, we considered the model of a bipartite $\mathcal{PT}$-symmetric system that consists of two oscillators located in two cavities with the balance between the gain and loss of energy. The cavities are coupled each other by a linear coupling. We have found the conditions determining where the phase-transition point of $\mathcal{PT}$-symmetry appears. We have concentrated to such values of the parameters for which the $\mathcal{PT}$-symmetry is unbroken

Next, we discussed various types of quantum correlations appearing in our model as follows:
First, we calculated the first- and the second-order correlation function with zero time delay and showed that we always achieve partial coherence in the system. The level of partial coherence in the system strongly depends on the rate of gain/loss of energy. For small rates of gain/loss of energy, the system rapidly changes its behavior between mostly full coherent and incoherent one. When the rate of energy gain/loss increases, the level of partial incoherence appearing in the system gradually decreases. The most interesting results are those concerning the situation when all the parameters correspond to the unbroken phase of $\mathcal{PT}$-symmetry. Fore such the case the level of coherence appearing in the system will be stable for the long-time regime. Moreover, the higher value of energy gain/loss is, one can achieve the higher level of the coherence for the stable-time regime. Such value does not change a lot, even when a nonlinear coupling is added. The presented results differ from those considered in our article [169].

Next, we continued to discuss the quantum entanglement in our model. to determine that, we have calculated the negativity N_{12}. We have shown that the entanglement between two subsystems strongly depends on the rate of energy gain/loss. For very small values of the rate of energy gain/loss, the strength of entanglement periodically changes, and finally disappears after sufficiently long period of time. When we increase that rate, the disappearance of entanglement occurs faster. However, if we increase the value of the rate of he energy gain/loss hat is close to the phase-transition point, the entanglement between subsystems tends to be its stable nonzero value. The higher is the value of the rate of energy gain/loss, the higher level of entanglement appears in the system. The mentioned here results have been published in [170].

Finally, we discussed quantum steering in our model. to do that, we have found the quantum steering parameters S_{12} and S_{21} that respectively shows the steering possibility in the direction from the active cavity to the passive one and in the opposite direction. The results showed that, depending of the parameters describing the system, the steering between subsystems can be a one-way steering, symmetric steering and finally, asymmetric steering. The kind of the steering that appears in the system does not depend on the rate of energy gain/loss, but also on the initial state of our system. For very small rates of energy gain/loss, the active and passive cavity alternately take their turn to steer the other one in time. The higher value of the rate of energy gain/losses assumed, the faster disappearance of steering can be achieved. If the

system is initially excited only in the passive cavity, the steerings between two cavities are approximately the same. For the second scenario, the steering ability of the active cavity is stronger than that corresponding to that passive one. The results presented her have been published in the article [171]

In the next chapter, we will continue the discussion of quantum correlation, but for the model involving three cavities interacting each other.

Chapter 4

Quantum correlations in tripartite $\mathcal{PT}$-symmetric models

4.1 The tripartite model of the $\mathcal{PT}$-symmetric system

In this chapter, we continue our discussion concerning quantum correlations in a model of linearly coupled cavities. Contrary to the previous chapter, the model considered here involves three cavities instead of two. Two of them directly interact with an external environment by the gain/loss of energy, and interact with a neutral cavity that is located between them. We will consider the general case in which the active and passive cavity also can interact to each other (a triangle configuration), and then, the special case in which the active and passive cavity do not interact to each other (a linear system).

In the general case, the system consists of three different cavities. The first cavity (labeled by 1) and the third one (labeled by 3) directly exchange the energy with an external environment. They are active cavity (cavity 1) and passive one (cavity 3) with the rates of the gain (γ_1) and loss (γ_2) of energy, respectively. The other cavity (labeled by 2) that does not exchange energy with the external environment is called a neutral one. Both three cavities interact with each other in which the interaction between the active and passive cavities is much smaller than the interaction between the other pairs of cavities. Thus, the Hamiltonian describing the system can be written as follows

$$\begin{aligned} \hat{H} &= (\omega - i\gamma_1)\,\hat{a}_1^\dagger \hat{a}_1 + \omega \hat{a}_2^\dagger \hat{a}_2 + (\omega + i\gamma_2)\,\hat{a}_3^\dagger \hat{a}_3 \\ &+ \beta\left(\hat{a}_1^\dagger \hat{a}_2 + \hat{a}_2^\dagger \hat{a}_1 + \hat{a}_2^\dagger \hat{a}_3 + \hat{a}_3^\dagger \hat{a}_2\right) + \chi\left(\hat{a}_1^\dagger \hat{a}_3 + \hat{a}_3^\dagger \hat{a}_1\right), \end{aligned} \tag{4.1}$$

where $\hat{a}_j^\dagger$ and $\hat{a}_j$ (j=1,2,3) are the bosonic creation and annihilation operators of the j-th cavity, χ characterizes the strength of interaction between the passive and active cavities while β describes the strength of interaction between the neutral cavity and the others. So, we assume that $\chi \ll \beta$. All oscillators representing three cavities are assumed to have the same resonance frequency ω. We also assume that our system achieves a balance between the gain and loss of energy. It means that $\gamma_1 = \gamma_2 = \gamma$. For such a case, the system will be $\mathcal{PT}$-symmetric, and the Hamiltonian (4.1) can be

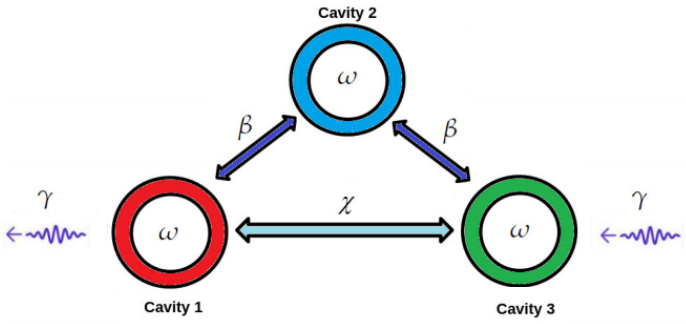

Fig. 4.1: Schematic illustration of a tripartite $\mathcal{PT}$-symmetric system. The cavities are labeled as 1 (active), 2 (neutral) and 3 (passive).

expressed in the matrix form:

$$\hat{H} = \begin{pmatrix} \hat{a}_1^\dagger & \hat{a}_2^\dagger & \hat{a}_3^\dagger \end{pmatrix} \begin{pmatrix} \omega - i\gamma & \beta & \chi \\ \beta & \omega & \beta \\ \chi & \beta & \omega + i\gamma \end{pmatrix} \begin{pmatrix} \hat{a}_1 \\ \hat{a}_2 \\ \hat{a}_3 \end{pmatrix} = \begin{pmatrix} \hat{a}_1^\dagger & \hat{a}_2^\dagger & \hat{a}_3^\dagger \end{pmatrix} \hat{\mathcal{H}} \begin{pmatrix} \hat{a}_1 \\ \hat{a}_2 \\ \hat{a}_3 \end{pmatrix}. \tag{4.2}$$

For a certain set of values of parameters, there will be an exceptional point called phase-transition point that separates two different phases of $\mathcal{PT}$-symmetry. In the first phase, all the eigenvalues of the Hamiltonian $\hat{\mathcal{H}}$ are real, and the system is in the unbroken phase of $\mathcal{PT}$-symmetry. In the opposite case, there is an existence of imaginary eigenvalues of Hamiltonian $\hat{\mathcal{H}}$, and the system will be in the broken phase of $\mathcal{PT}$-symmetry. Thus, Fig.4.2 shows that the sum of absolute values of eigenvalues's imaginary parts (λ). We can see that it strongly depends on the values of γ/β and χ/β. The system will be in the unbroken phase of $\mathcal{PT}$-symmetry if all the eigenvalues are real. It mean the absolute value of all the eigenvalue's imaginary parts have to be zero. Therefore, it is easy to realize (see Fig.4.2) that our system will be in the unbroken phase of $\mathcal{PT}$-symmetry if the interaction between the active and passive cavity is weak, and the rate of gain/loss energy is small enough.

The Fig.4.3 again depicts the sum of imaginary parts of the Hamiltonian's eigenvalues as a function of γ/β but for $\omega = 5\beta$. We consider here three cases when $\chi/\beta = \{0.01, 0.05, 0.1\}$. When $\chi = 0.01\beta$, the phase-transition point is located at $\gamma \simeq 1.363\beta$. When $\chi = 0.05\beta$, it can be found at $\gamma \simeq 1.267\beta$, whereas when $\chi = 0.1\beta$, its position moves to $\gamma \simeq 1.165\beta$.

Because our system exchanges energy with external environment, we describe its state by a density matrix $\hat{\rho}(t) = |xyz\rangle\langle xyz|$, where $|xyz\rangle = |x\rangle \otimes |y\rangle \otimes |z\rangle$. Here, the same as in the previous chapter we are interested in the phase for which the $\mathcal{PT}$-symmetry is unbroken. So, for such the case, we follow the ideas presented in [162] and [163], and describe its evolution with the application of the following master equation:

$$\frac{d}{dt}\hat{\rho}(t) = \frac{1}{i}\left[\hat{H}_0, \hat{\rho}(t)\right] + \hat{\mathcal{L}}\hat{\rho}(t), \tag{4.3}$$

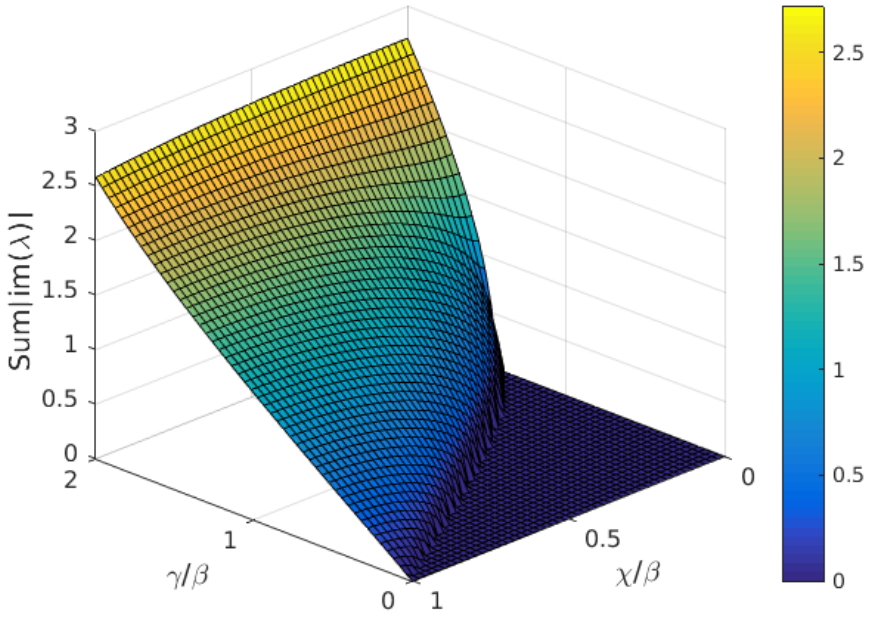

Fig. 4.2: The sum of imaginary parts of the Hamiltonian's eigenvalues as function of γ/β and χ/β when $\omega = 5\beta$.

where $\hat{H}_0$ is the Hamiltonian of the system neglecting the exchange energy with surrounding environment

$$\hat{H}_0 = \omega\left(\hat{a}_1^\dagger\hat{a}_1 + \hat{a}_2^\dagger\hat{a}_2 + \hat{a}_3^\dagger\hat{a}_3\right) + \beta\left(\hat{a}_1^\dagger\hat{a}_2 + \hat{a}_2^\dagger\hat{a}_3 + H.c\right) + \chi\left(\hat{a}_1^\dagger\hat{a}_3 + \hat{a}_3^\dagger\hat{a}_1\right), \tag{4.4}$$

$\hat{\mathcal{L}}$ is Liouvillian superoperator that acts on the density matrix $\hat{\rho}(t)$ as follows

$$\hat{\mathcal{L}}\hat{\rho}(t) = \gamma\left[\left(2\hat{a}_1\hat{\rho}(t)\hat{a}_1^\dagger - \hat{a}_1^\dagger\hat{a}_1\hat{\rho}(t) - \hat{\rho}(t)\hat{a}_1^\dagger\hat{a}_1\right) + \left(2\hat{a}_3^\dagger\hat{\rho}(t)\hat{a}_3 - \hat{a}_3\hat{a}_3^\dagger\hat{\rho}(t) - \hat{\rho}(t)\hat{a}_3\hat{a}_3^\dagger\right)\right] \tag{4.5}$$

For the special case mentioned above, when the first and the third cavities do not intereact each other directly, the value of χ appearing in (4.1) is equal to zero. As a result, the Hamiltonian that describes the system takes the following form [138]

$$\hat{H} = (\omega - i\gamma)\,\hat{a}_1^\dagger\hat{a}_1 + \omega\hat{a}_2^\dagger\hat{a}_2 + (\omega + i\gamma)\,\hat{a}_3^\dagger\hat{a}_3 + \beta\left(\hat{a}_1^\dagger\hat{a}_2 + \hat{a}_2^\dagger\hat{a}_1 + \hat{a}_2^\dagger\hat{a}_3 + \hat{a}_3^\dagger\hat{a}_2\right). \tag{4.6}$$

In this case, the Hamiltonian H_0 in (4.3) can be written as follows

$$\hat{H}_0 = \omega\left(\hat{a}_1^\dagger\hat{a}_1 + \hat{a}_2^\dagger\hat{a}_2 + \hat{a}_3^\dagger\hat{a}_3\right) + \beta\left(\hat{a}_1^\dagger\hat{a}_2 + \hat{a}_2^\dagger\hat{a}_3 + H.c\right). \tag{4.7}$$

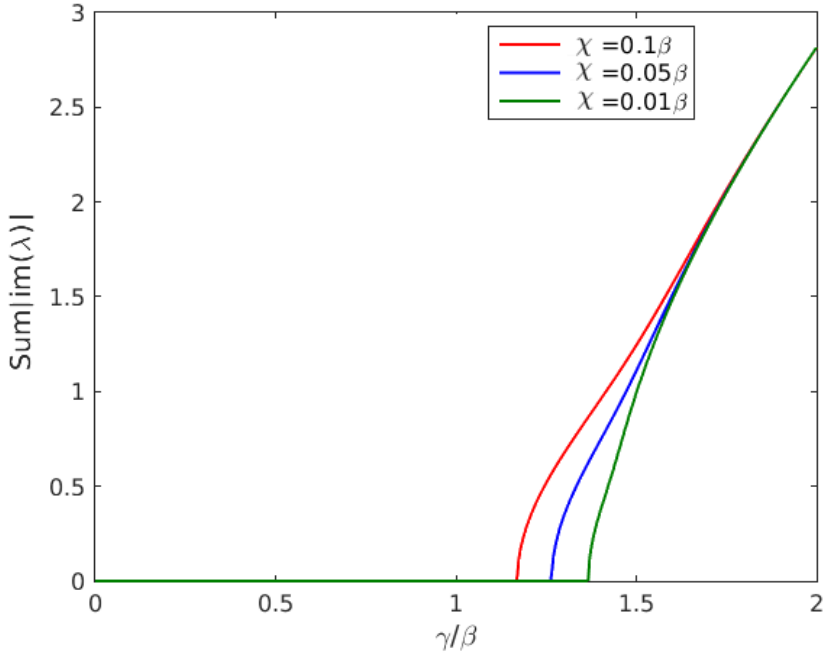

Fig. 4.3: The same as in Fig.4.2 but for $\omega = 5\beta$ and various values of χ/β.

The same as previously, one can rewrite the Hamiltonian (4.6) in the matrix form:

$$\hat{H} = \begin{pmatrix} \hat{a}_1^\dagger & \hat{a}_2^\dagger & \hat{a}_3^\dagger \end{pmatrix} \begin{pmatrix} \omega - i\gamma & \beta & 0 \\ \beta & \omega & \beta \\ 0 & \beta & \omega + i\gamma \end{pmatrix} \begin{pmatrix} \hat{a}_1 \\ \hat{a}_2 \\ \hat{a}_3 \end{pmatrix}. \tag{4.8}$$

Thus, the eigenvalues' equation of the Hamiltonian takes the form

$$X = \begin{vmatrix} \omega - i\gamma - E_n & \beta & 0 \\ \beta & \omega - E_n & \beta \\ 0 & \beta & \omega + i\gamma - E_n \end{vmatrix} = 0, \tag{4.9}$$

where E_n are eigenvalues of $\hat{H}$. We can rewrite the left hand side of equation (4.9) as following

$$\begin{aligned} X &= (\omega - E_n) \begin{vmatrix} \omega - i\gamma - E_n & 0 \\ 0 & \omega + i\gamma - E_n \end{vmatrix} - \beta \begin{vmatrix} \beta & \beta \\ 0 & \omega + i\gamma - E_n \end{vmatrix} - \beta \begin{vmatrix} \omega + i\gamma - E_n & 0 \\ \beta & \beta \end{vmatrix} \\ &= (\omega - E_n) \left[(\omega - i\gamma) - E_n \right] \left[(\omega + i\gamma) - E_n \right] - 2\beta^2 (\omega - E_n) \\ &= (\omega - E_n) \left[(\omega - i\gamma)(\omega + i\gamma) - E_n (\omega + i\gamma + \omega - i\gamma) + E_n^2 \right] - 2\beta^2 (\omega - E_n) \\ &= (\omega - E_n) \left[\omega^2 + \gamma^2 - 2\omega E_n + E_n^2 \right] - 2\beta^2 (\omega - E_n) \\ &= (\omega - E_n) \left[E_n^2 - 2\omega E_n + \omega^2 + \gamma^2 - 2\beta^2 \right]. \end{aligned}$$

Thus, we can solve the equation (4.9) and get the following eigenvalues of the Hamiltonian:

$$E_1 = \omega, \tag{4.10}$$

$$E_2 = \omega + \sqrt{2\beta^2 - \gamma^2}, \tag{4.11}$$

and

$$E_3 = \omega - \sqrt{2\beta^2 - \gamma^2}. \tag{4.12}$$

We can see that when $2\beta^2 > \gamma$, the eigenvalues' spectrum is real, and the system is in the unbroken $\mathcal{PT}$-symmetric phase. When $2\beta^2 < \gamma$, the symmetry becomes broken, and the eigenvalues become complex with non-zero imaginary parts

$$E_1 = \omega, \tag{4.13}$$

$$E_2 = \omega + i\sqrt{\gamma^2 - 2\beta^2}, \tag{4.14}$$

$$E_3 = \omega - i\sqrt{\gamma^2 - 2\beta^2}. \tag{4.15}$$

The point for which $2\beta^2 = \gamma$ is the phase-transition point. At this point, the only one eigenvalue of Hamiltonian exist and is $E = \omega$. The dependence of eigenvalue spectrum on the ratio between γ and β is illustrated in Fig. 4.4.

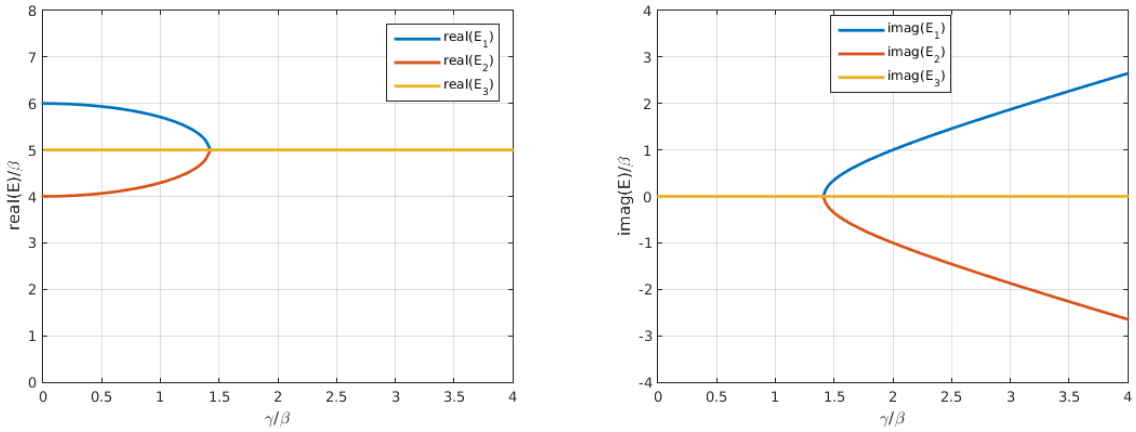

Fig. 4.4: The dependence of real and imaginary parts of the eigenvalues in on γ/β when $\omega = 5\beta$ and $\chi = 0$.

In the following sections, we discuss the quantum entanglement and steering appearing in our system for the case in which the $\mathcal{PT}$-symmetry is not broken. That means that the values of γ and β will be assumed so that the condition $2\beta^2 > \gamma$ is always satisfied.

4.2 Quantum entanglement in tripartite $\mathcal{PT}$-symmetric models

In this section, we will concentrate on the quantum entanglement. We start our consideration from the general model in which the direct interaction between the active

and passive cavities is present. To find the evolution of the system, we solve equation (4.3) assuming some initial states of the system corresponding to the situation when only one of three cavities is excited while the others are in the vacuum states, *i.e.*, $\hat{\rho}(0) = |100\rangle\langle 100|$, $\hat{\rho}(0) = |010\rangle\langle 010|$ or $\hat{\rho}(0) = |001\rangle\langle 001|$.

Analogously to the previous chapter concerning the system involving two cavities, to quantify the bipartite entanglement in the system we apply the negativity already introduced in equation 3.12 As we deal here with the tripartite system, it can be adapted for our purposes and written as:

$$N_{ij}\left(\hat{\rho}_{ij}\right) = \frac{\left\|\hat{\rho}_{ij}^{T_i}\right\| - 1}{2}, \tag{4.16}$$

where $\hat{\rho}_{ij}^{T_i}$ is the partial transpose of $\hat{\rho}_{ij}$ with respect to subsystem i, $\hat{\rho}_{ij}$ is the reduced density matrix of the whole density matrix $\hat{\rho}$, and $\left\|\hat{\rho}_{ij}^{T_i}\right\|$ shows the trace norm of $\hat{\rho}_{ij}^{T_i}$. Thus, N_{ij} that shows the strength of entanglement between subsystems i and j. It should be noted that the density matrix $\hat{\rho}_{ij}$ is a reduced one, and can be obtained by tracing out of the third subsystem from the full density matrix $\hat{\rho}_{ijk}$ describing the whole system. For the model considered here we calculate the bipartite negativities between three different pairs of the cavities, N_{12}, N_{23}, and N_{13}.

Here, we focus only on the case when $\chi = 0.1\beta$, and then, the corresponding phase-transition point is $\gamma = 1.165\beta$. The chosen values of γ are $\gamma = 0001\beta$, $\gamma = 001\beta$, $\gamma = 01\beta$ and $\gamma = 08\beta$. It is easy to see that, for all assumed here values of γ, the $\mathcal{PT}$-symmetry is not broken. For each of the values of γ/β, we consider three different scenarios corresponding to the different system's initial state. The results are shown in the subsequent figures.

In the first scenario, the system starts its evolution from the state in which only the active cavity is excited. It means that the density matrix $\hat{\rho}(0) = |100\rangle\langle 100|$. From Fig.4.5 one can see, that the entanglement between subsystems strongly depends on the value of γ/β. In other words, the entanglement between two subsystems strongly directly depends on the rate of gain/loss energy γ and the coupling strength between subsystems as long as the balance between gain and loss is preserved, and the condition for the unbroken phase of $\mathcal{PT}$-symmetry is still fulfilled. When $\gamma/\beta = 0.001$, at the beginning of the system's evolution, the negativities corresponding to the entanglement between $1 \leftrightarrow 3$ and $2 \leftrightarrow 3$, start their evolution from zero, while some amount of the entanglement $1 \leftrightarrow 2$ is already present for that time(see Fig.4.5a). Next, N_{12} and N_{23} periodically change in time with the same period of oscillation, and their amplitudes for each period of such oscillations are approximately the same, and decrease after sufficiently long time to the value close to zero. Meanwhile, although N_{13} also periodically changes in time, the period of its oscillations is smaller than that of N_{12} and N_{23}. On the other hand, the amplitude of its oscillations increases in time instead of decreasing as we observed for N_{12} and N_{23}. Moreover, although N_{12} and N_{23} do not reach their maximal values at the same moment of time, they get their minima simultaneously. We can see that the entanglement $1 \leftrightarrow 3$ in this case is even stronger than those denoted between the

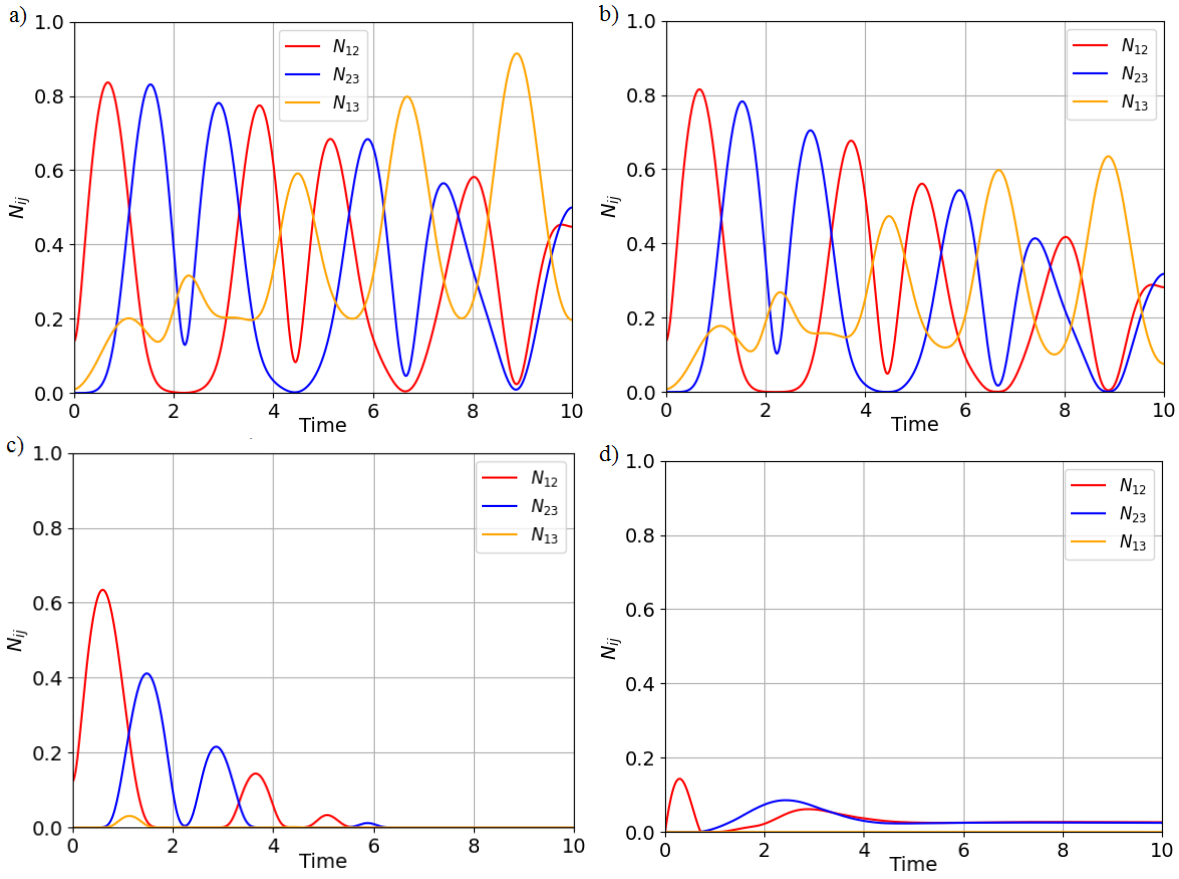

Fig. 4.5: The time evolution of negativities N_{ij} for (**a**) $\gamma = 0.001\beta$; (**b**) $\gamma = 0.01\beta$; (**c**) $\gamma = 0.1\beta$; (**d**) $\gamma = 0.8\beta$ when the initial state is $\hat{\rho}(t=0) = |100\rangle\langle 100|$, $\omega = 5\beta$, $\chi = 0.1\beta$. Time is scaled in $1/\beta$ units.

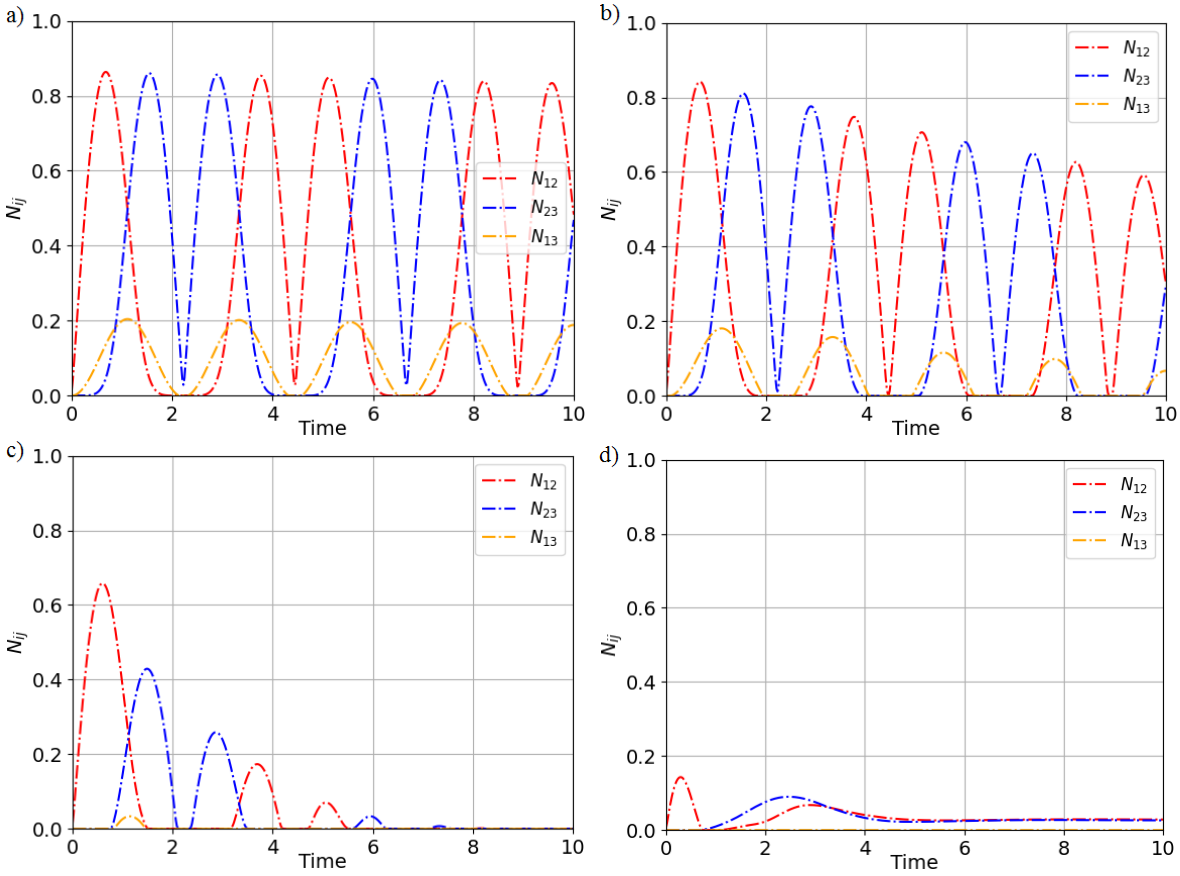

Fig. 4.6: The time evolution of negativities N_{ij} for (**a**) $\gamma = 0.001\beta$; (**b**) $\gamma = 0.01\beta$; (**c**) $\gamma = 0.1\beta$; (**d**) $\gamma = 0.8\beta$ when the initial state is $\hat{\rho}(t=0) = |100\rangle\langle 100|$, $\omega = 5\beta$, $\chi = 0$. Time is scaled in $1/\beta$ units.

pairs $1 \leftrightarrow 2$ and $2 \leftrightarrow 3$. The maximal values of N_{12} and N_{23} are approximately equal to 0.82 while the maximal value of N_{13} is approximately equal to 0.91. Interestingly, after several periods of oscillations, the value of N_{13} tends to reach its maximum, whereas the values of N_{12} and N_{23} are minimal. Besides that, N_{13} will is minimal when N_{12} and N_{23} have the same values. When $\gamma/\beta = 0.01$ (Fig.4.5b) all the negativities N_{12}, N_{23}, and N_{13} still periodically change in time. The periods of their oscillations are the same as those in the previous case. However, now, the amplitude of oscillations decrease faster in time. Besides that, the maximal value of N_{13} becomes smaller than its counterparts corresponding to N_{12} and N_{23}. When we continue to increase the value of γ/β up to $\gamma = 0.1\beta$ (Fig.4.5c), the value of N_{12} and N_{23} tend to be zero after several periods of oscillations, while the value of N_{13} is very small for a short interval of time before becoming close to zero in time. In such the case, the maximal value of N_{12} although is a little smaller than those corresponding to the previous cases, it is much greater than the maximal value of N_{23}. That means, that the bipartite entanglement $1 \leftrightarrow 2$ becomes much stronger than that for the pair $2 \leftrightarrow 3$, while the entanglement $1 \leftrightarrow 3$ is very weak and disappears after only a short interval of time. When $\gamma = 0.8\beta$, we can see from Fig.4.5d, that there is not bipartite entanglement between the active and passive cavity. At the beginning of system's evolution, only the bipartite entanglement $1 \leftrightarrow 2$ appears. After a short interval of time, the entanglement $2 \leftrightarrow 3$ becomes also visible. The value of N_{23}, firstly increases to its maximum, and next, decreases to a certain value. Meanwhile, the value of N_{12} firstly increases to a certain value and then, decreases to its minimum, and increases again to the maximal value before decreasing to a certain steady-state value. For such situation, the maximal values of N_{12} and N_{23} are much smaller than they were for the previously discussed cases. However, here the values of N_{12} and N_{23} finally tend to certain non-zero values instead of disappearing completely.

When the coupling between the active and passive cavities is removed, the form of the model changes from the triangular to the linear one. From Fig.4.6, it seems that the results for N_{12} and N_{23} are approximately the same as for the triangle configuration. It means, in this case, bipartite entanglement for the pairs $1 \leftrightarrow 2$ and $2 \leftrightarrow 3$ do not change very much. However, there is a considerable difference for N_{13} in two cases $\chi = 0.1\beta$ and $\chi = 0$. Firstly, when $\chi = 0.1\beta$, the amplitude of N_{13} increases in time, then decreases after reaching its maximal value. The maximal value of N_{13} in each period of its oscillation firstly increases to a greatest value that is can be close to 1, then decreases to zero. Meanwhile, when $\chi = 0$, the amplitude of N_{13} oscillations always decreases in time. the values of such maxim decreases in each period of oscillations from ~ 0.2 while the minimal value of N_{13} in this case is always approximately equal to zero. Secondly, for $\chi = 0.1\beta$, N_{13} reaches its maximal value in each period of oscillations when N_{12} and N_{23} get their minimal values, and it will be minimal when $N_{12} = N_{23}$. That means that bipartite entanglement $1 \leftrightarrow 3$ will be strongest for some moments in which the other ones are weakest, and it will be weakest when the other ones are of the same strength. Meanwhile, when $\chi = 0$, N_{13} reaches its maximal values when $N_{12} = N_{23}$, and it is equal to zero when N_{12} and N_{23} get their minimal values. It means, when we

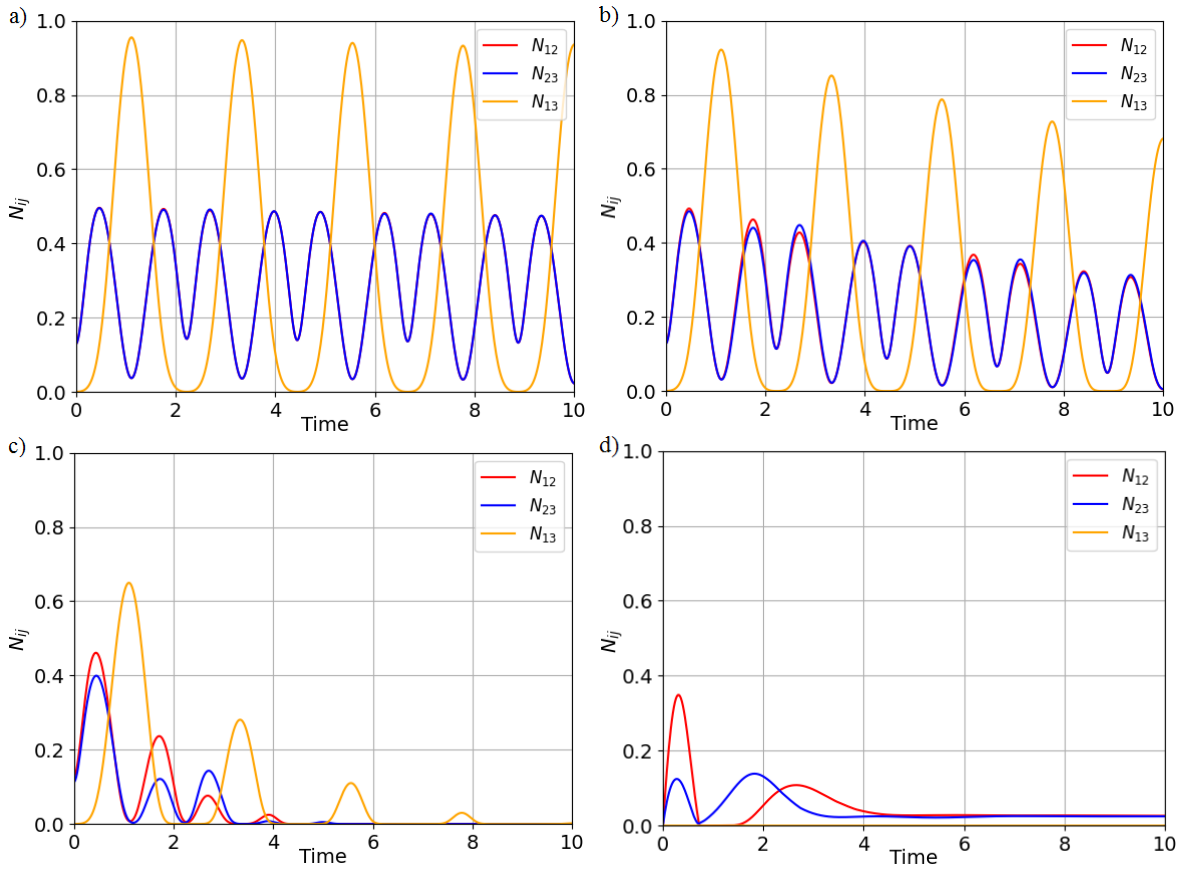

Fig. 4.7: The time evolution of negativities N_{ij} for (**a**) $\gamma = 0.001\beta$; (**b**) $\gamma = 0.01\beta$; (**c**) $\gamma = 0.1\beta$; (**d**) $\gamma = 0.8\beta$ when the initial state is $\hat{\rho}(t=0) = |010\rangle\langle 010|$, $\omega = 5\beta$, $\chi = 0.1\beta$. Time is scaled in $1/\beta$ units.

remove the coupling between the active and passive cavities, the entanglement $1 \leftrightarrow 3$ will be strongest when the entanglement for the other pairs have the same strength, and it disappears when the other bipartite entanglement reach their weakest strengths. Remarkably, those two differences are only appear for small value of ratio of gain/loss energy γ. When we increase the value of γ to the values that are close to the phase-transition points, the bipartite entanglement in both two cases of interaction between the active and passive cavities apparently get the same strength.

In the second scenario, the neutral cavity is the only excited one. The system starts its evolution from the state $\hat{\rho}(0) = |010\rangle\langle 010|$. We see (in Fig.4.7) that the strength of the bipartite entanglement produced strongly depends on the value of γ/β. When $\gamma = 0001\beta$ (Fig.4.7a) N_{ij} $(i, j = 1, 2, 3)$ periodically changes in time with the same periods of oscillations. Their amplitudes slightly decrease in time. We can also see that N_{12} and N_{23} change in the same way. They start their oscillations from non-zero values and then, oscillate between ~ 0.04 and ~ 0.48. Meanwhile, N_{13} starts its evolution from the value equal to zero, and its maximal value is close to 0.95. We can

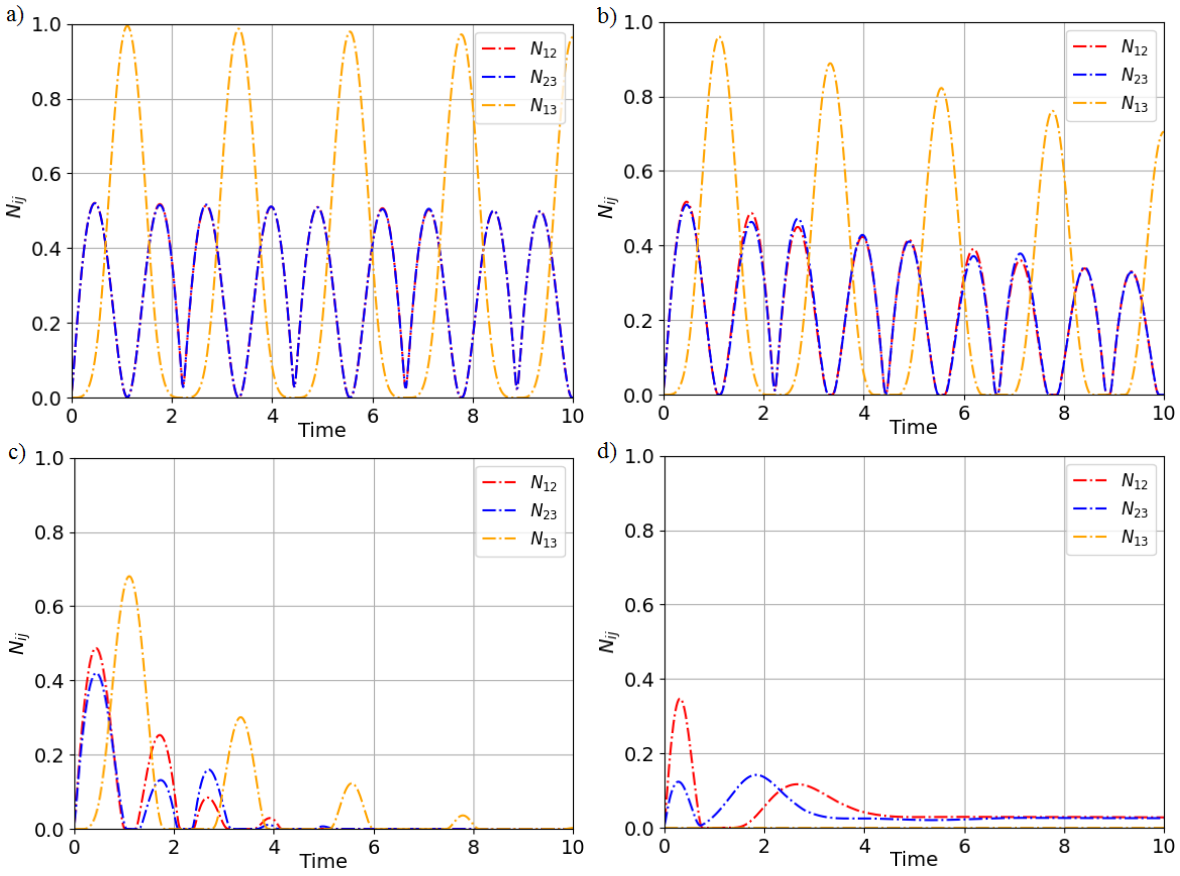

Fig. 4.8: The time evolution of negativities N_{ij} for (**a**) $\gamma = 0.001\beta$; (**b**) $\gamma = 0.01\beta$; (**c**) $\gamma = 0.1\beta$; (**d**) $\gamma = 0.8\beta$ when the initial state is $\hat{\rho}(t=0) = |010\rangle\langle 010|$, $\omega = 5\beta$, $\chi = 0$. Time is scaled in $1/\beta$ units.

say that, in this case, the strength of entanglement $1 \leftrightarrow 3$ is much stronger than the other ones. The value of N_{13} will be maximal at the moments of time in which the value of N_{12} and N_{23} are minimal. That means, the bipartite entanglement $1 \leftrightarrow 3$ will be the strongest at the moments when the entanglement for other pairs of cavities is the weakest. When $\gamma = 001\beta$, the entanglement for all pairs also change periodically (see Fig.4.7b). However, in this case, there are some details that differ from those discussed in the previous case. Firstly, the amplitudes of N_{12} and N_{23} start to be different from each other. Secondly, these amplitudes decrease more faster than they did in the previous case. Thirdly, in this case, the minimal values of all the negativities are equal to zero. Additionally, at some moments of time, all the negativities simultaneously get zero value. Besides that, at some other moments of time, the bipartite negativity N_{13} reaches its maximal value in each period when the other negativities are equal to zero. It means, that at those moments, the entanglement $1 \leftrightarrow 3$ is strongest when the other ones disappear. Finally, for some intervals of time, we can see that the entanglement suddenly disappears for a while before getting rebirth. When $\gamma = 01\beta$ (Fig.4.7c) the amplitudes of N_{ij} rapidly decrease in time, and their oscillations disappear after only several periods of oscillations. In such the case, the strength of the entanglement $1 \leftrightarrow 3$ is still much stronger than the others. The changes of N_{12} and N_{23} are more different from each others. However, they still get their maximal or minimal values at the same moments of time. After several periods of time, all negativities N_{ij} become equal zero. It means that all entanglements in our system will no longer be appearing. When $\gamma = 0.8\beta$ (Fig.4.7d) N_{12} and N_{23} also tend to get a certain final non-zero values while N_{13} is equal to zero for all moments of time as we saw it for the previous scenario, when $\hat{\rho}(0) = |100\rangle\langle 100|$ and $\gamma = 08\beta$. However, there are still some differences. Firstly, in this scenario, the entanglement $2 \leftrightarrow 3$ appears right at the beginning of system's evolution. Secondly, the maximal values of N_{12} and N_{23} are greater that they were in the previous scenario when $\gamma = 0.8\beta$. It means that the entanglement generation in this scenario is more efficient than that previously discussed for the same value of γ/β.

When we assume that the coupling between the active and passive cavity is washed out, and the system starts from the initial state in which only the neutral cavity is excited(in Fig.4.8), there are not changes for all considered here bipartite entanglements.

In the last scenario, only the active cavity is in one photon state while the other cavities are in vacuum states. The initial state of the system is $\hat{\rho}(0) = |001\rangle\langle 001|$. We can see (Fig.4.9a and b) that when $\gamma = 0.001\beta$ and $\gamma = 0.01\beta$, the changes of N_{ij} seem to be the same what they were in the scenario of $\hat{\rho}(0) = |100\rangle\langle 100|$ if we swap the roles of N_{12} and N_{23}. In the case of $\gamma = 0.1\beta$, we can see, in Fig.4.9c, that the entanglement $1 \leftrightarrow 3$ is much weaker than it was in the previous scenarios. When $\gamma = 0.8\beta$, this entanglement still appears with a small strength. Besides that, the other entanglements are stronger than those corresponding to the previous scenario. The maximal value of N_{12} is around 0.32 while the maximal value of N_{23} is around 0.5. For all scenarios, we can see that for the case of $\gamma = 0.8\beta$, the values of N_{12}, N_{23} and N_{13} eventually tend to get their final non-zero values values. When we remove the coupling between the active and passive cavities, and the system starts its evolution with excitation in the active cavity, we can

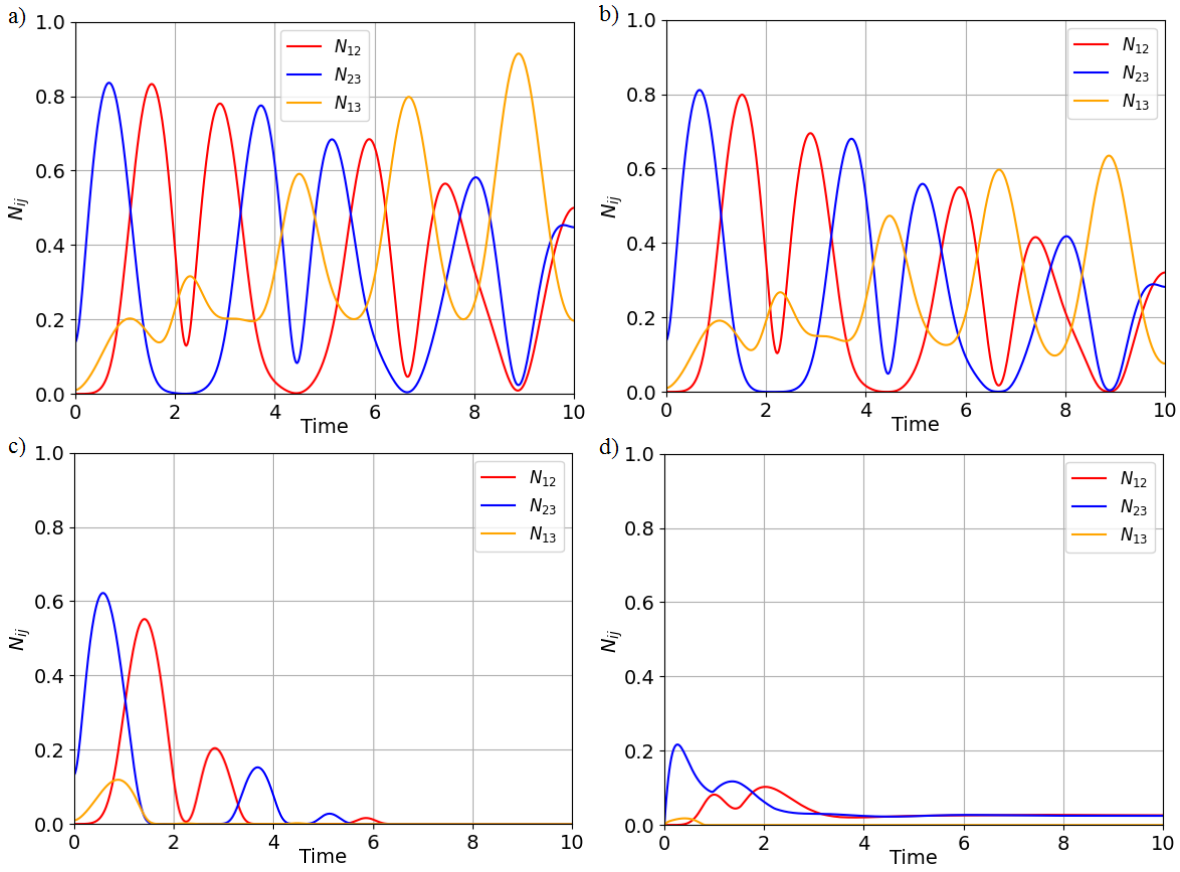

Fig. 4.9: The time-evolution of the negativities N_{ij} for (**a**) $\gamma = 0.001\beta$; (**b**) $\gamma = 0.01\beta$; (**c**) $\gamma = 0.1\beta$; (**d**) $\gamma = 0.8\beta$ when the initial state is $\hat{\rho}(t=0) = |001\rangle\langle 001|$, $\omega = 5\beta$, $\chi = 0.1\beta$. Time is scaled in $1/\beta$ units.

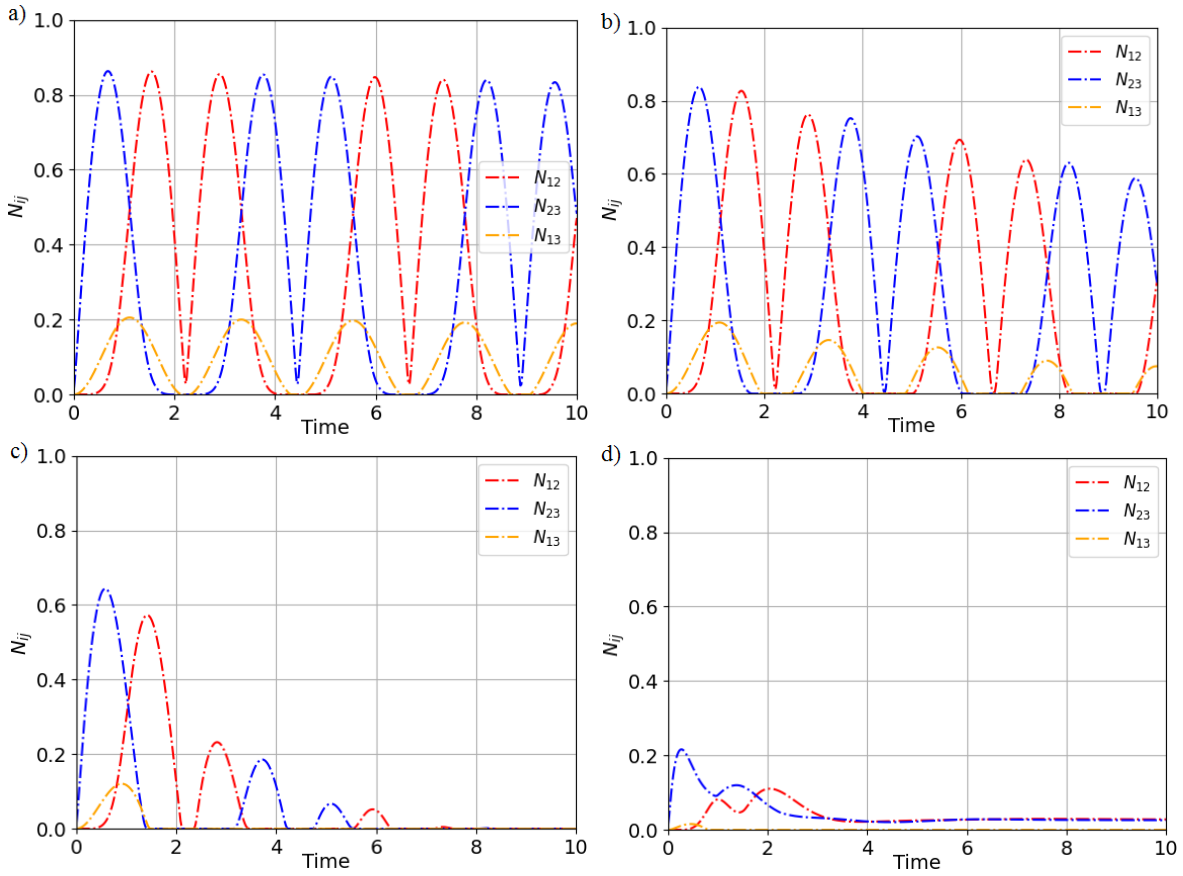

Fig. 4.10: The time evolution of negativities N_{ij} for (**a**) $\gamma = 0.001\beta$; (**b**) $\gamma = 0.01\beta$; (**c**) $\gamma = 0.1\beta$; (**d**) $\gamma = 0.8\beta$ when the initial state is $\hat{\rho}(t=0) = |001\rangle\langle 001|$, $\omega = 5\beta$, $\chi = 0$. Time is scaled in $1/\beta$ units.

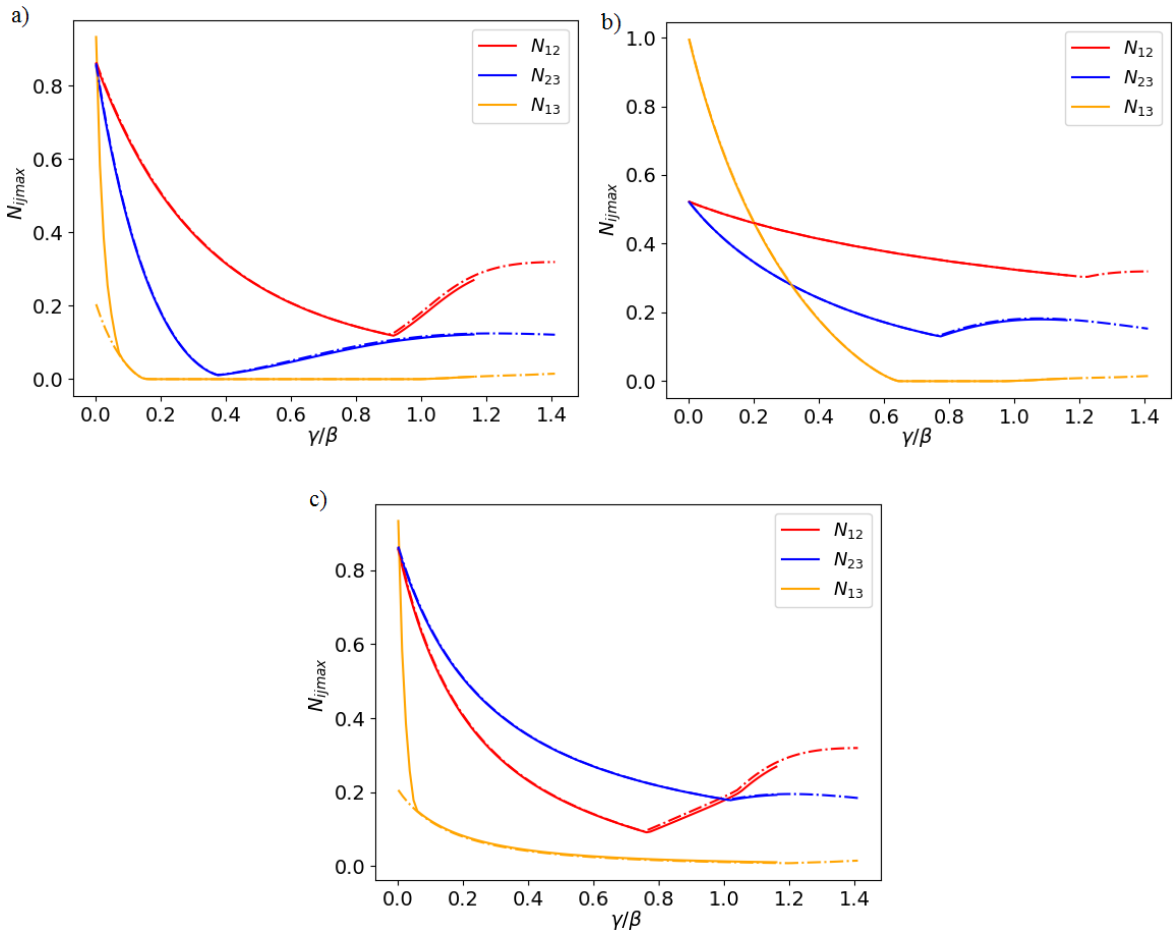

Fig. 4.11: The dependence of maximal values of negativities on γ/β for various of system's initial states: (**a**) $\hat{\rho}(t=0) = |100\rangle\langle 100|$; (**b**) $\hat{\rho}(t=0) = |010\rangle\langle 010|$; (**c**) $\hat{\rho}(t=0) = |001\rangle\langle 001|$ when $\gamma = 5\beta$, $\chi = 0.1\beta$ (solid lines) and $\chi = 0$ (dash-dotted lines).

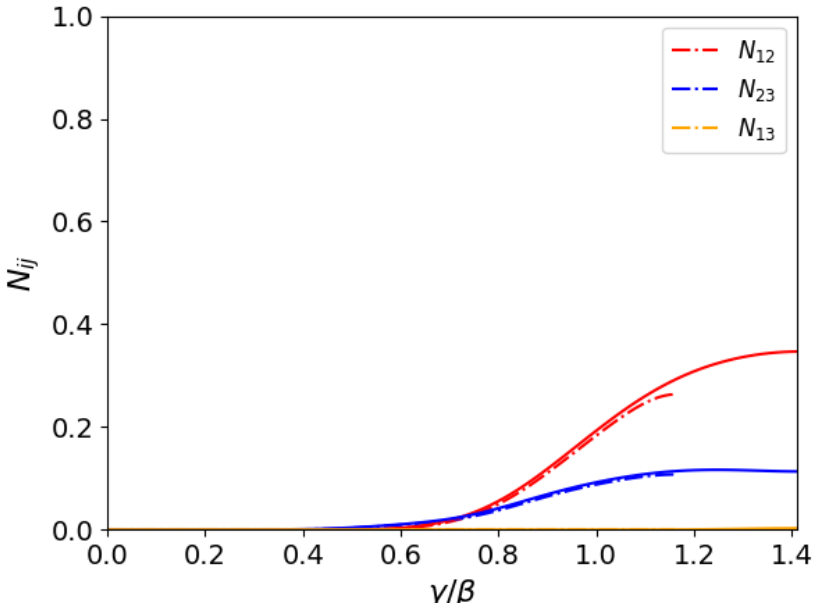

Fig. 4.12: Steady-solution for N_{ij} versus γ/β when $\omega = 5\beta$, $\chi = 0.1\beta$ (solid line) and $\chi = 0$ (dash-dotted line).

see (in Fig.4.10), the bipartite entanglement generated in the system differs from that for the triangle shaped system when $\gamma = 0.001\beta$ and $\gamma = 0.01\beta$. For $\gamma = 0.1\beta$ and $\gamma = 0.8\beta$, there are practically the same situation for the linear and triangle systems.

We can see that the strength of the entanglement between subsystems strongly depends on the value of γ/β. Therefore, it is desirable to find the maximal values of the negativities N_{ij} versus the value of γ/β corresponding to three different initial states of the system. Thus, Fig.4.11 depicts the results concerning those maximal values. For the first case, we assume that $\hat{\rho}(t = 0) = |100\rangle\langle 100|$. We see (Fig.4.11a), that when we increase the value of γ/β, the maximal value of N_{13} rapidly decreases from ~ 0.95. When $\gamma/\beta > 0.15$, the maximal value of N_{13} is close to zero. That means that for such values of γ/β, the bipartite entanglement $1 \leftrightarrow 3$ is very weak. Meanwhile, the maximal values of N_{12} and N_{23} firstly decrease from ~ 0.85 to their lowest value. Then, they increase again, when the value of γ/β becomes close to the phase-transition point of the strongest.

In the second case, the systems starts its evolution from the state $\hat{\rho}(t = 0) = |010\rangle\langle 010|$. Here, a big difference in the change of maximal values of the negativities is visible, as we compare them to those considered in the previous case (see Fig.4.11b). When we increase the value of γ/β, the maximal value of N_{13} gradually decreases from the value ~ 0.95 to that which is close to zero. For the values of $\gamma/\beta > 0.63$, the entanglement $1 \leftrightarrow 3$ is very weak. For very small values of γ/β, the maxima of N_{12} and N_{23} are approximately the same, and are equal to 0.51. When we increase the value of γ/β,

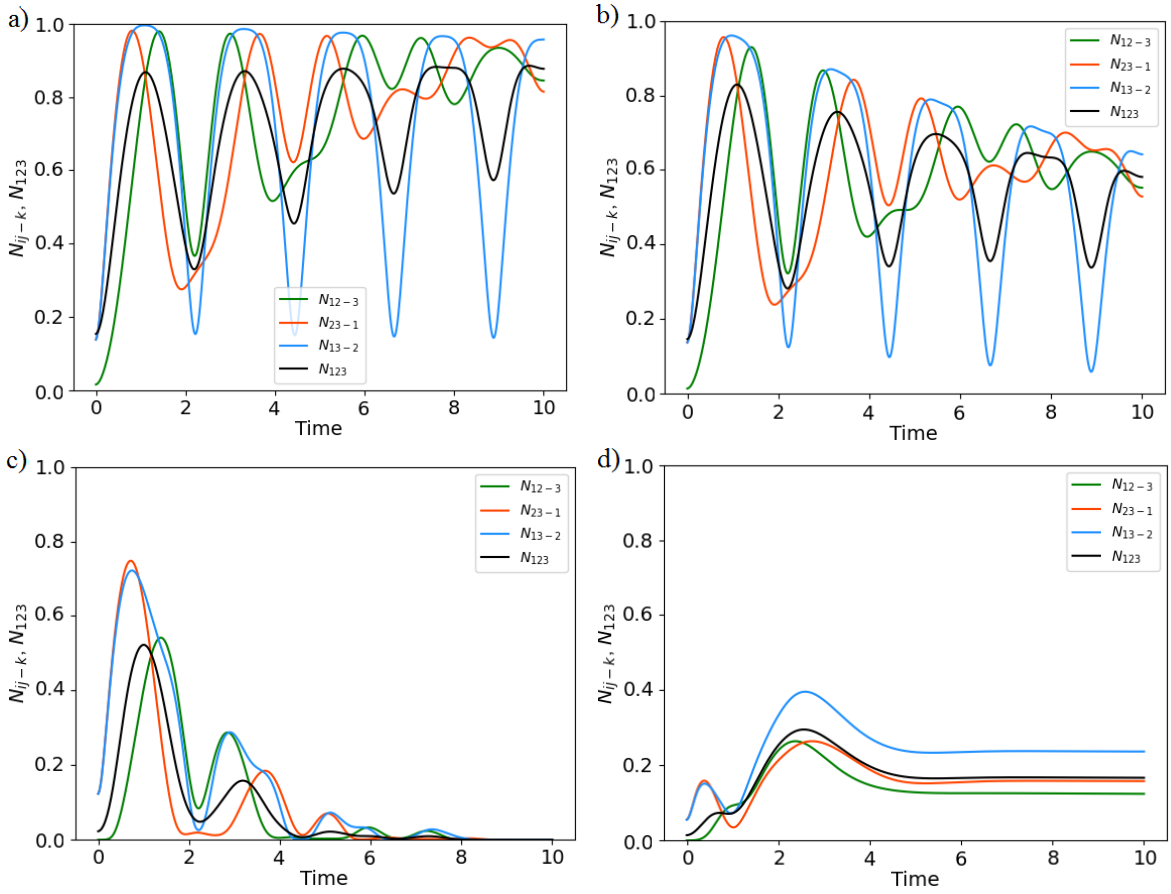

Fig. 4.13: The time evolution of negativities N_{ij-k} and N_{123} for (**a**) $\gamma = 0.001\beta$; (**b**) $\gamma = 0.01\beta$; (**c**) $\gamma = 0.1\beta$; (**d**) $\gamma = 0.8\beta$ when the initial state is $\hat{\rho}(t=0) = |100\rangle\langle 100|$, $\omega = 5\beta$, $\chi = 0.1\beta$. Time is scaled in $1/\beta$ units.

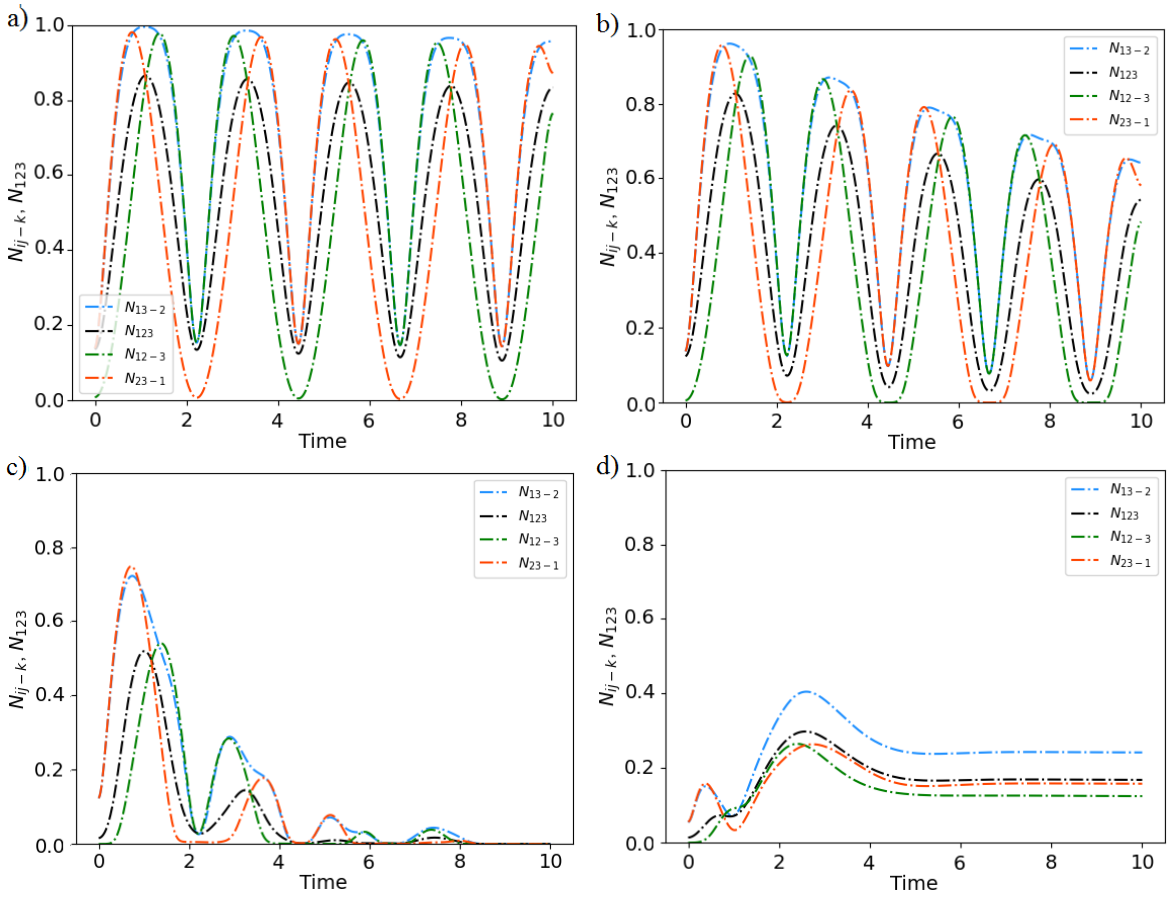

Fig. 4.14: The time evolution of negativities N_{ij-k} and N_{123} for (**a**) $\gamma = 0.001\beta$; (**b**) $\gamma = 0.01\beta$; (**c**) $\gamma = 0.1\beta$; (**d**) $\gamma = 0.8\beta$ when the initial state is $\hat{\rho}(t=0) = |100\rangle\langle 100|$, $\omega = 5\beta$, $\chi = 0$. Time is scaled in $1/\beta$ units.

those maximal values change in two different ways. The maximal value of N_{12} slightly decreases while the maximal value of N_{23} first, gradually decreases to its lowest value, and then increases to a certain value before decreasing again when γ/β is close to the phase-transition point. When $\gamma/\beta < 0.19$, the entanglement $1 \leftrightarrow 3$ becomes to be strongest. For the other values of γ/β, the entanglement $1 \leftrightarrow 2$ takes its turn to be the strongest.

Next, we shall concentrate on the situation when, the system starts its evolution from the state, $\hat{\rho}(t=0) = |001\rangle\langle 001|$. We can see (in Fig.4.11c) that, for $\gamma/\beta < 0.04$, the maximal value of N_{12} and N_{23} does not change very much. They seem to be the same for each value of γ/β. Meanwhile, in this range of γ/β, the maximal value of N_{13} rapidly changes from ~ 0.95 to ~ 0.16. When $0.04 < \gamma/\beta < 1.165$, the maximal value of N_{13} slightly decrease. Interestingly, the entanglement $1 \leftrightarrow 3$ does not disappear for all values of γ/β. Meanwhile, the maximal values of N_{12} and N_{23} seem to change in the same way. They firstly decrease to their minima, then they increase to reach certain values and next, slightly decrease again when γ/β becomes close to the phase-transition point of $\mathcal{PT}$-symmetry. We see that for the considered here scenario, the entanglement $1 \leftrightarrow 3$ is the strongest when γ/β is very small. For the other values of γ/β, the strongest entanglement is that corresponding to the pair $2 \leftrightarrow 3$.

As we showed above (Fig.4.5d, Fig.4.7d, and Fig.4.9d), when the value of γ/β is close to the phase-transition point of the $\mathcal{PT}$-symmetry, the values of N_{ij} tend to be stable. Therefore, it is necessary to find out the behavior of the system when it virtually approaches the steady-state. In this case, for $t \to \infty$, the state of our system is characterized by density matrix $\hat{\rho}_s$ obeying the following equation:

$$\frac{d}{dt}\hat{\rho}_s(t) = \frac{1}{i}\left[\hat{H}_0, \hat{\rho}_s(t)\right] + \hat{\mathcal{L}}\hat{\rho}_s(t) = 0. \tag{4.17}$$

Solving such equation allows to determine the system's state in the long-time limit and then, to find parameters describing the characteristics of the system. To study the bipartite entanglement for steady-solution, we calculate the values of bipartite negativities corresponding to that state. The results are depicted in Fig.4.12. We see that, for all considered here values of γ/β, the value of N_{13} is always equal to zero. In other words, in the case of the steady-state, there is no entanglement between the active and passive cavity, even when the direct interaction between them is present. For the value of γ/β satisfying $0.5 < \gamma/\beta < 1.165$, the N_{12}, N_{23} increase with γ/β. That means that the bipartite entanglement in the system can be significantly generated for the values of γ/β that are close to the phase-transition point. The closer to the phase-transition point, the stronger bipartite entanglements becomes. Besides that, bipartite entanglement $1 \leftrightarrow 2$ is always stronger than that of $2 \leftrightarrow 3$ for the all values of γ/β in the range in which we are interested in.

Next, we concentrate on the generation of tripartite entanglement in our system. To quantify such corelations, we calculate a quantity called tripartite negativity. Such a kind of quantity is considered as the one that can quantify tripartite entanglement

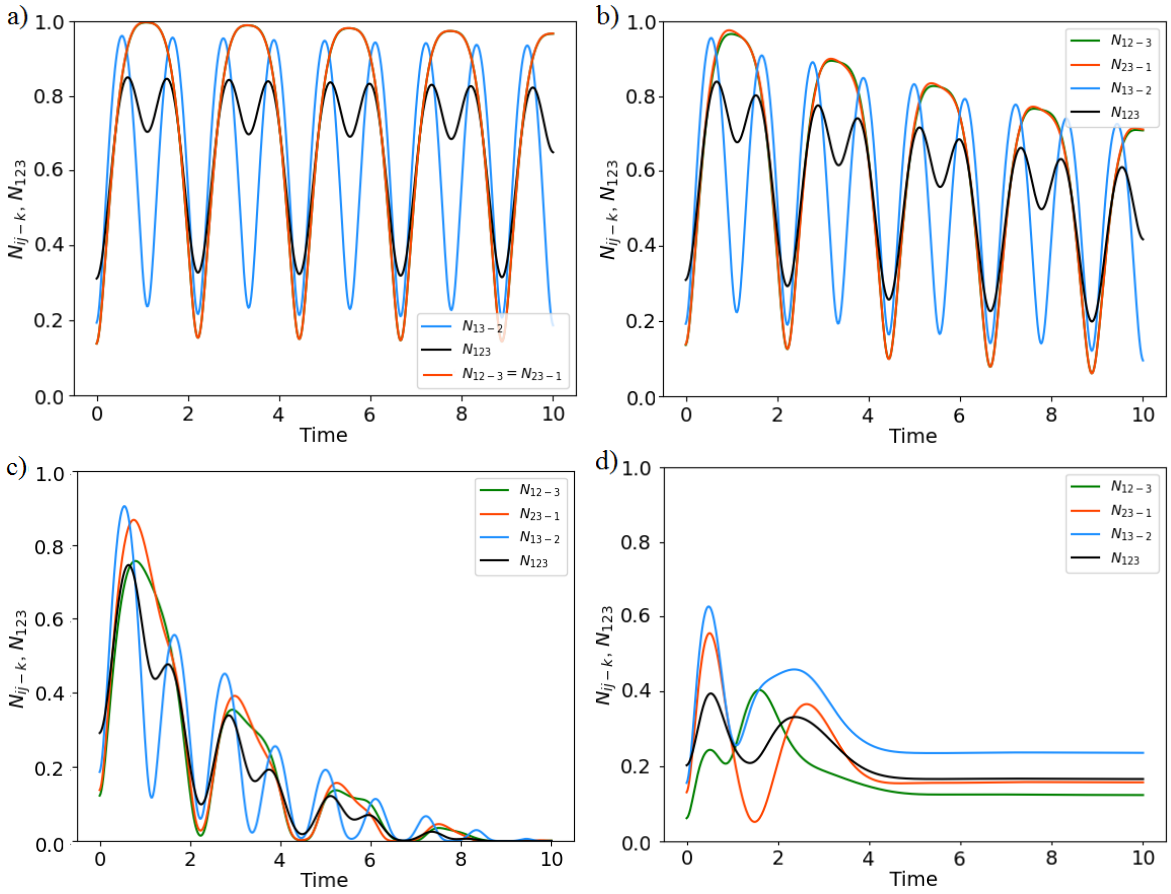

Fig. 4.15: The time evolution of the negativities N_{ij-k} and N_{123} for (**a**) $\gamma = 0.001\beta$; (**b**) $\gamma = 0.01\beta$; (**c**) $\gamma = 0.1\beta$; (**d**) $\gamma = 0.8\beta$ when the initial state is $\hat{\rho}(t=0) = |010\rangle\langle 010|$, $\omega = 5\beta$, $\chi = 0.1\beta$. Time is scaled in $1/\beta$ units.

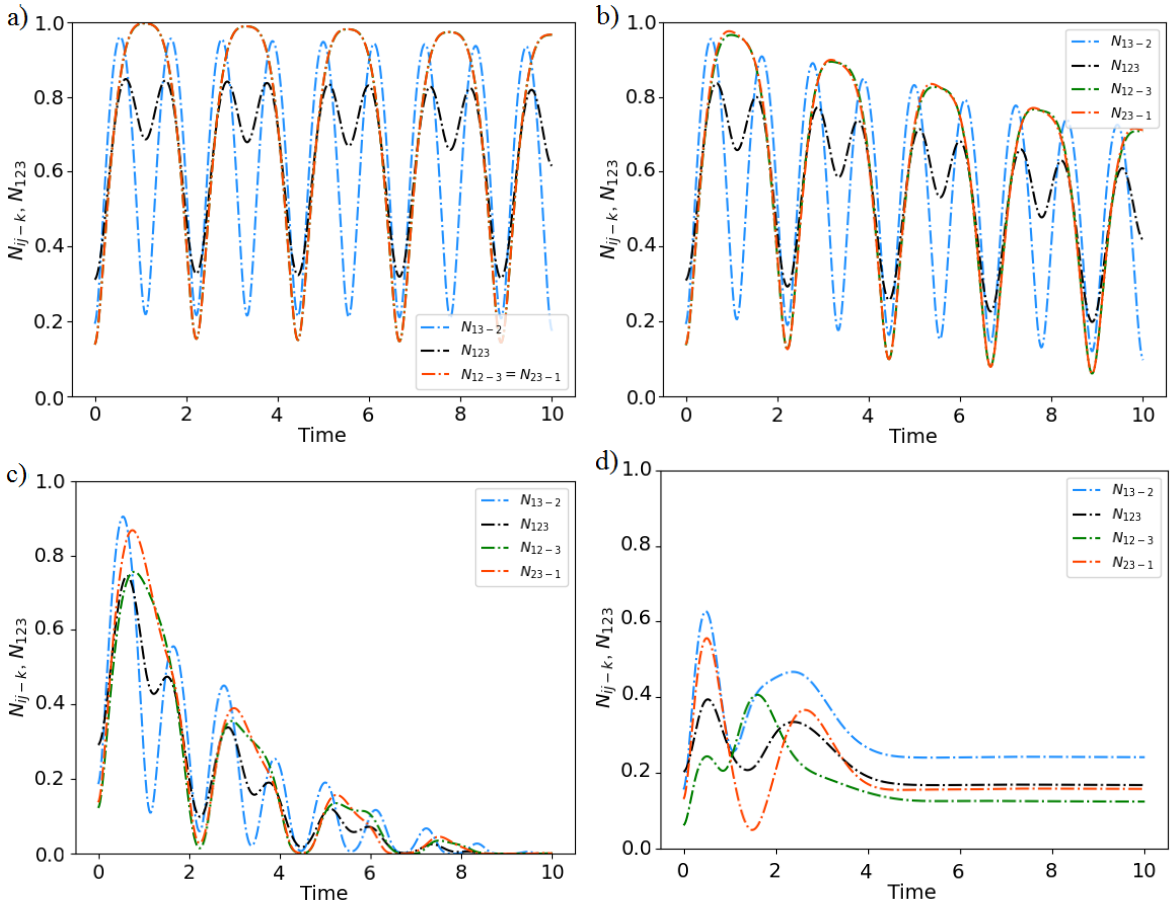

Fig. 4.16: The time evolution of negativities N_{ij-k} and N_{123} for (**a**) $\gamma = 0.001\beta$; (**b**) $\gamma = 0.01\beta$; (**c**) $\gamma = 0.1\beta$; (**d**) $\gamma = 0.8\beta$ when the initial state is $\hat{\rho}(t=0) = |010\rangle\langle 010|$, $\omega = 5\beta$, $\chi = 0$. Time is scaled in $1/\beta$ units.

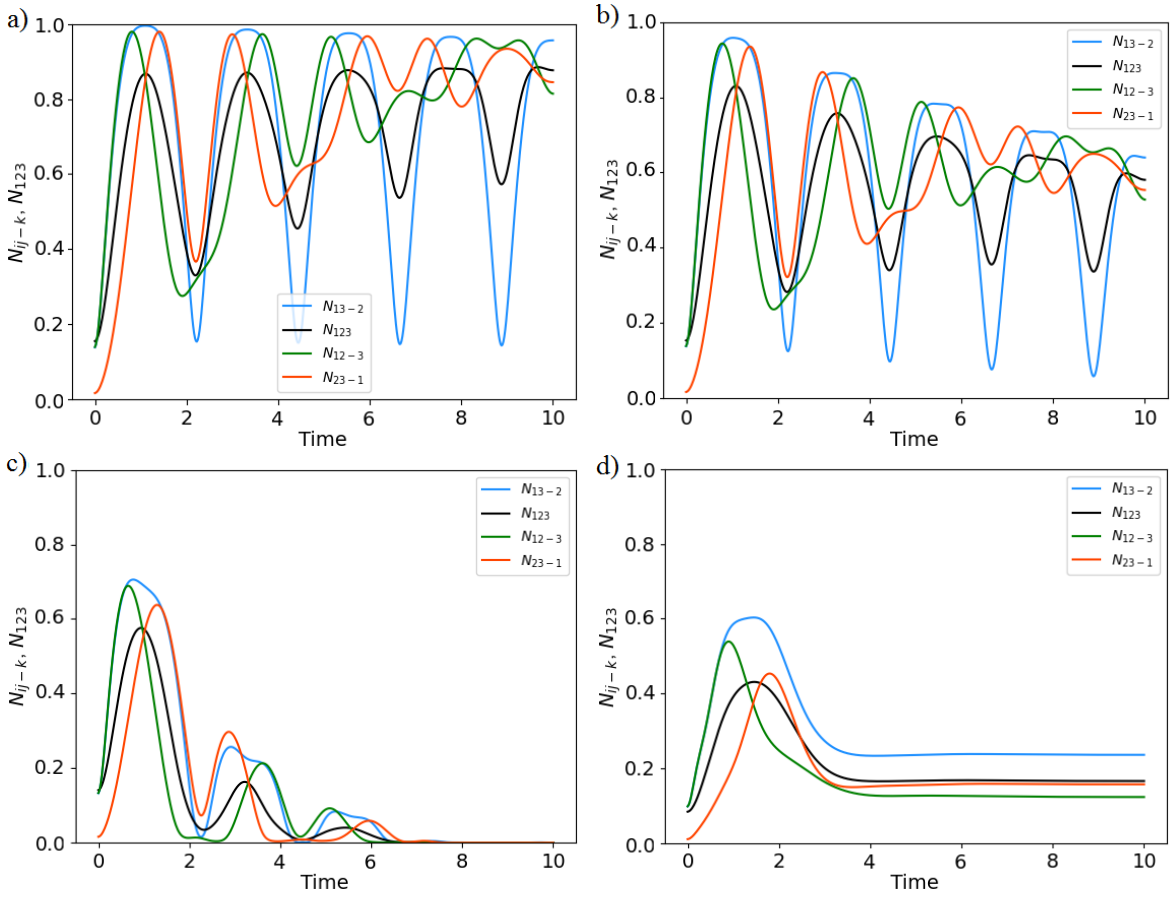

Fig. 4.17: The time evolution of negativities N_{ij-k} and N_{123} for (**a**) $\gamma = 0.001\beta$; (**b**) $\gamma = 0.01\beta$; (**c**) $\gamma = 0.1\beta$; (**d**) $\gamma = 0.8\beta$ when the initial state is $\hat{\rho}(t=0) = |001\rangle\langle 001|$, $\omega = 5\beta$, $\chi = 0.1\beta$. Time is scaled in $1/\beta$ units.

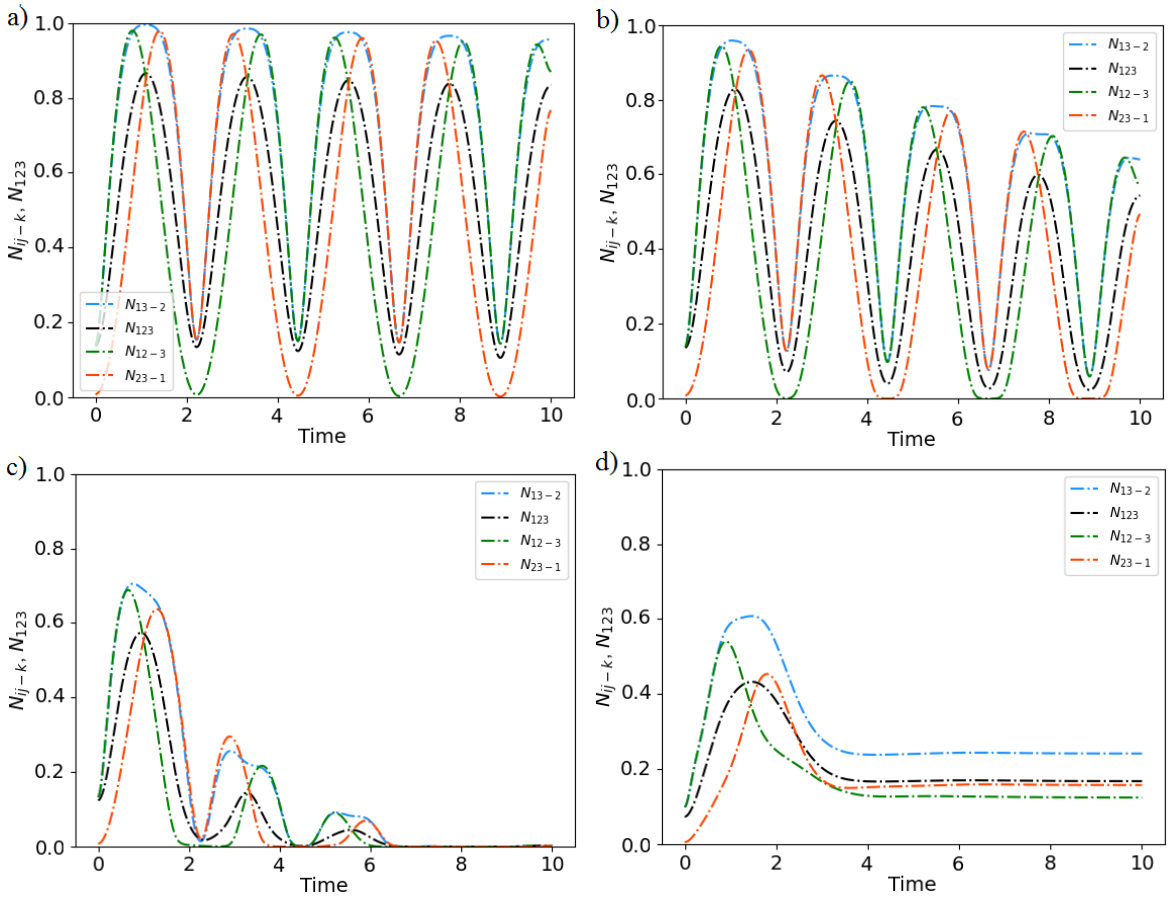

Fig. 4.18: The time evolution of negativities N_{ij-k} and N_{123} for (**a**) $\gamma = 0.001\beta$; (**b**) $\gamma = 0.01\beta$; (**c**) $\gamma = 0.1\beta$; (**d**) $\gamma = 0.8\beta$ when the initial state is $\hat{\rho}(t=0) = |001\rangle\langle 001|$, $\omega = 5\beta$, $\chi = 0$. Time is scaled in $1/\beta$ units.

between the subsystems in a system of three parties. It can be calculated as follows [39]

$$N_{123} = \sqrt[3]{N_{12-3}N_{23-1}N_{13-2}}, \tag{4.18}$$

where N_{ij-k} are the bipartite negativities between subsystem k and the others in which subsystems i and j are seemed as a whole, $k = (1, 2, 3)$, *i.e.* $(ij) = \{12, 23, 13\}$. In that sense, bipartite negativities N_{ij-k} can be calculated as

$$N_{ij-k} = -2\sum_n \lambda_n \left(\rho^{PT_k}\right), \tag{4.19}$$

where λ_n are negative eigenvalues of $\hat{\rho}^{PT_k}$ that is partial transposed density matrix of density matrix $\hat{\rho}$ respect to mode k. We also concentrate on the cases in which the system starts its evolution with excitation in only one of cavities. For such the case, we calculate the values of tripartite negativities corresponding to the four different values of γ: $\gamma = 0.001\beta$, $\gamma = 0.01\beta$, $\gamma = 0.1\beta$, and $\gamma = 0.8\beta$.

In the first scenario, the initial state of the system is $\hat{\rho}(t = 0) = |100\rangle\langle 100|$. The results of the bipartite negativities N_{ij-k} and the tripartite negativity N_{123} are shown in Fig.4.13 for $\chi = 0.1\beta$, and in Fig.4.14 for $\chi = 0$. Thus, Fig.4.13 shows that bipartite negativities N_{ij-k} strongly depend on the value of γ/β. When $\gamma = 0.001\beta$ (Fig.4.13a), N_{13-2} periodically changes in time with a certain period of oscillations, while the changes of N_{23-1} and N_{12-3} are not precisely periodical. Their maximal values in each interval of time slightly decrease from the values that are close to 1. The minimal value of N_{23-1} and N_{12-3} tend to increase in time. Meanwhile, the minimal value of N_{13-2} slightly decrease in time from a value close to 0.125. At the beginning, tripartite negativity N_{123} starts from a values close to 0.150, then it oscillates with the same period of oscillation as for N_{13-2}. It also get its minimal values when the value of N_{13-2} is minimal. Interestingly, the value of N_{123} reach its maximum in each period when N_{23-1} and N_{12-3} virtually get the same value, and its maximal value slightly increases in time. When $\gamma = 0.01\beta$, the results depicted in Fig.4.13b show that the period of oscillations of both N_{ij-k} and N_{123} do not change. However, their maximal and minimal values are smaller than those considered in the previous case and faster decrease in time. When $\gamma = 01\beta$, the value of the bipartite negativities N_{ik-k} tend to be equal zero after several periods of oscillations. Consequently, the value of the tripartite negativity N_{123} also rapidly decreases to zero after only several oscillations (see Fig.4.13c). In the last case, when $\gamma = 08\beta$ (Fig.4.13d), the values of N_{ik-k} reach their stable values after one period of oscillations. This leads to a consequence in which tripartite negativity N_{123} is also apparently constant for a long interval of time. It means, that for the values of γ close to the transition-point of $\mathcal{PT}$-symmetry, the tripartite entanglement is still generated. When we remove the coupling between the active and passive cavities (Fig.4.14) that the evolution of all bipartite and tripartite negativities seem to change more periodical than them when $\chi = 0.1\beta$. In this case, bipartite negativity N_{13-2} and tripartite negativity N_{123} reach there maximal values at right moments when N_{23-1} and N_{12-3} get the same value. On the other hand, both bipartite negativities N_{ij-k} and tripartite negativity N_{123} get their

minimal values at the same time. We can also see that, when the system is close to the transition point, even when we remove the interaction between the active and passive cavities, both bi- and tripartite negativities get the same stable values as what they got in the case of remaining that interaction.

In the second scenario, the initial state of our system is $\hat{\rho}(t=0) = |010\rangle\langle 010|$. Here (Fig.4.12), we can easily see that, when $\gamma/\beta = 0.001$, both bi- and tripartite negativities periodically change in time with the same period of oscillation. The value of N_{23-1} and N_{12-3} are exactly the same. In this case, both bi- and tripartite negativities reach their minimal values at the same time. However, tripartite negativity N_{123} only reaches its maximal value when all bipartite negativities N_{ij-k} apparently take the same value. When we increase the value of γ/β, the oscillation of both bi- and tripartite negativities tend to disappear after some periods. In cases of γ/β close to the phase transition point, they will get stable values when the values as what they behaved in the previous scenario of system's initial state. When we remove the coupling between the active and passive cavities, every change of bi- and tripartite entanglement seem to be similar to the case of remaining the coupling (see Fig.4.16).

In the last scenario, the system starts from the initial state $\hat{\rho}(t=0) = |001\rangle\langle 001|$. The changes of bi- and tripartite entanglements apparently are the same as for the scenario in which the system starts its evolution from the initial state $\hat{\rho}(t=0) = |100\rangle\langle 100|$ for both cases $\chi = 0.1\beta$ and $\chi = 0$ (see Fig.4.17 and Fig.4.18). However, in this scenario, there is an interchange of the roles between N_{12-3} and N_{23-1}. Beside that, in this case, both bi- and tripartite negativities get their stable values a little bit faster than what they did in the other scenarios.

In Fig.4.19, we can see that the maximal values of both bipartite negativities N_{ij-k} and tripartite negativity N_{123} are not only dependent on the value of γ/β, but also on the system's initial state. For all cases of system's initial states, the maximal value of N_{123} is different from zero. This also happened for all values of γ/β satisfying the condition of the unbroken phase of $\mathcal{PT}$ symmetry. As a result, we can say that our system can generate tripartite entanglement for all given cases of system's initial state and given values of γ/β as long as the it is still $\mathcal{PT}$ symmetric. In the first case, when the initial state of the system is $\hat{\rho}(t=0) = |100\rangle\langle 100|$, if we increase the value of γ/β, the maximal values of bipartite negativities N_{ij-k} will firstly decrease to their largest values that are close to 1 to their smallest values. These smallest values are respectively 0.182, 0.205, and 0.276 for N_{12-3}, N_{23-1}, and N_{13-2} when respective values of γ/β are 0.25, 0.704, and 0.507. Then, they increase when we continue to increase the value of γ/β. In this case, before N_{13-2} reaches its smallest value, the maximal values of N_{13-2} and N_{23-1} are mostly similar, and they are greater than the maximal value of N_{12-3}. It means that the strength of bipartite entanglements $23 \leftrightarrow 1$ and $13 \leftrightarrow 2$ are mostly similar, and they are stronger than bipartite entanglement $12 \leftrightarrow 3$ (see Fig.4.19a). For the values of γ/β close to the phase transition point, bipartite entanglement $13 \leftrightarrow 2$ is the strongest while bipartite entanglement $12 \leftrightarrow 3$ is the weakest one. Also in this case, tripartite negativity N_{123} starts with a value of 0.942 before rapid decreasing to its smallest value

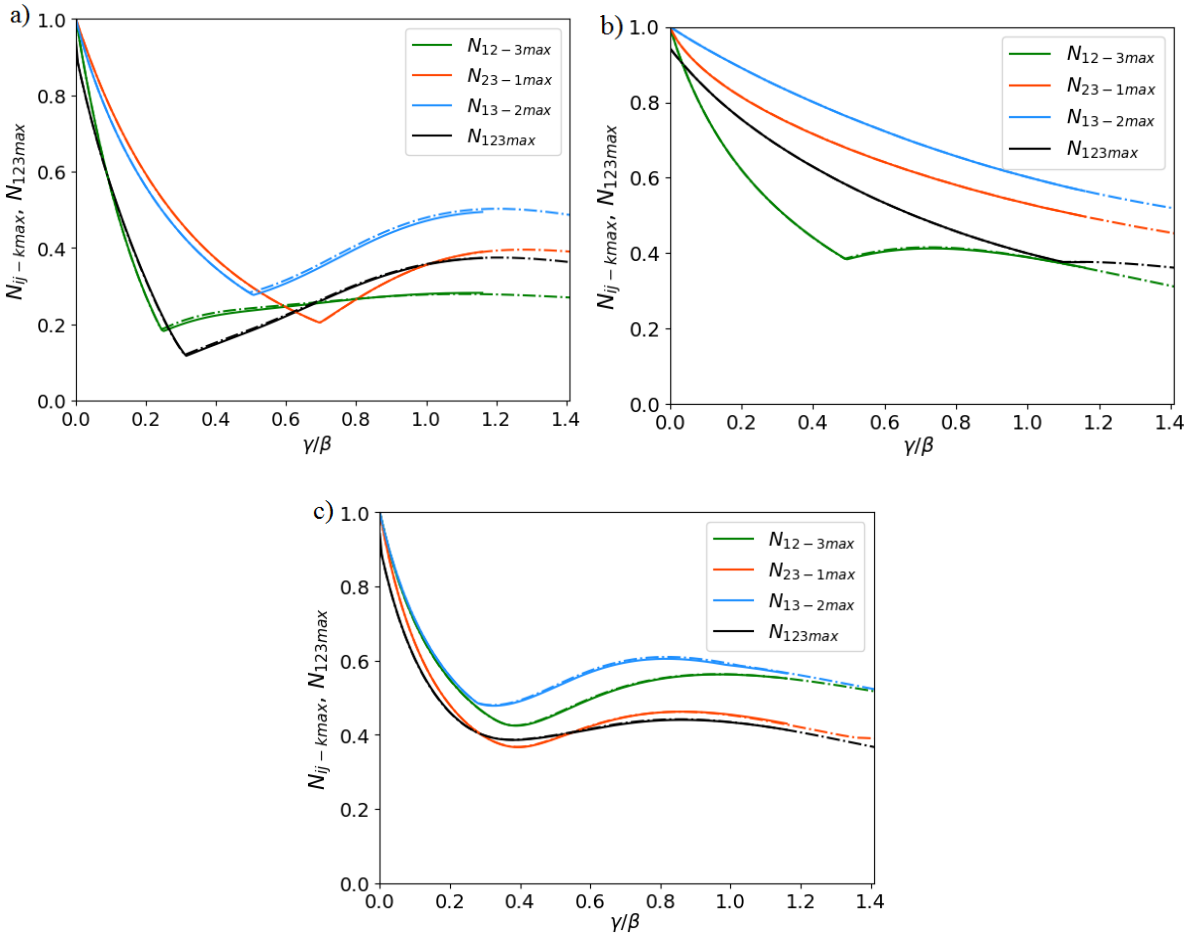

Fig. 4.19: The dependence of maximal values of bipartite negativity N_{ij-k} and tripartite negativity N_{123} on γ/β for various of system's initial states: (**a**) $\hat{\rho}(t=0) = |100\rangle\langle 100|$; (**b**) $\hat{\rho}(t=0) = |010\rangle\langle 010|$; (**c**) $\hat{\rho}(t=0) = |001\rangle\langle 001|$ when $\gamma = 5\beta$, $\chi = 0.1\beta$ (solid lines) and $\chi = 0$ (dash-dotted lines).

(0.117) when $\gamma/\beta = 0.314$. From this point, it gradually increases to 0.372 when we increase the value of γ/β.

In the second case, the system starts its evolution by being in the state $\hat{\rho}(t = 0) = |010\rangle\langle 010|$. Thus, we can see in Fig.4.19b, that when the value of γ/β increases, the maximal value of N_{13-2} and N_{23-1} gradually decreases from a value close to 1 while the maximal value of N_{12-3} firstly decreases to 0.384 at $\gamma = 0.495\beta$ and then slightly increases to 0.412 before decreasing again when we increase the values of γ/β to the phase-transition point of $\mathcal{PT}$-symmetry. In this case, the maximal value of N_{13-2} is always the largest while the maximal value of N_{12-3} is the smallest among bipartite negativities N_{ij-k}. It means bipartite entanglement $13 \leftrightarrow 2$ is always the strongest while $12 \leftrightarrow 3$ is the weakest entanglement. From the side of tripartite entanglement generation, we can see (in Fig. 4.19b) the value of tripartite negativity N_{123} gradually decreases from 0.942 to 0.376 when we increase the value of γ/β. It mostly take larger values than what it took in the previous case. Therefore, ee can say that, in this case, tripartite entanglement is stronger than it in the previous case of system's initial state. In the last case, the initial state of the system is $\hat{\rho}(t = 0) = |001\rangle\langle 001|$. The results in Fig. 4.19c show that both bi- and tripartite negativities change in the similar way. They firstly decrease from their largest values (close to 1) to certain values, then gradually increase to other certain values before slight decreasing. In this case, bipartite entanglement $13 \leftrightarrow 2$ is always the strongest while the weakest bipartite entanglement is $23 \leftrightarrow 1$. For all cases of system's initial state, we can see that when the coupling between the active and passive cavities is removed, the maximal values of bi- and tripartite negativities are almost the same with what they were when we remained this coupling. However, for the values of γ/β close to the phase-transition points of two systems, bipartite entanglement $13 \leftrightarrow 2$ is a little stronger than it was in the case when the coupling existed.

From Fig.4.13 to Fig.4.18, we can see that there is existence of steady-state solutions for the bi- and tripartite negativities when the value of γ/β is close to the phase transition point of the $\mathcal{PT}$-symmetry. In Fig.4.20 we show the dependence of these steady-solution on the value of γ/β for various initial states of our system. It is easy to see that the steady-solution of N_{13-2} will be different from zero when the value of $\gamma/\beta > 0.195$ while N_{12-3}, N_{23-1} and tripartite negativity N_{123} (consequently) take non-zero values when $\gamma/\beta > 0.376$. It means, for a long interval of time, our systems can generate tripartite entanglement when $\gamma/\beta > 0.376$ as long as it is still in the unbroken phase of $\mathcal{PT}$ symmetry. If we remove the coupling between the active and passive cavity, the value of N_{12-3} and N_{13-2} for steady-state solution is almost the same with what they were in the case of remaining the coupling.

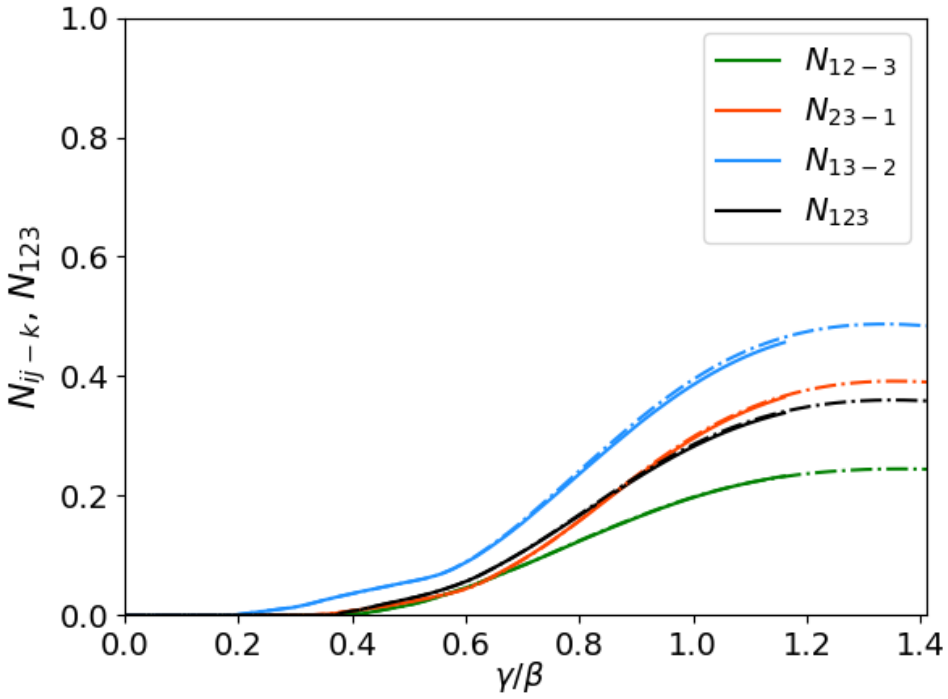

Fig. 4.20: Steady-state solution for N_{ij-k} and N_{123} versus γ/β when $\omega = 5\beta$, $\chi = 0.1\beta$ (solid lines) and $\chi = 0$ (dash-dotted lines).

4.3 Quantum steering in tripartite $\mathcal{PT}$-symmetric models

In this section, we concentrate on the quantum steering between subsystems of our model. To do that, we will show the time evolution of the steering parameters S_{ij} $(i, j = 1, 2, 3)$ that defined as in (3.13) and already described in the previous chapter. Here, we also consider three cases of system's initial state in which there is only one of the cavities is excited. For each case, we will concentrate on four different values of γ/β: $\gamma = 0.001\beta$, $\gamma = 0.01\beta$, $\gamma = 0.1\beta$, and $\gamma = 0.8\beta$.

In the first case, only the passive cavity is excited. It means that the system's initial state is $\hat{\rho}(t = 0) = |100\rangle\langle 100|$. The results are shown in Fig.4.21. We can see that when $\gamma = 0.001\beta$, the passive and active cavity can steer the others while the neutral cavity can not steer the others. Besides time intervals of steering, there are some other intervals of time in which all the subsystems loss their steering ability to the others. It means each subsystem can only steer another one in some certain intervals of time. The steering abilities of the passive and active cavity to the neutral one decrease in time. Meanwhile, the steering abilities of the passive and active cavity to each other firstly increase to their maxima be fore decreasing in time. We can say that, there is only one-way steering from the active or passive cavity to the neutral one. For the couple of passive and active cavity, the reciprocal steering is asymmetric. Interestingly, we can see that there are some intervals in which S_{21} and S_{31} simultaneously take positive values.

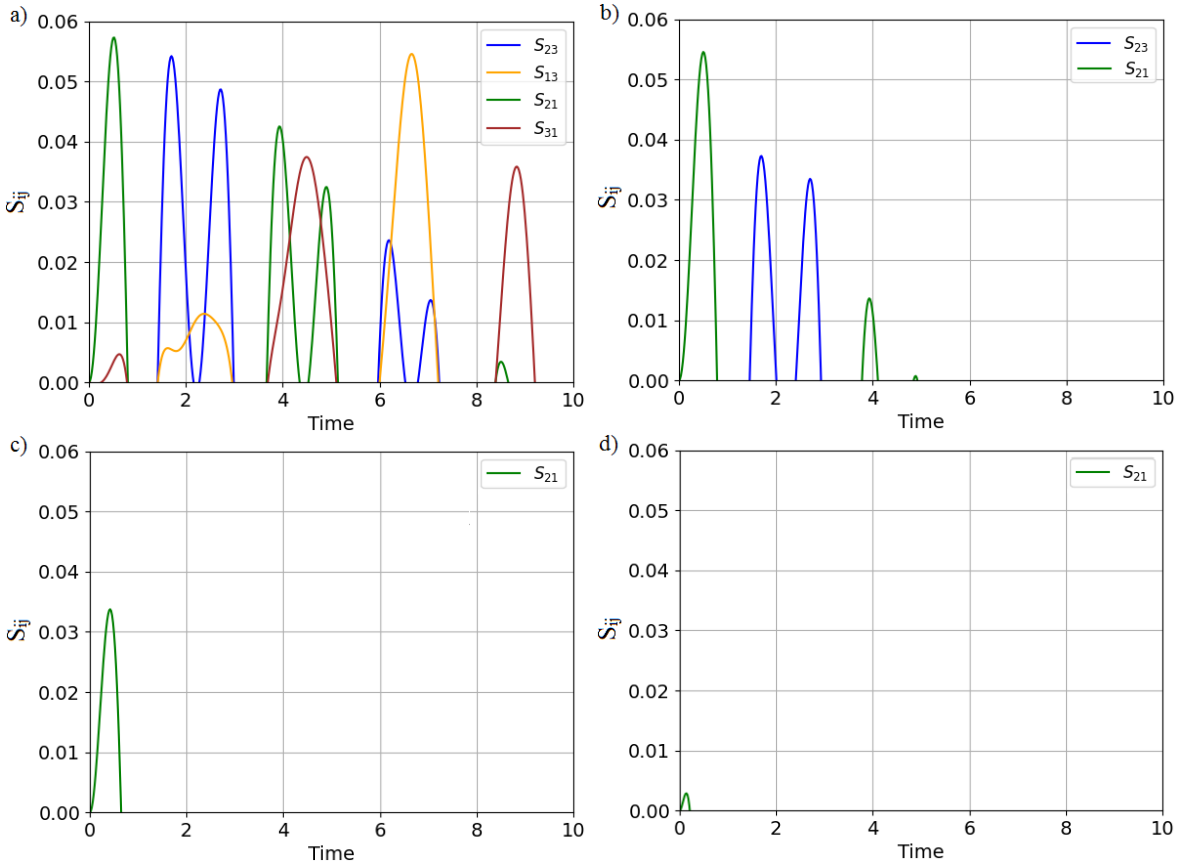

Fig. 4.21: The time evolution of steering parameters S_{ij} for (**a**) $\gamma = 0.001\beta$; (**b**) $\gamma = 0.01\beta$; (**c**) $\gamma = 0.1\beta$; (**d**) $\gamma = 0.8\beta$ when the initial state is $\hat{\rho}(t=0) = |100\rangle\langle 100|$, $\omega = 5\beta$, $\chi = 0.1\beta$. Time is scaled in $1/\beta$ units.

It means in those intervals of time, the passive cavity can simultaneously steer the active and neutral cavity. Similarly, there are some other intervals of time in which S_{23} and S_{13} simultaneously take positive values, and we can consequently say that the active cavity can also simultaneously steer the others for some certain intervals of time (see Fig.4.21a). When $\gamma = 0.01\beta$, the result on Fig.4.21b shows that only S_{23} and S_{21} take positive values. It means that the passive and active cavity loss their abilities steering to each other. They can only alternatively steer the neutral cavity for some intervals of time. Their abilities of steering decrease in time. The steering in our system for this case is also one-way. When $\gamma = 0.1\beta$, only S_{21} takes positive value. As a result, we can say that for this situation, the one-way steering happens in the only direction from the passive cavity to the neutral one. However this steering is only remained in a short beginning interval of time before disappearing. When we continue to increase the value of γ/β, this ability of steering will decreases (see Fig.4.21c and Fig.4.21d). If we remove the coupling between the active and passive cavities, we can see in Fig.4.22, there are some differences from the case in which the coupling between the active and passive cavities is maintained and the value of γ/β is very small. Firstly, although there are still steering abilities of the passive and active cavities to the others, the steering abilities are much weaker than what they were in the scenario of remaining the coupling between the active and passive cavities. Secondly, these steering abilities only appear for very short intervals of time, and decrease faster in time. Finally, the strength of steering abilities of the passive and active cavities to the neutral one slightly decrease in time in stead of rapidly decreasing as they did in the previous scenario. For the greater values of γ/β, the steering of subsystems in our system for both two scenarios is virtually the same.

In the second case, the initial state of our system is $\hat{\rho}(t = 0) = |010\rangle\langle 010|$. The results in Fig.4.23 show that the value of all steering parameters strongly depends on the value of γ/β. When $\gamma = 0.001\beta$, only S_{12} and S_{32} take positive values (see Fig.4.23a). It means that only the neutral cavity can steer the others with one-way steering. The steering abilities in the other directions are not available. We also see that the possibility of this steering only happens in some certain periods of time. A part from those periods of time, our system is out of steering for every directions. The maximal values of S_{12} and S_{32} in each period of steering time are apparently the same. It means that the steering abilities of the neutral cavity to the active and the passive ones are approximately equivalent. These steering abilities lightly decrease in time. Interestingly, S_{12} and S_{32} always take the positive values at the same moments of time. This directly indicates that the neutral cavity can simultaneously steer the active and passive ones. When $\gamma = 0.01\beta$, we can see in Fig.4.23b that the neutral cavity still remains its steering abilities to the others. However, in this situation, these steering abilities decrease faster than they did when $\gamma = 0.001\beta$. After several periods of time, they totally disappear. Besides that, the steering ability of the neutral cavity to the active cavity is weaker than its steering ability to the passive one. When $\gamma = 0.1\beta$, only S_{12} takes positive values. It means that the neutral cavity loss its steering ability to the active one. There is only steering in direction from the neutral cavity to the passive cavity. This steering appears in a short

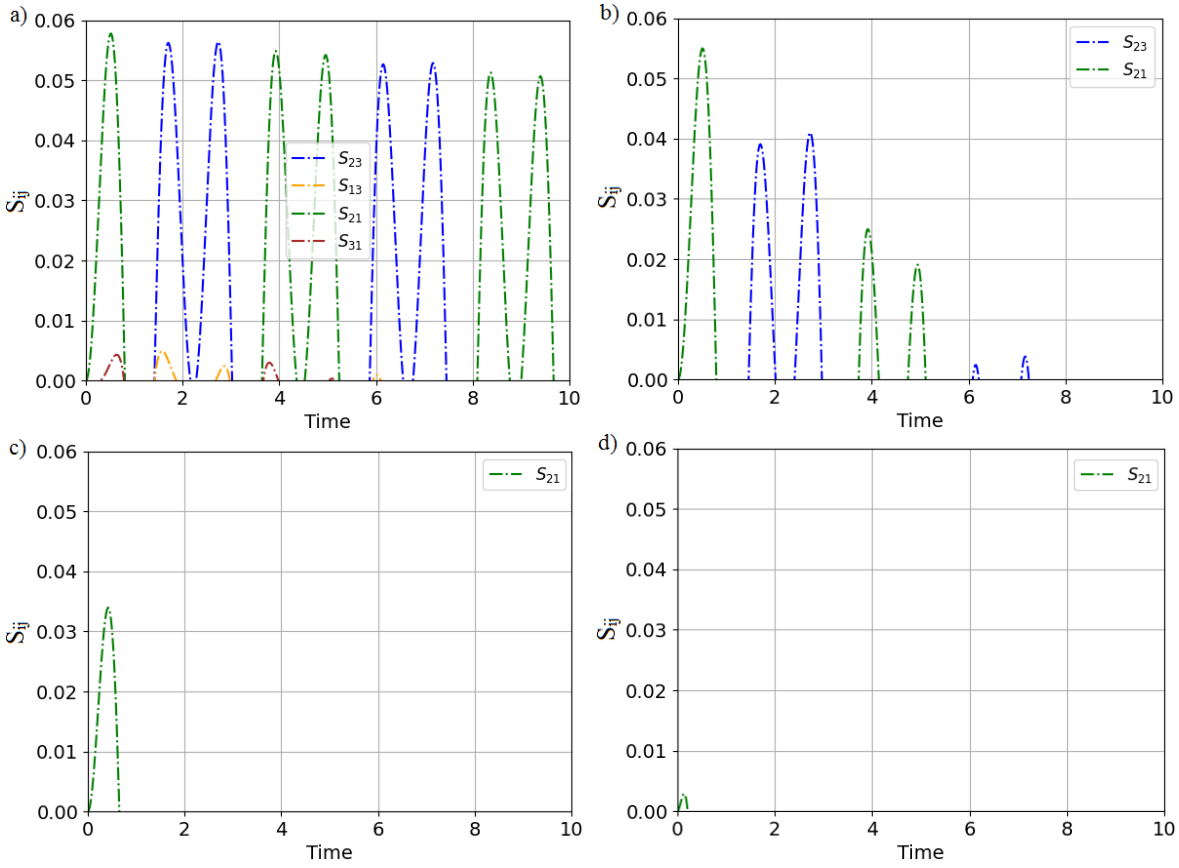

Fig. 4.22: The time evolution of steering parameters S_{ij} for (**a**) $\gamma = 0.001\beta$; (**b**) $\gamma = 0.01\beta$; (**c**) $\gamma = 0.1\beta$; (**d**) $\gamma = 0.8\beta$ when the initial state is $\hat{\rho}(t=0) = |100\rangle\langle 100|$, $\omega = 5\beta$, $\chi = 0$. Time is scaled in $1/\beta$ units.

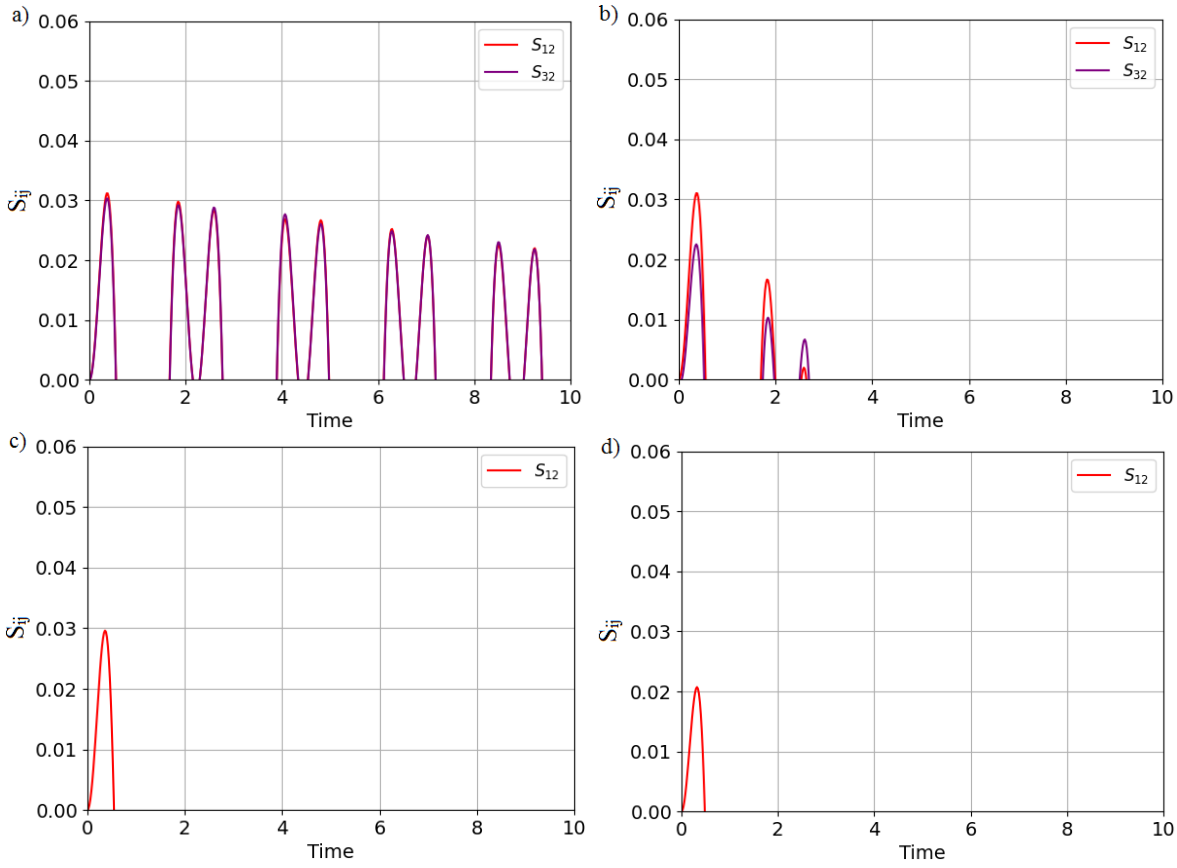

Fig. 4.23: The time evolution of steering parameters S_{ij} for (**a**) $\gamma = 0.001\beta$; (**b**) $\gamma = 0.01\beta$; (**c**) $\gamma = 0.1\beta$; (**d**) $\gamma = 0.8\beta$ when the initial state is $\hat{\rho}(t=0) = |010\rangle\langle 010|$, $\omega = 5\beta$, $\chi = 0.1\beta$. Time is scaled in $1/\beta$ units.

period of time before vanishing. When we continue to increase the value of γ/β to 0.8, the steering ability of the neutral cavity will be decreasing (see Fig.4.23c and Fig.4.23d). If we remove the coupling between the active and passive cavities, the results in Fig.4.24 show that there is nothing different from the scenario in which the coupling is remained. This indicate that if the system starts its evolution with excitation in the neutral cavity, the steering in our system is apparently not dependent on the interaction between the active and passive cavities.

In the last case, the system will start by the initial state $\hat{\rho}(t=0) = |001\rangle\langle 001|$. We can see in Fig.4.25 that, for both four different values of γ, the steering ability of the active cavity to the neutral one always appears at the beginning of system's evolution. When $\gamma = 0.001\beta$, we also see that the active and passive cavity can steer the neutral one. However, in this case of initial state, the evolution of S_{23} and S_{21} are reversed in the comparison to the case of initial state $\hat{\rho}(t=0) = |100\rangle\langle 100|$. Besides the steering abilities to the neutral cavity, the active and passive cavities can also steer each other. The evolution of S_{13} and S_{31} are also reversed compared to the case of $\hat{\rho}(t=0) = |100\rangle\langle 100|$

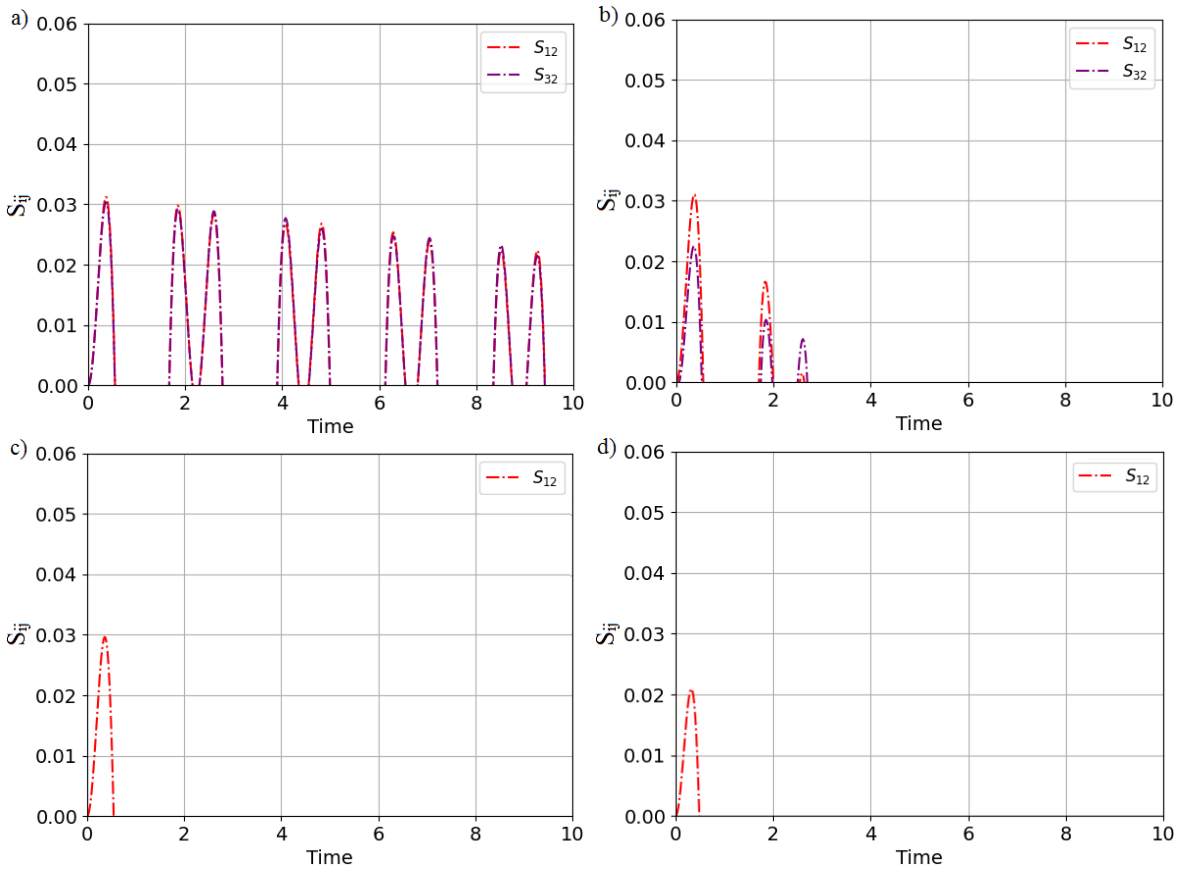

Fig. 4.24: The time evolution of steering parameters S_{ij} for (**a**) $\gamma = 0.001\beta$; (**b**) $\gamma = 0.01\beta$; (**c**) $\gamma = 0.1\beta$; (**d**) $\gamma = 0.8\beta$ when the initial state is $\hat{\rho}(t=0) = |010\rangle\langle 010|$, $\omega = 5\beta$, $\chi = 0$. Time is scaled in $1/\beta$ units.

(see Fig.4.25a). When $\gamma = 0.01\beta$, the results in Fig.4.25b show that the passive cavity losses its steering to the active one. However, in the opposite direction, the active cavity still can steer the passive one for a short interval of time at the beginning of system's evolution. Moreover, in this interval of time, the active can also simultaneously steer both the passive and the neutral cavity. When $\gamma = 0.1\beta$, we can see in Fig.4.25c that only the active cavity can steer the other ones. These steering abilities also simultaneously appear for a short interval of time before disappearing. When the value of γ increases to $\gamma = 0.8\beta$ the steering abilities of the active cavity to the others will be decreasing (see Fig.4.25d). If we remove the coupling between the active and passive cavities, the results of S_{ij} evolution will be mostly the same with what they were in the case of initial state $\hat{\rho}(t = 0) = |100\rangle\langle 100|$ when we invert the roles of S_{23} with S_{21}, and S_{13} with S_{31} (see Fig.4.22 and Fig.4.26). However, for the case of initial state $\hat{\rho}(t = 0) = |001\rangle\langle 001|$, the active cavity does not loss its steering to the passive one for both four different value of γ.

Next, we investigate the dependence of maximal values of S_{ij} that show the strength

of steering ability for each direction. In the first case, when the system starts with excitation in the passive cavity, we can see in Fig.4.27 that there are only four steering directions from the active or passive cavity to the others. The steering ability for each direction depends on the value of γ/β, and they only appear for a certain range of γ/β. Firstly, we will concentrate on the steering ability of the passive cavity. In this case of system's initial state, the maximal value of S_{21} is always different from zero for all value of γ/β that fulfilled the condition of the unbroken phase of $\mathcal{PT}$-symmetry, and it gradually decreases when we increase the value of γ/β. It means that the passive cavity can steer the neutral one as long as the system is in the unbroken phase of $\mathcal{PT}$-symmetry, and the steering ability in this direction decreases when the rate of gain/loss energy increases. This results are the same for both two scenarios $\chi = 0.1\beta$ and $\chi = 0$. Meanwhile, the maximal value of S_{31} rapidly decreases when we increase the value of γ/β, and it will be negative when $\gamma/\beta > 0.012$. When we remove the coupling between the active and passive cavity, the maximal value of S_{31} becomes much smaller than it takes when $\chi = 0.1\beta$, and it will be negative when $\gamma/\beta > 0.007$. It means that the passive cavity can only steer the active one for very small rates of gain/loss energy. Secondly, about the steering ability of the active cavity, we can see that the maximal values of S_{13} and S_{23} rapidly decrease from the value around 0.05 to zero when the value of γ/β increases to 0.030 (for S_{23}) and 0.011 (for S_{13}). It means that the steering ability of the active cavity only appears for very small values of γ/β. If we remove the coupling between the active and passive cavities, the steering ability of the active cavity to the passive one will become much weaker, and its steering ability to the neutral cavity is a little stronger than what they were in the scenario of remaining the coupling. We can also see that, in this case of systems′s initial state, the neutral cavity can not steer the others for all values of γ/β.

In the second case, the system starts by excitation in the neutral cavity. The results in Fig.4.28 show that in the unbroken phase of $\mathcal{PT}$-symmetry, only the neutral cavity can steer the others. When we increase the value of γ/β, the maximal value of S_{12} is always positive , and it slightly decreases from 0.032 to 0.018. Meanwhile, the maximal value of S_{32} rapidly decreases from 0.030 to zero when the value of γ/β increases from zero to 0.03. It means, the active cavity can steer the passive one for all values of gain/loss energy rate while its steering to the neutral only appears for very small value of gain/loss energy rate. This steering will disappear when $\gamma/\beta > 0.03$. We also see that, the maximal values of S_{12} and S_{32} apparently do not change when we remove the coupling between the active and passive cavities. It means that the steering ability of the neutral cavity in this case are virtually not influenced by the coupling between the other cavities.

In the last case, the system starts its evolution with excitation in the active cavity. The results are shown in Fig.4.29. We see that, in this case, only the active and passive cavities can steer the others. About the steering ability of the passive cavity, we can see that the maximal value of S_{21} and S_{31} are only positive for very small values of γ/β. It means that the steering abilities of the passive cavity to the others only appear for very small rates of gain/loss energy. When we increase the value of γ/β, the maximal

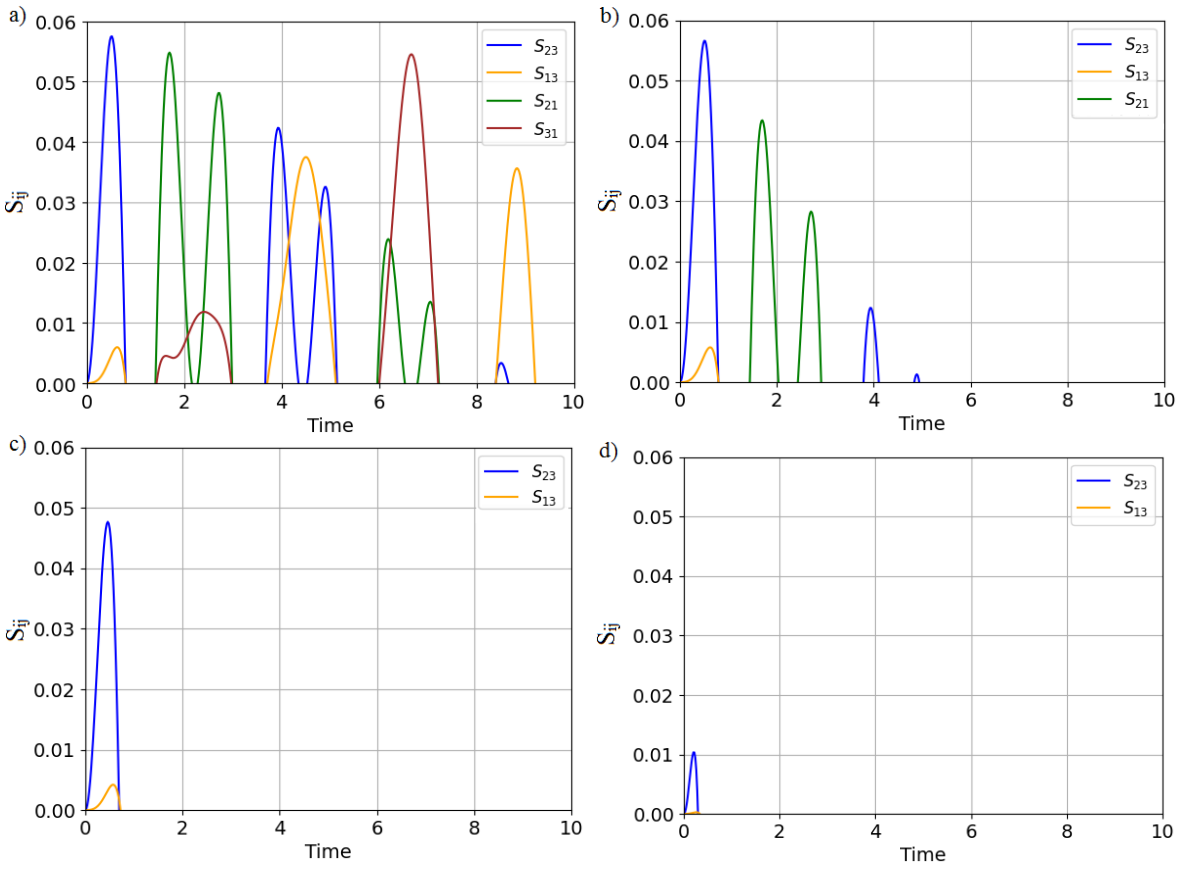

Fig. 4.25: The time evolution of steering parameters S_{ij} for (**a**) $\gamma = 0.001\beta$; (**b**) $\gamma = 0.01\beta$; (**c**) $\gamma = 0.1\beta$; (**d**) $\gamma = 0.8\beta$ when the initial state is $\hat{\rho}(t=0) = |001\rangle\langle 001|$, $\omega = 5\beta$, $\chi = 0.1\beta$. Time is scaled in $1/\beta$ units.

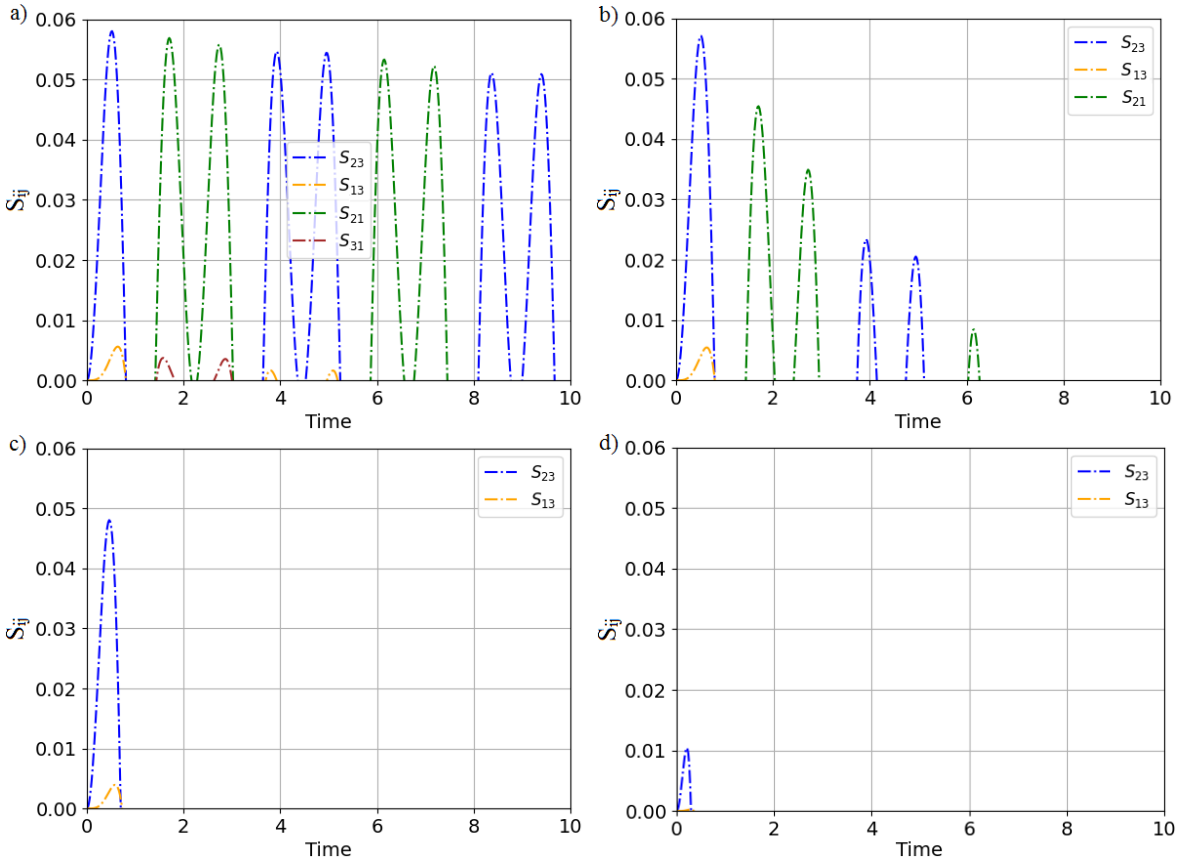

Fig. 4.26: The time evolution of steering parameters S_{ij} for (**a**) $\gamma = 0.001\beta$; (**b**) $\gamma = 0.01\beta$; (**c**) $\gamma = 0.1\beta$; (**d**) $\gamma = 0.8\beta$ when the initial state is $\hat{\rho}(t=0) = |001\rangle\langle 001|$, $\omega = 5\beta$, $\chi = 0$. Time is scaled in $1/\beta$ units.

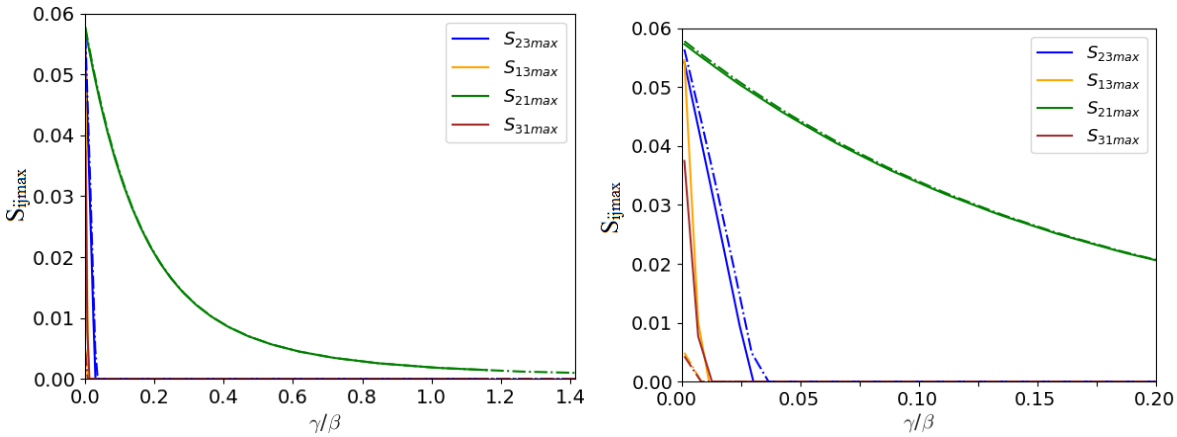

Fig. 4.27: The dependence of maximal values of steering parameter S_{ij} on γ/β for system's initial state $\hat{\rho}(t=0) = |100\rangle\langle 100|$ when $\gamma = 5\beta$, $\chi = 0.1\beta$ (solid lines) and $\chi = 0$ (dash-dotted lines).

values of S_{21} and S_{31} decrease from 0.055 to zero when the value of γ/β increases from zero to 0.038 (for S_{21}), and to 0.08 (for S_{31}). If we remove the coupling between the active and passive cavities ($\chi = 0$), the maximal value of S_{21} will be a little greater while the maximal value of S_{31} will be much smaller than what they were in the case of remaining the coupling ($\chi = 0.1\beta$). It indicates that the coupling between the active and passive cavities strongly intensifies the steering ability of the passive cavity to the active one. Concerning the steering ability of the active cavity, we can see that, the values of both S_{23} and S_{13} are positive for all the values of γ/β. It means, the active cavity can steer the others for all values of γ/β satisfying the condition of the unbroken phase of $\mathcal{PT}$-symmetry. However, its steering to neutral cavity is much stronger than its steering to the passive one. Besides that, the maximal values of S_{23} are approximately the same for both two scenarios $\chi = 0.1\beta$ and $\chi = 0$. However, it looks different for the maximal value of S_{13}. In the scenario of $\chi = 0.1\beta$, when we increase the value of γ/β, the maximal value of S_{13} rapidly decrease from 0.037 to 0.006 (at $\gamma/\beta = 0.012$), then slightly decreases for the rest values of γ/β in the unbroken phase of $\mathcal{PT}$-symmetry. Meanwhile, if $\chi = 0$, the maximal value of S_{13} slightly decrease from 0.006 to the value approximately equal to zero when we increase the value of γ/β. We can say that, the coupling between the active and passive cavities strongly influence the steering abilities between them, but approximately does not influence the steering ability of the neutral cavity.

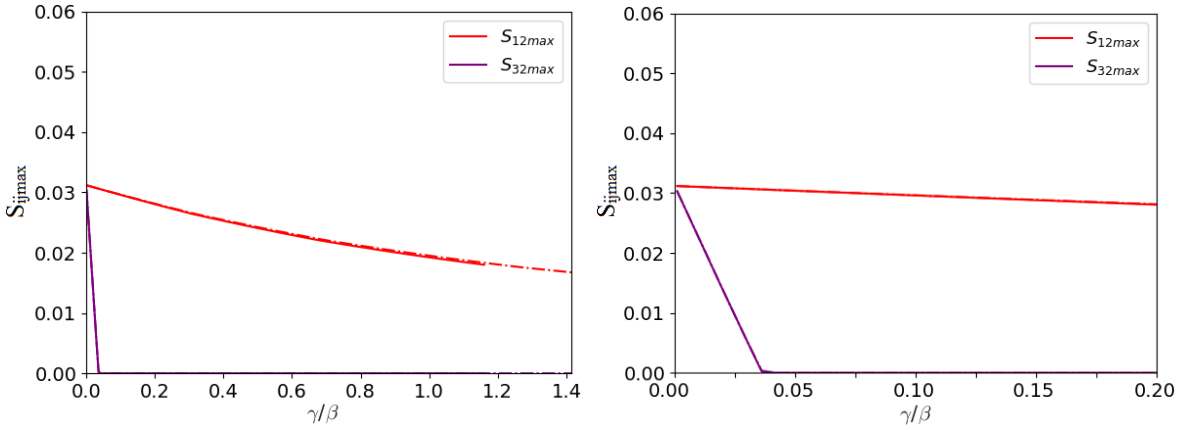

Fig. 4.28: The dependence of maximal values of steering parameter S_{ij} on γ/β for system's initial state $\hat{\rho}(t=0) = |010\rangle\langle 010|$ when $\gamma = 5\beta$, $\chi = 0.1\beta$ (solid lines) and $\chi = 0$ (dash-dotted lines).

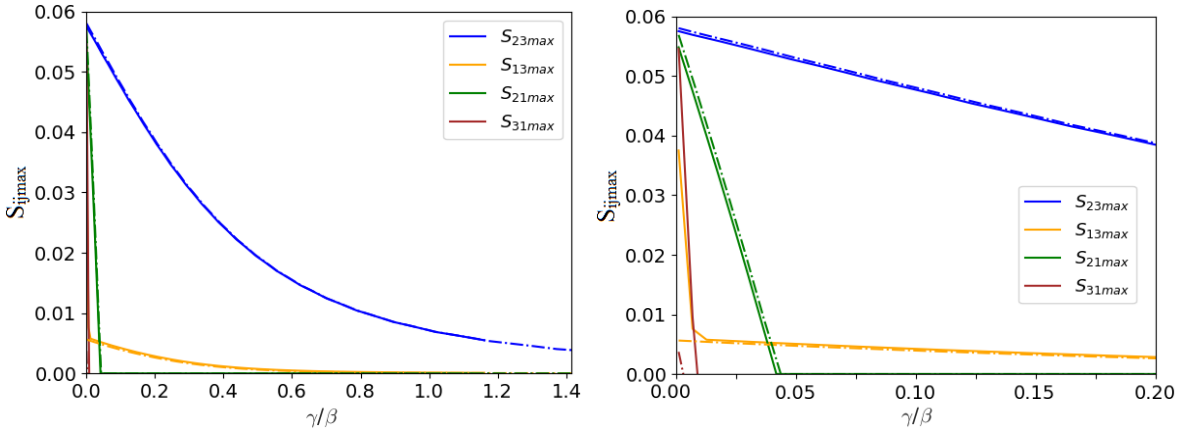

Fig. 4.29: The dependence of maximal values of steering parameter S_{ij} on γ/β for system's initial state $\hat{\rho}(t=0) = |001\rangle\langle 001|$ when $\gamma = 5\beta$, $\chi = 0.1\beta$ (solid lines) and $\chi = 0$ (dash-dotted lines).

4.4 Summary

In this chapter, we considered two models of tripartite $\mathcal{PT}$-symmetric systems that consist of three linear interacting cavities with a balance between gain and loss of energy. In those systems, the passive and active cavities are coupled to the neutral middle one. In the first model, it is not interaction between the active and passive cavities. Contrary to the second analyzed system, where those two cavities interact with each other. However, this coupling is much weaker than those between other cavities. After finding the phase-transition point for each system, we investigated the quantum correlation such as quantum entanglement and quantum steering.

Concerning quantum entanglement, we saw that, in both two systems, entanglements between subsystems change periodically in time. For higher rate of gain/loss of energy, entanglement decreases faster than for small values of this rate. When system is close to the phase-transition point, in both systems, stable bi- and tripartite entanglement is produced with realiable . What is relevant, the strength of entanglement depends on the rate of gain/loss of energy. If the system is without direct coupling between the active and passive cavities, the strength of bipartite entanglements between the neutral and the other two cavities are the same. Meanwhile, the entanglement between active and passive cavities is weaker than other entanglements generated in the system. The tripartite entanglement is also significantly generated. Those results is published in our article [170]. When the active cavity directly interacts with active one, the bipartite entanglement between the active and passive cavities is much stronger than those observed in the system without interaction between active and passive cavities. However, the tripartite entanglement generations in both two systems seem to be similar.

For quantum steering, we saw that the generation of steerable states strongly depends on the initial state of the systems. When the passive or active cavity is initially excited, only those two subsystems steer others, and the steerings in the opposite direction are not generated. However, if the neutral cavity is initially excited, there is only the neutral cavity steer the other subsystems. The additional interaction between the active and passive cavities significantly increases the strength of their steering abilities. However, this increase is only for the case of small values of the rate of gain/loss of energy. These results can be found in our published [171].

Conclusions

This dissertation is devoted to quantum correlations in the bi- and tripartite PT-symmetric systems. The first two chapters of the dissertation were focused on some basic concepts related to the quantum correlations and the PT-symmetry. The other two chapters were presented our results for bi- and tripartite PT-symmetric systems.

Bi- and tripartite $\mathcal{PT}$-symmetric systems have been researched both theoretically [132–140, 142] and experimentally [99, 100, 172] since Bender and his co-worker proposed the existence of $\mathcal{PT}$-symmetric systems. The researchers focused on showing the critical point of $\mathcal{PT}$-symmetry breaking [133–135, 137, 138, 142], photon transfer [99, 100, 139, 140, 172] in bi- and tripartite $\mathcal{PT}$-symmetric system. This dissertation contributes the results that show the possibility of quantum correlation generation in such systems that can be a good base for quantum computation and quantum information processing or waveguide fabricating.

The first considered model is the bipartite $\mathcal{PT}$-symmetric system that consists of two cavities with the balance between gain and loss of energy. The coupling between cavities is linear. For such a model, the coherence, quantum entanglement, and quantum steering are investigated by calculating correlation function, negativity, and quantum steering parameter, respectively. Our results showed that in the unbroken $\mathcal{PT}$-symmetry phase, the generation of the above quantum correlations is controllable by changing the value of the rate of gain/loss of energy and by choosing the initial state of the system. One of the most important results is that for the long-time limit, the quantum correlations are generated. What is relevant, our model ensures the possibility of producing stable quantum correlations such as coherence, entanglement [170], and steering. By changing the rate of gain/loss of energy, we can obtain strong quantum correlations. In the analyzed system, the quantum steering is produced in both directions: from the first subsystem to the second one and in the opposite direction. But the generated steering is asymmetric [171].

The second analyzed system consists of three cavities with a balanced gain and loss of energy. The passive cavity and the active one interact with the middle neutral cavity. But those two cavities (passive and active) do not directly interact with each other. In this case, we also see that the maximal values of bi- and tripartite negativities depend not only on the rate of gain/loss of energy but also on the initial system's state. The entanglement becomes weaker with increasing the rate of gain/loss of energy. When the rate of gain/loss of energy is high enough, and the system is close to the phase-transition point, the bipartite entanglements become stable, and the tripartite entanglement disappears. When the passive cavity or active cavity is initially excited, the bipartite entanglement between those two cavities is weak. However, if the neutral cavity is initially excited, for some rates of gain/loss of energy, the entanglement between the passive cavity and the active cavity dominates the others. As for entanglement, our results showed that the generation of steerable states strongly depends on the initial system's state. For instance, when the middle cavity is initially excited, only this one

steers the others. In the other cases, the passive and active cavity steer the other subsystems. But in all analyzed cases, only asymmetric steering is produced.

At last, in the tripartite model, we added a linear coupling between the active and the passive cavity. The results showed, that in the system with this additional coupling, the generated entanglement and steering between the passive and active cavity are stronger. The influence of the coupling between the active and passive cavity is more visible for the small rates of gain/loss of energy.

In the future, we will continue to investigate the quantum correlations in the various models with nonlinear coupling and parametric interaction between subsystems. Besides that, we plan also to consider some geometrical configurations of cavities connected by fibers in which the influence of phase factors on the phase-transition point of $\mathcal{PT}$-symmetry and quantum correlation generation is significant.

Articles and conference communications

Articles:

- V. Le Duc, J.K. Kalaga, W. Leoński, Quantum correlations in System of Kerr Nonlinear Coupler, *Acta Physica Polonica A*, **139**, 532-534 (2021).

- V. Le Duc, M. Nowotarski, J. Kalaga, The Bipartite and Tripartite Entanglement in PT-Symmetric System, Symmetry **13**, 203 (2021).

- V. Le Duc, M. Nowotarski, J. Kalaga, W. Leoński, K. Gruszka, Steering generation in two- and three-mode PT-symmetric system, Symmetry **13**, 2201 (2021).

Conference communications:

- V. Le Duc, W. Leoński, Entangled state generation by a nonlinear coupler pumped in two modes, The 12th Workshop on Current Problems in Physics, University of Zielona Gora, Zielona Gora, Poland, (2019).

- V. Le Duc, Entangled state - The work base of quantum computation and quantum teleportation, The Fourth Workshop of Vietnamese Students in Poland, University of Warsaw, Warsaw, Poland (2019).

- V. Le Duc, J. K. Kalaga, W. Leoński, Quantum correlations in a system of the Kerr nonlinear coupler, Applications of Physics in Mechanical and Material Engineering (APMME), (2021).

- V. Le Duc, J. K. Kalaga, W. Leoński, Quantum correlations in PT-symmetric systems, The 13th Workshop on Current Problems in Physics, Lviv (2021).

Bibliography

[1] C. M. Bender and S. Boettcher. Real Spectra in Non-Hermitian Hamiltonians Having $\mathcal{PT}$ Symmetry. *Physical Review Letters*, 80:5243–5246, 1998.

[2] F. David, T. Gudehus, and G. Kaiser. Space-time structure in high energy interactions. In *Fundamental Interactions at High Energy*. Gordon & Breach, 1968.

[3] C. H. Bennett. Logical reversibility of computation. *IBM journal of Research and Development*, 17(6):525, 1973.

[4] P. Benioff. The computer as a physical system: A microscopic quantum mechanical hamiltonian model of computers as represented by turing machines. *Journal of Statistical Physics*, 22(5):563, 1980.

[5] P. Benioff. Quantum mechanical hamiltonian models of turing machines. *Journal of Statistical Physics*, 29(3):515, 1982.

[6] Richard P. Feynman. *Feynman Lectures on Computation*. CRC Press, Taylor & Francis Group, 2000.

[7] I. L. Chuang, N. Gershenfeld, and M. Kubinec. Experimental implementation of fast quantum searching. *Physical Review Letters*, 80(15):3408, 1998.

[8] C. H. Bennett, G. Brassard, C. Crepeau, R. Jozsa, A. Peres, and W. K. Wootters. Teleporting an unknown quantum state via dual classical and Einstein-Podolsky-Rosen channels. *Physical Review Letters*, 70(13):1895, 1993.

[9] D. Boschi, S. Branca, F. De Martini, L. Hardy, and S. Popescu. Experimental realization of teleporting an unknown pure quantum state via dual classical and Einstein-Podolsky-Rosen channels. *Physical Review Letters*, 80(6):1121, 1998.

[10] D. Bouwmeester, J. Pan, K. Mattle, M. Eibl, H. Weinfurter, and A. Zeilinger. Experimental quantum teleportation. *Nature*, 390(6660):575, 1997.

[11] Q. Zhang, A. Goebel, C. Wagenknecht, Y. Chen, B. Zhao, T. Yang, A. Mair, J. Schmiedmayer, and J. W. Pan. Experimental quantum teleportation of a two-qubit composite system. *Nature Physics*, 2(10):678, 2006.

[12] W. Pfaff, B. J. Hensen, H. Bernien, S. B. van Dam, M. S. Blok, T. H. Taminiau, M. J. Tiggelman, R. N. Schouten, M. Markham, and D. J. Twitchen. Unconditional quantum teleportation between distant solid-state quantum bits. *Science*, 345(6196):532, 2014.

[13] Xiao-Song Ma, Thomas Herbst, Thomas Scheidl, Daqing Wang, Sebastian Kropatschek, William Naylor, Bernhard Wittmann, Alexandra Mech, Johannes Kofler, Elena Anisimova, Vadim Makarov, Thomas Jennewein, Rupert Ursin, and Anton Zeilinger. Quantum teleportation over 143 kilometres using active feed-forward. *Nature*, 489(7415):269, 2012.

[14] J. Ren, P. Xu, H. L. Yong, L. Zhang, S. K. Liao, J. Yin, W. Y. Liu, W. Q. Cai, M. Yang, and L. Li. Ground-to-satellite quantum teleportation. *Nature*, 549(7670):70, 2017.

[15] N. Linden and S. Popescu. Good dynamics versus bad kinematics: Is entanglement needed for quantum computation? *Physical Review Letters*, 87(4):047901, 2001.

[16] R. Uola, A. C. S. Costa, H. C. Nguyen, and O. Gühne. Quantum steering. *Reviews of Modern Physics*, 92(1):015001, 2020.

[17] J. R. Schaibley, A. P. Burgers, G. A. McCracken, L. M. Duan, P. R. Berman, D. G. Steel, A. S. Bracker, D. Gammon, and L. J. Sham. Demonstration of quantum entanglement between a single electron spin confined to an InAs quantum dot and a photon. *Physical Review Letters*, 110(16):167401, 2013.

[18] J. Hu and H. Yu. Quantum entanglement generation in de sitter spacetime. *Physical Review D*, 88(10):104003, 2013.

[19] M. D. Lukin and P. R. Hemmer. Quantum entanglement via optical control of atom-atom interactions. *Physical Review Retters*, 84(13):2818, 2000.

[20] X. Tian, Y. Liu, C. Cui, and J. Wu. Population transfer and quantum entanglement implemented in cold atoms involving two Rydberg states via an adiabatic passage. *Physical Review A*, 92(6):063411, 2015.

[21] Y. Lin, D. R. Leibrandt, D. Leibfried, and C. Chou. Quantum entanglement between an atom and a molecule. *Nature*, 581(7808):273, 2020.

[22] R. Riedinger, A. Wallucks, I. Marinkovic, C. Loschnauer, M. Aspelmeyer, S. Hong, and S. Groblacher. Remote quantum entanglement between two micromechanical oscillators. *Nature*, 556(7702):4, 2018.

[23] G. Giavaras, J. H. Jefferson, A. Ramsak, T. P. Spiller, and C. J. Lambert. Quantum entanglement generation with surface acoustic waves. *Physical Review B*, 74(19):195341, 2006.

[24] C. M. Bender, S. Boettcher, and P. N. Meisinger. *PT-symmetric quantum mechanics*, volume 40. American Institute of Physics, 1999.

[25] E. Turilova. Completeness of inner product spaces induced by states on jordan and c algebras. *International Journal of Theoretical Physics*, 54(12):4229, 2015.

[26] G. Jaeger and B. Terhal. Quantum information: An overview. *Physics Today*, 61(3):53, 2008.

[27] B. Thaller. *Advanced visual quantum mechanics*. Springer Science and Business Media, 2005.

[28] M. A. Nielsen and I. L. Chuang. *Quantum computation and quantum information*. Cambridge University Press, 2010.

[29] L. Aolita, F. De Melo, and L. Davidovich. Open-system dynamics of entanglement: a key issues review. *Reports on Progress in Physics*, 78(4):042001, 2015.

[30] R. F. Werner. Quantum states with einstein-podolsky-rosen correlations admitting a hidden-variable model. *Physical Review A*, 40(8):4277, 1989.

[31] M. Horodecki, P. Horodecki, and R. Horodecki. Mixed-state entanglement and distillation: Is there a bound entanglement in nature? *Physical Review Letters*, 80(24):5239, 1998.

[32] F. Pan, D. Liu, G. Lu, and J. P. Draayer. Simple entanglement measure for multipartite pure states. *International Journal of Theoretical Physics*, 43(5):1241, 2004.

[33] W. Cao, D. Liu, F. Pan, and G. Long. Entropy product measure for multipartite pure states. *Science in China Series G: Physics, Mechanics and Astronomy*, 49(5):606, 2006.

[34] W. K. Wootters. Entanglement of formation of an arbitrary state of two qubits. *Physical Review Letters*, 80(10):2245, 1998.

[35] F. Mintert, M. Kuś, and A. Buchleitner. Concurrence of mixed bipartite quantum states in arbitrary dimensions. *Physical Review Letters*, 92(16):167902, 2004.

[36] M. Nawareg. Concurrence of multiqubit bound entangled states constructed from unextendible product bases. *Physical Review A*, 101(3):032342, 2020.

[37] C. Yu and H. Song. Free entanglement measure of multiparticle quantum states. *Physics Letters A*, 330(5):377, 2004.

[38] G. Vidal and R. F. Werner. Computable measure of entanglement. *Physical Review A*, 65(3):032314, 2002.

[39] C. Sabín and G. García-Alcaine. A classification of entanglement in three-qubit systems. *The European Physical Journal D*, 48(3):435, 2008.

[40] A. Einstein, B. Podolsky, and N. Rosen. Can quantum-mechanical description of physical reality be considered complete? *Physical Review*, 47(10):777, 1935.

[41] E. Schrödinger. Discussion of probability relations between separated systems. In *Mathematical Proceedings of the Cambridge Philosophical Society*, volume 31, page 555. Cambridge University Press, 1935.

[42] E. Schrödinger. Probability relations between separated systems. In *Mathematical Proceedings of the Cambridge Philosophical Society*, volume 32, page 446. Cambridge University Press, 1936.

[43] H. M. Wiseman, S. J. Jones, and A. C. Doherty. Steering, entanglement, nonlocality, and the Einstein-Podolsky-Rosen paradox. *Physical Review Letters*, 98(14):140402, 2007.

[44] D. Cavalcanti and P. Skrzypczyk. Quantum steering: a review with focus on semidefinite programming. *Reports on Progress in Physics*, 80(2):024001, 2016.

[45] P. Skrzypczyk, M. Navascués, and D. Cavalcanti. Quantifying einstein-podolsky-rosen steering. *Physical Review Letters*, 112(18):180404, 2014.

[46] M. Lewenstein and A. Sanpera. Separability and entanglement of composite quantum systems. *Physical Review Letters*, 80(11):2261, 1998.

[47] G. Vidal and R. Tarrach. Robustness of entanglement. *Physical Review A*, 59(1):141, 1999.

[48] R. Gallego and L. Aolita. Resource theory of steering. *Physical Review X*, 5(4):041008, 2015.

[49] A. Aspect, P. Grangier, and G. Roger. Experimental realization of Einstein-Podolsky-Rosen-Bohm-Gedanken experiment: a new violation of bell's inequalities. *Physical Review Letters*, 49(2):91, 1982.

[50] B. Hensen, H. Bernien, A. E. Dreau, A. Reiserer, N. Kalb, M. S. Blok, J. Ruitenberg, R. F. L. Vermeulen, R. N. Schouten, and C. Abellan. Loophole-free bell inequality violation using electron spins separated by 1.3 kilometres. *Nature*, 526(7575):682, 2015.

[51] L. K. Shalm, E. Meyer-Scott, B. G. Christensen, P. Bierhorst, M. A. Wayne, M. J. Stevens, T. Gerrits, S. Glancy, D. R. Hamel, and M. S. Allman. Strong loophole-free test of local realism. *Physical Review Letters*, 115(25):250402, 2015.

[52] M. Giustina, M. A. M. Versteegh, S. Wengerowsky, J. Handsteiner, A. Hochrainer, K. Phelan, F. Steinlechner, J. Kofler, J. Larsson, and C. Abellan. Significant loophole-free test of Bell theorem with entangled photons. *Physical Review Letters*, 115(25):250401, 2015.

[53] N. D. Mermin. Extreme quantum entanglement in a superposition of macroscopically distinct states. *Physical Review Letters*, 65(15):1838, 1990.

[54] E. G. Cavalcanti, C. J. Foster, M. D. Reid, and P. D. Drummond. Bell inequalities for continuous-variable correlations. *Physical Review Letters*, 99(21):210405, 2007.

[55] M. Hillery and M. S. Zubairy. Entanglement conditions for two-mode states. *Physical Review Letters*, 96(5):050503, 2006.

[56] Y. Cai and S. Zhu. Ghost interference with partially coherent radiation. *Optics Letters*, 29(23):2716, 2004.

[57] L. Mandel and E. Wolf. *Optical coherence and quantum optics*. Cambridge University Press, 1995.

[58] R. Loudon. *The quantum theory of light*. Oxford University Press, 2000.

[59] D. F. Walls and G. J. Milburn. Quantum coherence and measurement theory. In *Quantum Optics*, page 283. Springer, 2008.

[60] C. Gerry, P. Knight, and P. L. Knight. *Introductory quantum optics*. Cambridge University Press, 2005.

[61] M. A. Nielsen and I. Chuang. Quantum computation and quantum information, 2002.

[62] R. H. Brown and R. Q. Twiss. A test of a new type of stellar interferometer on sirius. *Nature*, 178(4541):1046, 1956.

[63] A. G. Arutyunyan, S. A. Akhmanov, Y. D. Golyaev, V. G. Tunkin, and A. S. Chirkin. Spatial field and intensity correlation functions of laser radiation. *Journal of Experimental and Theoretical Physics*, 64:1511, 1973.

[64] H. J. Kimble, M. Dagenais, and L. Mandel. Photon antibunching in resonance fluorescence. *Physical Review Letters*, 39(11):691, 1977.

[65] A. Imamoglu, H. Schmidt, G. Woods, and M. Deutsch. Strongly interacting photons in a nonlinear cavity. *Physical Review Letters*, 79(8):1467, 1997.

[66] G. M. D'Ariano, L. Maccone, M. G. A. Paris, and M. F. Sacchi. Optical fock-state synthesizer. *Physical Review A*, 61(5):053817, 2000.

[67] W. Leonski and R. Tanas. Possibility of producing the one-photon state in a kicked cavity with a nonlinear Kerr medium. *Physical Review A*, 49(1):R20, 1994.

[68] I. Carusotto and C. Ciuti. Quantum fluids of light. *Reviews of Modern Physics*, 85(1):299, 2013.

[69] K. M. Birnbaum, A. Boca, R. Miller, A. D. Boozer, T. E. Northup, and H. J. Kimble. Photon blockade in an optical cavity with one trapped atom. *Nature*, 436(7047):87, 2005.

[70] R. H. Brown and R. Q. Twiss. Correlation between photons in two coherent beams of light. *Nature*, 177(4497):27, 1956.

[71] A. B. U'Ren, C. Silberhorn, J. L. Ball, K. Banaszek, and I. A. Walmsley. Characterization of the nonclassical nature of conditionally prepared single photons. *Physical Review A*, 72(2):021802, 2005.

[72] F. Bussieres, J. A. Slater, N. Godbout, and W. Tittel. Fast and simple characterization of a photon pair source. *Optics Express*, 16(21):17060, 2008.

[73] D. L. Boiko, N. J. Gunther, N. Brauer, M. Sergio, C. Niclass, G. B. Beretta, and E. Charbon. A quantum imager for intensity correlated photons. *New Journal of Physics*, 11(1):013001, 2009.

[74] G. Scarcelli, A. Valencia, and Y. Shih. Experimental study of the momentum correlation of a pseudothermal field in the photon-counting regime. *Physical Review A*, 70(5):051802, 2004.

[75] E. D. Lopaeva and M. V. Chekhova. Ghost imaging with the use of the variance of the difference photocurrent. *Journal of Experimental and Theoretical Physics Letters*, 91(9):447, 2010.

[76] M. Avenhaus, K. Laiho, M. V. Chekhova, and C. Silberhorn. Accessing higher order correlations in quantum optical states by time multiplexing. *Physical Review Letters*, 104(6):063602, 2010.

[77] S. Chopra and L. Mandel. Higher-order correlation properties of a laser beam. *Physical Review Letters*, 30(2):60, 1973.

[78] O. A. Ivanova, T. S. Iskhakov, A. N. Penin, and M. V. Chekhova. Multiphoton correlations in parametric down-conversion and their measurement in the pulsed regime. *Quantum Electronics*, 36(10):951, 2006.

[79] A. Glindemann. Introduction to spatial interferometry. *European Southern Observatory*, 2011.

[80] R. J. Glauber. The quantum theory of optical coherence. *Physical Review*, 130(6):2529, 1963.

[81] R. Loudon. The quantum theory of light. 1983.

[82] J. Rubinstein, P. Sternberg, and Q. Ma. Bifurcation diagram and pattern formation of phase slip centers in superconducting wires driven with electric currents. *Physical Review Letters*, 99(16):167003, 2007.

[83] S. Assawaworrarit, X. Yu, and S. Fan. Robust wireless power transfer using a nonlinear parity–time-symmetric circuit. *Nature*, 546(7658):387, 2017.

[84] N. Bender, S. Factor, J. D. Bodyfelt, H. Ramezani, D. N. Christodoulides, F. M. Ellis, and T. Kottos. Observation of asymmetric transport in structures with active nonlinearities. *Physical Review Letters*, 110(23):234101, 2013.

[85] J. Schindler, A. Li, M. C. Zheng, F. M. Ellis, and T. Kottos. Experimental study of active lrc circuits with PT-symmetries. *Physical Review A*, 84(4):040101, 2011.

[86] P. A. Kalozoumis and D. Petrosyan. Self-organized PT-symmetry of exciton-polariton condensate in a double-well potential. *Applied Sciences*, 11(16):7372, 2021.

[87] M. Partanen, J. Goetz, K. Y. Tan, K. Kohvakka, V. Sevriuk, R. E. Lake, R. Kokkoniemi, J. Ikonen, D. Hazra, and A. Mäkinen. Exceptional points in tunable superconducting resonators. *Physical Review B*, 100(13):134505, 2019.

[88] J. Huber and P. Rabl. Active energy transport and the role of symmetry breaking in microscopic power grids. *Physical Review A*, 100(1):012129, 2019.

[89] N. M. Chtchelkatchev, A. A. Golubov, T. I. Baturina, and V. M. Vinokur. Stimulation of the fluctuation superconductivity by PT-symmetry. *Physical Review Letters*, 109(15):150405, 2012.

[90] R. El-Ganainy, K. G. Makris, D. N. Christodoulides, and Z. H. Musslimani. Theory of coupled optical PT-symmetric structures. *Optics Letters*, 32(17):2632, 2007.

[91] J. Huerta Morales, Julio Guerrero, Servando L. A., and B. Rodríguez-Lara. Revisiting the optical PT-symmetric dimer. *Symmetry*, 8(9):83, 2016.

[92] A. A. Sukhorukov, Z. Xu, and Y. S. Kivshar. Nonlinear suppression of time reversals in PT-symmetric optical couplers. *Physical Review A*, 82(4):043818, 2010.

[93] I. V. Barashenkov. Hamiltonian formulation of the standard PT-symmetric nonlinear schrödinger dimer. *Physical Review A*, 90(4):045802, 2014.

[94] Y. Lumer, Y. Plotnik, M. C. Rechtsman, and M. Segev. Nonlinearly induced PT-transition in photonic systems. *Physical Review Letters*, 111(26):263901, 2013.

[95] H. Ramezani, T. Kottos, R. El-Ganainy, and D. N. Christodoulides. Unidirectional nonlinear PT-symmetric optical structures. *Physical Review A*, 82(4):043803, 2010.

[96] K. Li, P. G. Kevrekidis, and B. A. Malomed. Nonlinear modes and symmetries in linearly coupled pairs of-invariant dimers. *Studies in Applied Mathematics*, 133(3):281, 2014.

[97] R. Driben and B. A. Malomed. Stability of solitons in parity-time-symmetric couplers. *Optics Letters*, 36(22):4323, 2011.

[98] A. Guo, G. J. Salamo, D. Duchesne, R. Morandotti, M. Volatier-Ravat, V. Aimez, G. A. Siviloglou, and D. N. Christodoulides. Observation of PT-symmetry breaking in complex optical potentials. *Physical Review Letters*, 103(9):093902, 2009.

[99] C. E. Rüter, K. G. Makris, R. El-Ganainy, D. N. Christodoulides, M. Segev, and D. Kip. Observation of parity-time symmetry in optics. *Nature Physics*, 6(3):192, 2010.

[100] L. Chang, X. Jiang, S. Hua, C. Yang, J. Wen, L. Jiang, G. Li, G. Wang, and M. Xiao. Parity–time symmetry and variable optical isolation in active–passive-coupled microresonators. *Nature Photonics*, 8(7):524, 2014.

[101] H. Vemuri, V. Vavilala, T. Bhamidipati, and Y. N. Joglekar. Dynamics, disorder effects, and PT-symmetry breaking in waveguide lattices with localized eigenstates. *Physical Review A*, 84(4):043826, 2011.

[102] H. Vemuri and Y. N. Joglekar. PT-symmetric lattices with a local degree of freedom. *Physical Review A*, 87(4):044101, 2013.

[103] S. Longhi. Bound states in the continuum in PT-symmetric optical lattices. *Optics Letters*, 39(6):1697, 2014.

[104] A. A. Sukhorukov, S. V. Dmitriev, S. V. Suchkov, and Y. S. Kivshar. Nonlocality in PT-symmetric waveguide arrays with gain and loss. *Optics Letters*, 37(11):2148, 2012.

[105] Y. N. Joglekar, C. Thompson, D. D. Scott, and G. Vemuri. Optical waveguide arrays: quantum effects and PT symmetry breaking. *The European Physical Journal-Applied Physics*, 63(3), 2013.

[106] W. Walasik and N. M. Litchinitser. Phase transition in multimode nonlinear parity-time-symmetric waveguide couplers. *Scientific Reports*, 6(1):1, 2016.

[107] P. G. Kevrekidis, D. E. Pelinovsky, and D. Y. Tyugin. Nonlinear dynamics in PT-symmetric lattices. *Journal of Physics A: Mathematical and Theoretical*, 46(36):365201, 2013.

[108] K. G. Makris, R. El-Ganainy, D. N. Christodoulides, and Z. H. Musslimani. Beam dynamics in PT-symmetric optical lattices. *Physical Review Letters*, 100(10):103904, 2008.

[109] M. C. Zheng, D. N. Christodoulides, R. Fleischmann, and T. Kottos. PT optical lattices and universality in beam dynamics. *Physical Review A*, 82(1):010103, 2010.

[110] A. Regensburger, C. Bersch, M. Miri, G. Onishchukov, D. N. Christodoulides, and U. Peschel. Parity–time synthetic photonic lattices. *Nature*, 488(7410):167, 2012.

[111] Z. H. Musslimani, K. G. Makris, R. El-Ganainy, and D. N. Christodoulides. Optical solitons in PT periodic potentials. *Physical Review Letters*, 100(3):030402, 2008.

[112] A. A. Naeimi, E. Darabi, A. Mortezapour, and G. Naeimi. Phase-controlled optical PT-symmetry and asymmetric light diffraction in one-and two-dimensional optical lattices. *The European Physical Journal Plus*, 135(10):1, 2020.

[113] Y. He, X. Zhu, D. Mihalache, J. Liu, and Z. Chen. Solitons in PT-symmetric optical lattices with spatially periodic modulation of nonlinearity. *Optics Communications*, 285(15):3320, 2012.

[114] Y. V. Kartashov, C. Hang, G. Huang, and L. Torner. Three-dimensional topological solitons in PT-symmetric optical lattices. *Optica*, 3(10):1048, 2016.

[115] H. Wang, Z. Li, X. Ren, and Y. Weng. Two-dimensional solitons in parity-time-symmetric optical lattices with nonlocal defocusing nonlinearity. *Optics Express*, 24(20):23063, 2016.

[116] J. Huang, Y. Weng, and H. Wang. Stability and internal interaction of multipole solitons in nonlocal PT-symmetric lattices. *Optics Express*, 26(9):11667, 2018.

[117] L. Ge, M. Shen, T. Zang, C. Ma, and L. Dai. Stability of optical solitons in parity-time-symmetric optical lattices with competing cubic and quintic nonlinearities. *Physical Review E*, 91(2):023203, 2015.

[118] Y. V. Kartashov, V. A. Vysloukh, V. V. Konotop, and L. Torner. Diffraction control in PT-symmetric photonic lattices: From beam rectification to dynamic localization. *Physical Review A*, 93(1):013841, 2016.

[119] X. Zhang, J. Chai, J. Huang, Z. Chen, Y. Li, and B. A. Malomed. Discrete solitons and scattering of lattice waves in guiding arrays with a nonlinear PT-symmetric defect. *Optics Express*, 22(11):13927, 2014.

[120] A. J. Martinez, M. I. Molina, S. K. Turitsyn, and Y. S. Kivshar. Nonlinear multicore waveguiding structures with balanced gain and loss. *Physical Review A*, 91(2):023822, 2015.

[121] J. T. Cole, K. G. Makris, Z. H. Musslimani, D. N. Christodoulides, and S. Rotter. Twofold PT-symmetry in doubly exponential optical lattices. *Physical Review A*, 93(1):013803, 2016.

[122] S. Longhi. Bloch oscillations in complex crystals with PT-symmetry. *Physical Review Letters*, 103(12):123601, 2009.

[123] S. Longhi. Invisibility in-symmetric complex crystals. *Journal of Physics A: Mathematical and Theoretical*, 44(48):485302, 2011.

[124] Y. Takasu, T. Yagami, Y. Ashida, R. Hamazaki, Y. Kuno, and Y. Takahashi. PT-symmetric non-hermitian quantum many-body system using ultracold atoms in an optical lattice with controlled dissipation. *Progress of Theoretical and Experimental Physics*, 2020(12):12A110, 2020.

[125] L. Ge and R. El-Ganainy. Nonlinear modal interactions in parity-time (PT) symmetric lasers. *Scientific Reports*, 6(1):1, 2016.

[126] M. Liertzer, L. Ge, A. Cerjan, A. D. Stone, H. E. Treci, and S. Rotter. Pump-induced exceptional points in lasers. *Physical Review Letters*, 108(17):173901, 2012.

[127] Y. D. Chong, L. Ge, and A. D. Stone. PT-symmetry breaking and laser-absorber modes in optical scattering systems. *Physical Review Letters*, 106(9):093902, 2011.

[128] M. Farhat, M. Yang, Z. Ye, and P. Chen. PT-symmetric absorber-laser enables electromagnetic sensors with unprecedented sensitivity. *ACS Photonics*, 7(8):2080, 2020.

[129] D. Yu and F. Vollmer. Spontaneous PT-symmetry breaking in lasing dynamics. *Communications Physics*, 4(1):1, 2021.

[130] K. V. Kepesidis, T. J. Milburn, J. Huber, K. G. Makris, S. Rotter, and P. Rabl. PT-symmetry breaking in the steady state of microscopic gain-loss systems. *New Journal of Physics*, 18(9):095003, 2016.

[131] B. Peng, Ş. K. Özdemir, F. Lei, F. Monifi, M. Gianfreda, G. L. Long, S. Fan, F. Nori, C. M. Bender, and L. Yang. Parity-time-symmetric whispering-gallery microcavities. *Nature Physics*, 10(5):394, 2014.

[132] A. Purkayastha, M. Kulkarni, and Y. N. Joglekar. PT-symmetry from lindblad dynamics in a linearized optomechanical system. *Physical Review Research*, 2:043075, 2020.

[133] E. Lange, G. Chimczak, A. Kowalewska-Kudłaszyk, and K. Bartkiewicz. Rotation-time symmetry in bosonic systems and the existence of exceptional points in the absence of PT-symmetry. *Scientific Reports*, 10(1):1, 2020.

[134] J. Peřina and A. Lukš. Quantum behavior of a PT-symmetric two-mode system with cross-kerr nonlinearity. *Symmetry*, 11(8):1020, 2019.

[135] J. Peřina Jr, A. Lukš, J. K. Kalaga, W. Leoński, and A. Miranowicz. Nonclassical light at exceptional points of a quantum PT-symmetric two-mode system. *Physical Review A*, 100(5):053820, 2019.

[136] A. Purkayastha, M. Kulkarni, and Y. N. Joglekar. Emergent PT-symmetry in a double-quantum-dot circuit qed setup. *Physical Review Research*, 2(4):043075, 2020.

[137] I. I. Arkhipov, A. Miranowicz, F. Minganti, and F. Nori. Quantum and semiclassical exceptional points of a linear system of coupled cavities with losses and gain within the scully-lamb laser theory. *Physical Review A*, 101(1):013812, 2020.

[138] L. F. Xue, Z. R. Gong, H. B. Zhu, and Z. H. Wang. PT-symmetric phase transition and photonic transmission in an optical trimer system. *Optics Express*, 25(15):17249, 2017.

[139] S. Felicetti, G. Romero, D. Rossini, R. Fazio, and E. Solano. Photon transfer in ultrastrongly coupled three-cavity arrays. *Physical Review A*, 89(1):013853, 2014.

[140] K. Li, P. G. Kevrekidis, D. J. Frantzeskakis, C. E. Rüter, and D. Kip. Revisiting the-symmetric trimer: bifurcations, ghost states and associated dynamics. *Journal of Physics A: Mathematical and Theoretical*, 46(37):375304, 2013.

[141] S. V. Suchkov, F. Fotsa-Ngaffo, A. Kenfack-Jiotsa, A. D. Tikeng, T. C. Kofane, Y. S. Kivshar, and A. A. Sukhorukov. Non-hermitian trimers: PT-symmetry versus pseudo-hermiticity. *New Journal of Physics*, 18(6):065005, 2016.

[142] J. Naikoo, K. Thapliyal, S. Banerjee, and A. Pathak. Quantum zeno effect and nonclassicality in a PT-symmetric system of coupled cavities. *Physical Review A*, 99(2):023820, 2019.

[143] M. Duanmu, K. Li, R. L. Horne, P. G. Kevrekidis, and N. Whitaker. Linear and nonlinear parity-time-symmetric oligomers: a dynamical systems analysis. *Philosophical Transactions of the Royal Society A: Mathematical, Physical and Engineering Sciences*, 371(1989):20120171, 2013.

[144] S. V. Suchkov, A. A. Sukhorukov, J. Huang, S. V. Dmitriev, C. Lee, and Y. S. Kivshar. Nonlinear switching and solitons in PT-symmetric photonic systems. *Laser and Photonics Reviews*, 10(2):177, 2016.

[145] G. S. Agarwal and K. Qu. Spontaneous generation of photons in transmission of quantum fields in PT-symmetric optical systems. *Physical Review A*, 85(3):031802, 2012.

[146] J. Li, X. Zhan, C. Ding, D. Zhang, and Y. Wu. Enhanced nonlinear optics in coupled optical microcavities with an unbroken and broken parity-time symmetry. *Physical Review A*, 92(4):043830, 2015.

[147] H. Schomerus. Quantum noise and self-sustained radiation of PT-symmetric systems. *Physical Review Letters*, 104(23):233601, 2010.

[148] M. Zhang, W. Sweeney, C. W. Hsu, L. Yang, A. D. Stone, and L. Jiang. Quantum noise theory of exceptional point amplifying sensors. *Physical Review Letters*, 123(18):180501, 2019.

[149] S. Bittner, B. Dietz, U. Gunther, H. L. Harney, M. Miski-Oglu, A. Richter, and F. Schäfer. PT-symmetry and spontaneous symmetry breaking in a microwave billiard. *Physical Review Letters*, 108(2):024101, 2012.

[150] B. Dietz, H. L. Harney, O. N. Kirillov, M. Miski-Oglu, A. Richter, and F. Schafer. Exceptional points in a microwave billiard with time-reversal invariance violation. *Physical Review Letters*, 106(15):150403, 2011.

[151] S. Bittner, B. Dietz, H. L. Harney, M. Miski-Oglu, A. Richter, and F. Schafer. Scattering experiments with microwave billiards at an exceptional point under broken time-reversal invariance. *Physical Review E*, 89(3):032909, 2014.

[152] N. Lazarides and G. P. Tsironis. Gain-driven discrete breathers in PT-symmetric nonlinear metamaterials. *Physical Review Letters*, 110(5):053901, 2013.

[153] G. P. Tsironis and N. Lazarides. PT-symmetric nonlinear metamaterials and zero-dimensional systems. *Applied Physics A*, 115(2):449, 2014.

[154] L. Feng, Y. Xu, W. S. Fegadolli, M. Lu, J. Oliveira, V. R. Almeida, Y. Chen, and A. Scherer. Experimental demonstration of a unidirectional reflectionless parity-time metamaterial at optical frequencies. *Nature Materials*, 12(2):108, 2013.

[155] G. Castaldi, S. Savoia, V. Galdi, A. Alu, and N. Engheta. PT metamaterials via complex-coordinate transformation optics. *Physical Review Letters*, 110(17):173901, 2013.

[156] S. Weinberg. The quantum theory of fields (cambridge), 1995.

[157] A. Mostafazadeh. On the pseudo-hermiticity of a class of PT-symmetric hamiltonians in one dimension. *Modern Physics Letters A*, 17(30):1973, 2002.

[158] C. M. Bender, D. C. Brody, and H. F. Jones. Complex extension of quantum mechanics. *Physical Review Letters*, 89(27):270401, 2002.

[159] Dennis Dast, Daniel Haag, Holger Cartarius, and Günter Wunner. Quantum master equation with balanced gain and loss. *Phys. Rev. A*, 90:052120, 2014.

[160] Jiahua Li, Rong Yu, and Ying Wu. Proposal for enhanced photon blockade in parity-time-symmetric coupled microcavities. *Phys. Rev. A*, 92:053837, 2015.

[161] Dennis Dast, Daniel Haag, Holger Cartarius, Jörg Main, and Günter Wunner. Bose-einstein condensates with balanced gain and loss beyond mean-field theory. *Phys. Rev. A*, 94:053601, 2016.

[162] V. Peřinová, A. Lukš, and J. Křepelka. Quantum description of a $\mathcal{PT}$-symmetric nonlinear directional coupler. *J. Opt. Soc. Am. B*, 36:855, 2019.

[163] S. Scheel and A. Szameit. $\mathcal{PT}$-symmetric photonic quantum systems with gain and loss do not exist. *Europhys. Lett.*, 122:34001, 2018.

[164] K. Z˙ yczkowski, P. P. Horodecki, M. Horodecki, and R. Horodecki. Dynamics of quantum entanglement. *Physical Review A*, 65:012101, 2001.

[165] T. Yu and J. H. Eberly. Finite-time disentanglement via spontaneous emission. *Physical Review Letters*, 93:140404, 2004.

[166] Z. Ficek and R. Tana s. Dark periods and revivals of entanglement in a two-qubit system. *Physical Review A*, 74:024304, 2006.

[167] Z. Ficek and R. Tana s. Delayed sudden birth of entanglement. *Physical Review A*, 77:054301, 2008.

[168] E. G. Cavalcanti, Q. Y. He, M. D. Reid, and H. M. Wiseman. Experimental criteria for steering and the Einstein-Podolsky-Rosen paradox. *Physical Review A*, 84:032115, 2011.

[169] V. Le Duc, J. K. Kalaga, and W. Leoński. Quantum correlations in system of kerr nonlinear coupler. *Acta Physica Polonica, A*, 139(5):532, 2021.

[170] V. Le Duc, M. Nowotarski, and J. K. Kalaga. The bipartite and tripartite entanglement in PT-symmetric system. *Symmetry*, 13(2):203, 2021.

[171] V. Le Duc, J. K. Kalaga, W. Leoński, M. Nowotarski, K. Gruszka, and M. Kostrzewa. Quantum steering in two-and three-mode-symmetric systems. *Symmetry*, 13(11):2201, 2021.

[172] Y. Sun, W. Tan, H. Li, J. Li, and H. Chen. Experimental demonstration of a coherent perfect absorber with PT phase transition. *Physical Review Letters*, 112(14):143903, 2014.